

**TECHNISCHE  
UNIVERSITÄT  
DRESDEN**

---

Fakultät für Maschinenwesen, Institut für Werkstoffwissenschaft

---

# Development of an *in vitro* blood flow model to evaluate antimicrobial coatings for blood-contacting devices

Von der Fakultät Maschinenwesen  
der Technischen Universität Dresden  
zur Erlangung des akademischen Grades

**Doktor-Ingenieur (Dr.-Ing.)**

angenommene

DISSERTATION

von

**Juliane Valtin, M.Sc.**

geboren am 03.03.1992 in Dresden

Tag der Einreichung: 04.08.2022

Tag der Verteidigung: 21.12.2022

**Gutachter:**

Prof. Dr. rer. medic. Hans-Peter Wiesmann, TU Dresden

Prof. Dr. rer. nat. Carsten Werner, TU Dresden

**Vorsitzender der Promotionskommission:**

Prof. Dr.-Ing. habil. Jochen Fröhlich, TU Dresden

Die Dissertation wurde im Zeitraum von 06/2018 bis 07/2022  
am Leibniz-Institut für Polymerforschung e.V. angefertigt.



“Whatever you do, always give 100%.  
Unless you're donating blood“

**Bill Murray**

# Abstract

Pre-clinical evaluation of novel antimicrobial coatings for blood-contacting devices commonly relies on the performance of animal studies since alternative *in vitro* models do not adequately represent the interactions between blood, bacteria, and material surfaces as they occur *in vivo*. To reduce the need of these cost-intensive and controversial animal tests, this project was dedicated to the development of a new model setup that overcomes this limitation and allows *in vitro* evaluation under *in vivo*-like conditions. This newly developed model was intended to be directly applied to evaluate recently in-house developed antimicrobial coatings, so-called anchor polymers. Therefore, the project was divided into two parts.

The first part of the project focused on the evaluation of the anchor polymer coatings concerning their applicability in blood-contacting devices. For this purpose, the PEGylated styrene-maleic acid copolymers were intensively studied using established laboratory tests. These examinations showed very promising results regarding adsorption and stability on relevant polymer substrates, antimicrobial efficacy, and biological safety of the coatings, thus revealing their great potential for future applications in medical devices. Moreover, this basic characterization was meant to allow a subsequent comparison of the new *in vitro* model with state-of-the-art *in vitro* tests.

The second part of the thesis focused on the development of the realistic *in vitro* model. Here, a single-pass flow system realized the implementation of adjustable flow conditions. Furthermore, incubation with freshly drawn human blood provided a physiological nutrient environment and included the influence of an immune response. *Staphylococcus aureus* were chosen as representative microorganisms, as they are responsible for a majority of device-related blood stream infections. The resulting blood flow model was validated with one anti-adhesive and one contact-killing anchor polymer coating, confirming the model's ability to differentiate the investigated surfaces. Inflammatory and coagulant blood activation correlated slightly with bacterial coverage, which in turn was strongly dependent on the investigated material surface. Incubation with varying flow conditions demonstrated the model's capability to reflect the well-documented dependence of bacterial colonization and occurring flow conditions. In contrast to the state-of-the-art *in vitro* tests, the simultaneous incubation of test surface, bacteria and whole blood allowed the analysis of mutual interactions of the three parameters. Thus, the model represents an excellent method for pre-clinical evaluation of novel antimicrobial coatings for blood-contacting devices.

# Acknowledgements

At the end of my time as a PhD student, I would like to look back and thank all the people who have accompanied and supported me along the way.

First and foremost, I would like to express my deepest gratitude to **Prof. Carsten Werner**, who gave me the opportunity to join his inspiring research group and provided me with continuous support and scientific guidance throughout my time at his institute. Furthermore, I would like to sincerely thank **Prof. Hans-Peter Wiesmann** for taking over the official supervision of the dissertation, for reviewing the thesis, as well as for his scientific advice during the project.

A special thank goes to **Dr. Manfred Maitz** and **Dr. Lars Renner**, who supported me with their broad expertise throughout my doctoral studies. Thank you for your professional guidance, support inside and outside of the lab, and numerous discussions that enormously contributed to the success of this project.

Furthermore, I would like to express my gratitude to **Dr. Frank Sonntag** and his research group from the Fraunhofer IWS for the successful cooperation. Thank you for the good communication, provisioning of the pumping setup, and the prompt assistance in case of troubles. Beyond that, special thanks to Stephan Behrens and Florian Schmieder for the entertaining company at the DGBMT conference that unfortunately remained my only on-site conference due to COVID-19 restrictions.

Further thanks goes to the “Anchor polymer”-Team (André Ruland, Melissa Sikosana, and Tina Helmecke), with whom I spent most of my time in the IPF labs. Thank you for the professional exchange, the mutual motivation, and for sharing this journey with me. You made countless hours in the lab and in the office much more fun!

Moreover, I would like to thank everyone at the IPF for the pleasant working atmosphere, where mutual support is a matter of course. I express my great appreciation to everyone who agreed to donate her/his blood for my experiments – this project could have never been realized without you! Also, I am very grateful for the technical support I received from Stefanie Hänsel, Lisa Ferdinand, Luise Hampel, Milauscha Grimmer, Kevin Richter, and Isabell Jeglinski. Lots of thanks to Dr. Lucas Schirmer for his helping hand during troubles with the microscope and his assistance with the 3D-printer, and to Dr. Ralf Helbig who was always willing to share his microbiology-related expertise with me. Further thanks goes to my part-time office mates, who always helped to stay positive, even during stressful phases. Thank you Alessia, André, Anna, Beatrise, Caro, Claudia, Felix, Nicole, Sina, and Tina for our fruitful



discussions, entertaining lunch breaks at the rooftop, and fun trips outside work. Moreover, I would like to take this opportunity to thank all the motivated cake and muffin bakers who sweetened our days sooo many times.

Finally, I wish to thank my family and friends. Here, I have received not only moral support, but also professional assistance. At this point, I would like to express a great thanks to Lydia and Matti for providing me their expertise and a helping hand during the design and assembly of the rotation device. A special thanks goes to my sister Kati, my grandma and especially to my parents. Thank you for your continuous support, belief in me and for keeping the balance between motivating and distracting me during work-loaded evenings and weekends. I would never have made it this far without you! Finally, I wish to express my greatest gratitude to my partner Pascal. Thanks for being my best friend in every situation of life, for supporting and believing in me, and for always giving me a hug when I needed it most. Our little motivational dances kept me going!

# Contents

|   |            |
|---|------------|
| <b>Abstract</b>   | <b>I</b>   |
| <b>Acknowledgements</b>   | <b>II</b>  |
| <b>List of abbreviations</b>  | <b>VII</b> |
| <b>1 Introduction</b>   | <b>1</b>   |
| 1.1 Motivation . . . . .  | 1          |
| 1.2 State of the art . . . . .  | 2          |
| 1.3 Approach . . . . .  | 4          |
| <b>2 Fundamentals</b>   | <b>6</b>   |
| 2.1 Device-related blood stream infections . . . . .                  | 6          |
| 2.1.1 Relevance . . . . .   | 6          |
| 2.1.2 Biofilm formation . . . . .                                     | 7          |
| 2.1.3 Influence of flow conditions on bacteria . . . . .              | 11         |
| 2.1.4 Host defense to bacterial invasion . . . . .                    | 12         |
| 2.2 Prevention of bacterial colonization on medical devices . . . . . | 16         |
| 2.2.1 Antimicrobial materials . . . . .                               | 16         |
| 2.2.2 Host reaction to biomaterials . . . . .                         | 19         |
| 2.3 Approval of medical devices . . . . .                             | 21         |
| 2.3.1 The evolution of an idea to a medical product . . . . .         | 21         |
| 2.3.2 Evaluation according to harmonized standards . . . . .          | 23         |
| <b>3 Coating evaluation</b>   | <b>25</b>  |
| 3.1 Objective . . . . .   | 25         |
| 3.2 Background . . . . .  | 26         |
| 3.2.1 Anchor polymer coatings . . . . .                               | 26         |
| 3.2.2 Polymer substrates . . . . .                                    | 27         |
| 3.3 Characterization of anti-adhesive coatings . . . . .              | 28         |
| 3.3.1 Quartz crystal microbalance . . . . .                           | 28         |
| 3.3.2 Contact angle . . . . .   | 30         |
| 3.3.3 Protein adsorption . . . . .                                    | 32         |
| 3.3.4 Long-term stability . . . . .                                   | 34         |
| 3.3.5 Hemocompatibility . . . . .                                     | 36         |
| 3.3.6 Antimicrobial activity . . . . .                                | 38         |
| 3.4 Characterization of contact-killing coatings . . . . .            | 40         |
| 3.4.1 Hemocompatibility . . . . .                                     | 40         |
| 3.4.2 Antimicrobial activity . . . . .                                | 42         |
| 3.5 Discussion . . . . .  | 44         |
| <b>4 Model development</b>  | <b>50</b>  |
| 4.1 Objective . . . . .   | 50         |
| 4.2 Requirements . . . . .  | 51         |

|          |  |            |
|----------|--|------------|
| 4.3      | Design rationale . . . . .                                     | 52         |
| 4.3.1    | Selection of an incubation system . . . . .                    | 52         |
| 4.3.2    | Incubation of the test surface . . . . .                       | 56         |
| 4.3.3    | Accumulation of activation products . . . . .                  | 57         |
| 4.3.4    | Sedimentation of blood cells . . . . .                         | 58         |
| 4.3.5    | Incubation time . . . . .                                      | 60         |
| 4.3.6    | Detection of bacteria after blood contact . . . . .            | 61         |
| 4.4      | Model setup . . . . .  | 64         |
| 4.4.1    | Overview . . . . .   | 64         |
| 4.4.2    | Optimization . . . . .   | 66         |
| 4.4.3    | Hemodynamic pumping behavior . . . . .                         | 71         |
| 4.5      | Verification . . . . .   | 73         |
| 4.6      | Validation . . . . .   | 75         |
| 4.6.1    | Differentiation of antimicrobial surfaces . . . . .            | 76         |
| 4.6.2    | Influence of wall shear stress . . . . .                       | 79         |
| 4.7      | Discussion . . . . .   | 81         |
| <b>5</b> | <b>Summary and outlook</b>                                     | <b>85</b>  |
| <b>6</b> | <b>Experimental part</b>                                       | <b>89</b>  |
| 6.1      | Surface preparation . . . . .                                  | 89         |
| 6.1.1    | Polycarbonate . . . . .  | 89         |
| 6.1.2    | Thermoplastic polyurethane . . . . .                           | 89         |
| 6.1.3    | Teflon AF . . . . .  | 90         |
| 6.1.4    | Glass . . . . .  | 90         |
| 6.2      | Anchor polymer coatings . . . . .                              | 90         |
| 6.2.1    | Synthesis of modified styrene-maleic acid copolymers . . . . . | 90         |
| 6.2.2    | Hexetidine functionalization . . . . .                         | 92         |
| 6.2.3    | Fluorescence functionalization . . . . .                       | 93         |
| 6.2.4    | Application . . . . .  | 93         |
| 6.3      | Characterisation . . . . .                                     | 93         |
| 6.3.1    | Quartz crystal microbalance . . . . .                          | 93         |
| 6.3.2    | Contact angle . . . . .  | 94         |
| 6.3.3    | Protein adsorption . . . . .                                   | 94         |
| 6.3.4    | Long-term stability . . . . .                                  | 94         |
| 6.3.5    | Hemocompatibility . . . . .                                    | 95         |
| 6.3.6    | Bacteria experiments . . . . .                                 | 98         |
| 6.4      | <i>In vitro</i> flow model . . . . .                           | 99         |
| 6.4.1    | Rotation device . . . . .                                      | 99         |
| 6.4.2    | Model setup . . . . .  | 100        |
| 6.4.3    | Micro-particle image velocimetry . . . . .                     | 101        |
| 6.4.4    | Workflow . . . . .   | 102        |
| 6.5      | Statistical analysis . . . . .                                 | 103        |
|          | <b>List of Figures</b>   | <b>ii</b>  |
|          | <b>List of Tables</b>  | <b>iii</b> |

|   |            |
|---|------------|
| <b>Bibliography</b>                                     | <b>iii</b> |
| <b>A Appendix</b>                                       | <b>xxi</b> |
| A.1 Supplementary results . . . . .                     | xxi        |
| A.2 Source code . . . . .                               | xxvii      |
| A.3 Technical drawings . . . . .                        | xxix       |
| A.4 Publications and conference contributions . . . . . | xxxii      |
| A.5 Selbstständigkeitserklärung . . . . .               | xxxiii     |

# List of abbreviations

|                   |   |
|-------------------|---|
| ANOVA             | one-way analysis of variance                |
| AP                | anchor polymer                              |
| bpm               | beats per minute                            |
| BSA               | bovine serum albumin                        |
| C5a               | complement fragment 5a                      |
| CAD               | computer-aided design                       |
| CFU               | colony forming unit                         |
| CVC               | central venous catheter                     |
| DAPI              | 4,6-diamidine-2-phenylindole-dihydrochlorid |
| DCM               | dichloromethane                             |
| DEHP              | di-2-ethylhexyl phthalate                   |
| DiOC <sub>6</sub> | 3,3'-dihexyl-oxacarbocyaniniodid            |
| DMF               | dimethylformamide                           |
| <i>E. coli</i>    | <i>Escherichia coli</i>                     |
| eDNA              | extracellular deoxyribonucleic acid         |
| EDTA              | ethylenediaminetetraacetic acid             |
| ELISA             | enzyme-linked immunosorbent assay           |
| EPS               | extracellular polymeric substances          |
| EVA               | ethylene-vinyl acetate                      |
| F                 | factor                                      |
| F1+2              | prothrombin fragment 1+2                    |
| FACS              | fluorescence-activated cell scanning        |
| FGN               | fibrinogen                                  |
| FISH              | fluorescence <i>in situ</i> hybridization   |
| GFP               | green fluorescent protein                   |
| HMDS              | hexamethyldisilazane                        |
| LB                | lysogeny broth                              |
| LPS               | lipopolysaccharides                         |
| MDD               | Medical Device Directive                    |
| MDR               | Medical Device Regulation                   |
| micro-PIV         | micro-particle image velocimetry            |
| NET               | neutrophil extracellular trap               |

|                    |                                       |
|--------------------|---------------------------------------|
| PAMP               | pathogen-associated molecular pattern |
| PBS                | phosphate buffered saline             |
| PC                 | polycarbonate                         |
| PEG                | poly(ethylene) glycol                 |
| PES                | polyethersulfone                      |
| PF4                | platelet factor 4                     |
| PMN                | polymorphonuclear leukocyte           |
| PRR                | pattern recognition receptor          |
| PS                 | polystyrene                           |
| PVC                | polyvinyl chloride                    |
| QCM                | quartz crystal microbalance           |
| RCA                | Radio Corporation of America          |
| RT                 | room temperature                      |
| <i>S. aureus</i>   | <i>Staphylococcus aureus</i>          |
| SEM                | scanning electron microscopy          |
| SMA                | styrene-maleic acid                   |
| SMA <sub>anh</sub> | styrene-maleic anhydride              |
| THF                | tetrahydrofuran                       |
| TLR                | toll-like receptor                    |
| TPU                | thermoplastic polyurethane            |
| Tris               | tris-(hydroxymethyl)-aminomethan      |
| WSS                | wall shear stress                     |

# 1 Introduction

## 1.1 Motivation

The pre-clinical evaluation of novel biomaterials and medical devices often relies on extensive animal testing. However, animal studies are highly controversial and frequently criticized by both public and experts. Beyond that, they are very cost-intensive, time-consuming, and in many cases a non-reliable predictor for human reaction to exposure [1–3]. The poor transferability of data is often attributed to an inappropriate methodological design of the studies [1, 4], as well as to differences between animals and humans regarding physiology, behavior, pharmacokinetics, and genetics [5].

The problematic nature of animal studies has been acknowledged for a long time. In 1960, the British scientists William Russel und Rex Burch published a book entitled „The Principles of Humane Experimental Technique“ [6], providing a framework for more humane animal experimentation. Their principle of 3Rs has been considered a guideline for experimental work with animals ever since. The 3Rs stand for “Replacement, Reduction, and Refinement”, encouraging to replace animal testing by alternative methods such as cell culture, computer simulations, or imaging methods, to reduce them through statistical and methodological optimization, and to refine them in order to minimize suffering of the animals to an absolute minimum. The relevance of this principle was reconfirmed in 2010 when it was integrated into the Directive 2010/63/EU on the protection of animals used for scientific purposes of the European Union. To implement this guideline, it is recommended to employ “alternative [...] testing strategies, such as the use of *in vitro* and other methods” [7]. The goal of such *in vitro* models is to test drugs and medical devices under realistic conditions to obtain information beyond those obtained from established laboratory tests, thus reducing, if not completely replacing, the need for subsequent animal testing.

The objective of this thesis was to develop such an *in vitro* model for the evaluation of antimicrobial materials for blood-contacting devices. These antimicrobial materials aim to minimize bacterial adhesion and biofilm formation on medical devices to reduce the incidence of device-related bloodstream infections. Although numerous *in*

*vitro* models already exist and have greatly contributed to an approved understanding of bacterial adhesion and biofilm formation, they often do not adequately reflect *in vivo* conditions. This discrepancy explains the poor predictive capabilities of *in vitro* models for pre-clinical *in vivo* testing and clinical outcome [8–10]. Roberts *et al.* [9] identified the following limitations of existing *in vitro* models: (1) unrepresentative nutrients, (2) unrepresentative microorganisms, (3) uncharacteristic nutrient flow, and (4) missing immune response. One way to address most of these aspects is the dynamic incubation of bacteria with human blood - an approach that has been chosen for this thesis.

## 1.2 State of the art

Only few existing *in vitro* models work with human blood to simulate an *in vivo* environment and evaluate antimicrobial substances and materials under more realistic conditions. One way to do this, is the co-incubation of bacteria with blood plasma [11] or relevant blood cells, such as leukocytes [12] or erythrocytes [13]. Using these methods, selected aspects of the natural immune response to bacteria are involved in the evaluation of the materials. However, both the immune and coagulation systems require the complex interplay of both blood cells and blood plasma (see Chapter 2.1.4). Consequently, only the utilization of whole blood can realistically represent the complex immune processes.

Another approach to consider blood-bacteria interactions when evaluating antimicrobial materials is the preconditioning of the material with whole blood prior to bacterial exposure. This procedure facilitates the formation of a conditioning layer of organic macromolecules such as fibronectin and fibrinogen, strongly influencing the subsequent adhesion of bacteria. This strategy was previously applied by our group [14] to analyze the antiseptic activity of silver-functionalized poly(ethylene glycol)-heparin hydrogels. Here, pre-incubation with whole blood reduced the number of initially adhered bacteria on polystyrene surfaces for *Pseudomonas aeruginosa* and *Staphylococcus epidermidis*. However, the vitality of adherent bacteria did not change, indicating that pre-adsorbed blood cells and proteins did not possess any antimicrobial effects but rather shielded the material surfaces. Another *in vitro* model, presented by Murga *et al.* [15], employs a similar principle to investigate the influence of whole blood on bacterial adhesion and biofilm formation on central venous catheter (CVC) connectors. After exposing the connector surfaces to a dilution of blood and physiological saline (ratio of 1:10) for one hour, a bacterial suspension was pumped over the connectors for a period of 13 days. Subsequent analysis of the connectors found that bacterial counts were higher on the pre-conditioned surfaces for all three



Gram-negative bacterial strains studied. A major advantage of this system was the implementation of flow conditions, allowing biofilm formation under relevant wall shear stress (WSS). However, due to the successive incubation of blood and bacteria, the interplay of the human immune system and bacteria could not be adequately reflected.

In contrast, Sapatnekar *et al.* [16, 17] developed a flow model that allowed simultaneous incubation of whole blood with bacteria. Here, *Staphylococcus epidermidis* were either pre-seeded on the material surface or directly injected with the freshly drawn blood. Interestingly, the correlation between bacteria and protein adsorption were highly dependent on the mode of incubation. While pre-seeded bacteria evoked a high level of subsequent protein adsorption, injected bacteria appeared to compete with proteins, resulting in a low protein adsorption when numerous bacteria managed to adhere. In contrast, platelets and leukocytes adhesion increased in the presence of bacteria. When assessing the potential of this model to evaluate antimicrobial materials, a few weaknesses were identified. First, the circulation of blood does not allow the removal of killed bacteria and apoptotic phagocytes, thus triggering an immune response even if the antimicrobial material fulfilled its purpose. And second, the model is not designed to adjust defined WSS, although they are known to strongly influence bacterial adhesion and biofilm formation. These points were meant to be addressed in the *in vitro* model developed as part of this thesis.

### 1.3 Approach

As mentioned above, the objective of this thesis project was the development of an *in vitro* flow model that enables the evaluation of antimicrobial surfaces under realistic conditions. This newly developed model should be directly applied to assess recently in-house developed antimicrobial coatings, so-called anchor polymers (APs) [18], concerning their applicability in blood-contacting devices. To achieve these goals, the project was divided into two parts (see Figure 1.1).

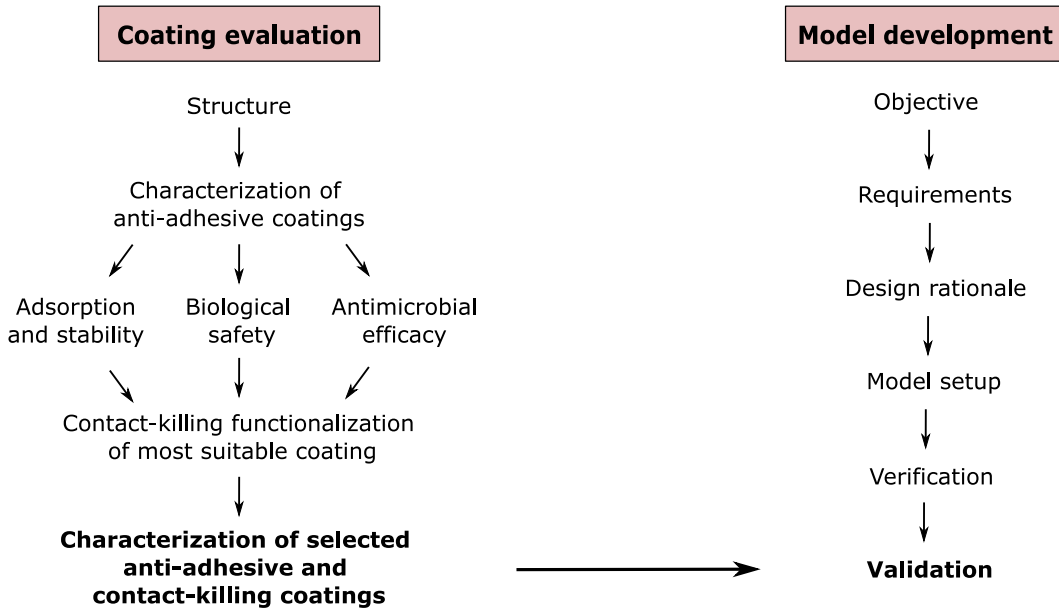


**Figure 1.1:** Approach of the thesis project, divided into two parts: Coating evaluation and model development.

#### Coating Evaluation

The first part of the project focused on a preliminary evaluation of APs coatings in terms of their applicability on blood-contacting materials. The AP technology is based on styrene-maleic acid copolymers that were functionalized with poly(ethylene) glycol (PEG), thus exhibiting anti-adhesive properties. Thanks to their well-balanced amphiphilicity, they maintain a high water solubility and strong binding affinity towards various polymer surfaces. The properties of the resulting APs can be adjusted by adapting the molecular weight and maleic acid percentage of the copolymer backbone, the PEG-styrene ratio, as well as the molecular weight of the PEG chains.

To analyze the influence of the different parameters on the properties of the resulting coatings, five APs were selected and characterized concerning their adsorption and stability on relevant polymer materials, antimicrobial efficacy and biological safety. These examinations were carried out with established static laboratory tests according to the state of the art. Subsequently, the most promising AP was chosen for further biocide functionalization. Here, a biocidal agent was covalently coupled to the PEG chains to provide an additional antimicrobial functionality, thus creating a contact-killing surface.

Finally, both anti-adhesive and contact-killing APs were tested concerning their antimicrobial activity and hemocompatibility. The resulting values were later employed for the validation of the *in vitro* model.

## Model development

The second part of the thesis dealt with the development an *in vitro* model that is able to evaluate antimicrobial coatings under more realistic conditions than existing models. To allow subsequent validation of the model, clear objectives were defined in the first step. These stated that the model should be able to distinguish different antimicrobial surfaces, represent the well-documented dependence between flow conditions and bacterial coverage, and provide information about antimicrobial coatings that cannot be obtained with established laboratory tests (as performed in the first part). Additionally, several requirements were defined to realize the implementation of the realistic *in vitro* model.

Subsequently, various decisions had to be made regarding the model design. These related, among others, to the selection of the pumping system, incubation mode of the test surface, and detection of bacteria after blood contact. Once the basic model setup was established, various parameters had to be re-adjusted to ensure optimal blood compatibility. After this optimization step, the *in vitro* model was further characterized, in particular the level of occurring WSS in dependence of the pump settings.

After the characterization was completed, the final model setup had to undergo a verification and a validation process. During verification, it was checked whether all previously defined requirements were met by the newly developed *in vitro* model. In contrast, validation was meant to verify whether the objective of the model could be fulfilled. For this process, the pre-characterized AP coatings from the first part of the work were tested in the *in vitro* model. For a subsequent evaluation, the measurement values of both parts were compared with each other and put in relation to literature data of coatings with comparable mode of action.

## 2 Fundamentals

### 2.1 Device-related blood stream infections

#### 2.1.1 Relevance

Intravascular devices play a significant role in current healthcare. Numerous widespread diseases such as arteriosclerosis, diabetes, or kidney failure demand the insertion of stents, catheters, ports, or other devices. However, the insertion of intravascular devices always bears the risk of a bacterial infection. In general, it is estimated that approximately 25 % of all healthcare-associated infections are related to medical devices [19]. The rate of device-associated infections highly depends on patient population, underlying medical conditions, and hygienic conditions. Accordingly, data vary widely between different studies; for catheters, numbers of clinically detectable infections per 1,000 catheter-days range from 0.8 to 4.1 [20, 21]. Even though improved surgical techniques, antibiotic prophylaxis and novel antimicrobial materials have significantly reduced the number of infections, the problem persists.

The high susceptibility to infection after the insertion of medical devices was first described by Elek and Cohen in 1957 [22]. The scientists discovered that the presence of foreign bodies increased the risk of wound infection by a factor of 10,000. Only 100 colony forming unit (CFU) of staphylococci were sufficient to trigger a purulent infection in healthy individuals in conjunction with a subcutaneously placed silk suture. Without the suture, at least 1,000,000 CFU were required to cause an infection. This correlation can be explained by the fact that bacteria are less susceptible to host immune defense mechanisms once they have attached to a surface. In particular, the phagocytic function of polymorphonuclear leukocytes (PMNs) is hindered by the formation of extracellular polymeric substances around the bacteria [23, 24].

Microorganisms that colonize medical devices originate from various sites. For catheters, most infections can be attributed to three different pathways (Figure 2.1): (1) invasion of the catheter lumen by a contaminated hub or infusate, (2) colonization of the outer catheter surface during insertion with bacteria from the natural skin flora, and (3) hematogenous seeding of the catheter from another infected site in the organism [25]. While infection by skin microorganisms plays the major

role for short-term catheters, the other two infection routes become increasingly relevant with advancing dwell time [26]. Accordingly, the most frequently isolated pathogens are those that naturally occur on the human skin flora. These include mainly Gram-positive strains such as coagulase-negative staphylococci as well as *Staphylococcus aureus* (*S. aureus*), each accounting for roughly 20 - 40 % of all infections [27, 28]. Infections with Gram-negative bacteria such as *Pseudomonas aeruginosa* and *Klebsiella pneumoniae* occur less frequently but vary greatly depending on hygiene and environmental conditions, catheter characteristics, pre-existing diseases and resistant strains in the hospital [26, 29, 30].

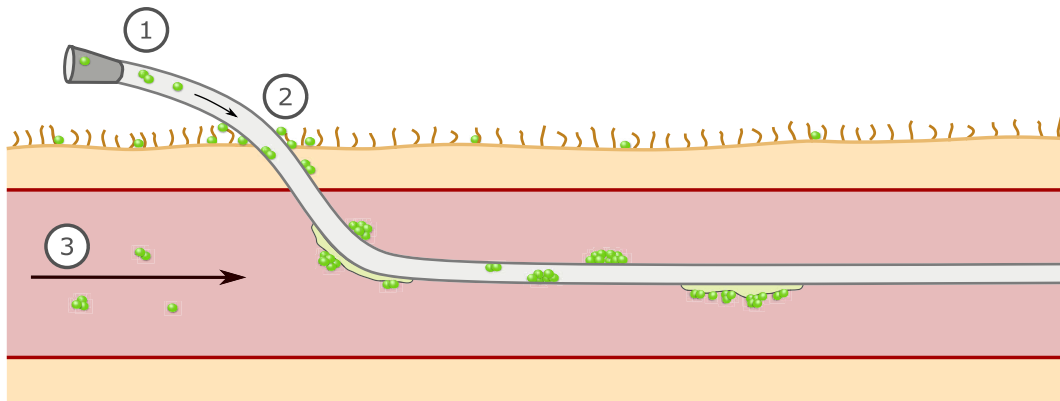


**Figure 2.1:** Infection pathways of medical devices illustrated by the example of a catheter: (1) Invasion of the catheter lumen by a contaminated hub or infusate, (2) Colonization of the outer catheter surface during insertion with bacteria from the natural skin flora, and (3) Hematogenous seeding of the catheter from another infected site in the organism; derived from [25] and [31].

### 2.1.2 Biofilm formation

In natural environments, bacteria occur almost exclusively in the form of biofilms [32]. Those are communities of well-organized microorganisms attached to a substrate and embedded in a self-producing extracellular matrix [33]. This way of living offers bacteria various survival advantages compared to their free-swimming, so-called planktonic, state. On the one hand, nutrients in aqueous environments also tend to accumulate at the solid-liquid interface and therefore provide nourishment for adherent bacteria. On the other hand, the adhesion of the bacteria stimulates their production of extracellular polymeric substances that enclose bacteria in a protective layer. This protective layer does not only provide mechanical stability to the bacteria, but also shields them from environmental influences such as drugs (e.g. antimicrobials), host immune attacks (e.g. phagocytes, antibodies), and shear forces (e.g. blood flow) [33, 34]. It is reported that bacteria organized in biofilms are at least 10 to 10,000 times

more resistant to antibiotic treatment than their planktonic counterparts [35].

Even though naturally occurring biofilms are often composed of multiple species, biofilm research predominantly focuses on the study of single-species biofilms for reasons of simplicity [36]. This study concentrates on the development of *S. aureus* biofilms as they play a major role in medical device-related infections and are utilized as model strain in this thesis. One of the latest *S. aureus* biofilm models from Moormeier *et al.* [37] divides biofilm formation in five phases: attachment, multiplication, exodus, maturation, and dispersal. These five phases are visualized in Figure 2.2 and described in more detail below.

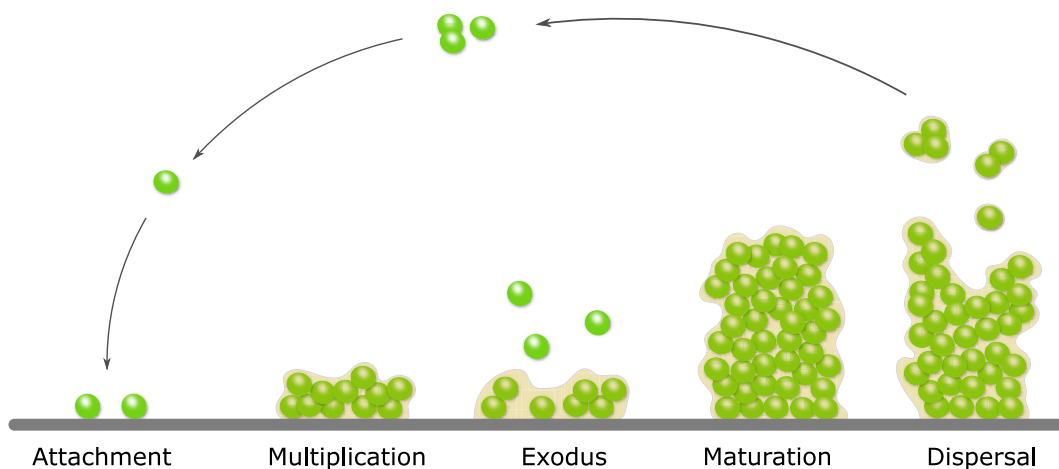


**Figure 2.2:** Biofilm life cycle showing the five phases of biofilm development: Attachment, multiplication, exodus, maturation, and dispersal; derived from [37] and [38].

### Attachment

The attachment of bacterial cells is the initial step of biofilm formation and can occur within seconds on both biotic and abiotic surfaces. On biotic surfaces, the initial attachment of planktonic *S. aureus* is mainly mediated by cell wall-anchored proteins that are highly specific for different host matrix components such as fibronectin [39], fibrinogen [40], and collagen [41]. In contrast, cell wall-anchored proteins only play a minor role during *S. aureus* attachment to abiotic surfaces. Here, adherence is mainly mediated by electrostatic and hydrophobic interactions, van der Waals forces and other physicochemical parameters of both material surface and bacteria cell [37, 42, 43]. Previous studies have shown that varying the charge of polymer surfaces lead to great alternations in cell attachment and overall biofilm development [44]. Also, teichoic acids – highly charged cell wall components - have shown to play a significant role in cell attachment due to their polyanionic properties [43].

## Multiplication

After having attached to a surface, the adherent *S. aureus* cells undergo a multiplication stage. In the presence of sufficient nutrients, the bacterial cells start to proliferate and accumulate on the surface. However, the newly formed daughter cells are highly susceptible to detachment, particularly in the presence of shear stress due to blood flow. In order to prevent detachment, *S. aureus* cells produce various factors that support the stabilization of cells. These include accumulation-associated protein SasG [45] as well as several cell wall-anchored proteins that already contributed to initial attachment phase (e.g. FnBPs, ClfB, and SdrC) [46]. In parallel, deceased bacterial cells lyse and release extracellular deoxyribonucleic acid (eDNA) and cytoplasmic proteins into the extracellular milieu, enclosing the microcolonies in a mixture of cytoplasmic proteins and genomic DNA [47, 48]. It is assumed that these extracellular polymeric substances (EPS) are further stabilized by immunodominant surface antigen B [49], beta-hemolysis [50], and extracellular proteins such as phenol soluble modulins [51].

## Exodus

One phase that has only recently been discovered and does not appear in elderly biofilm development models, is the stage of exodus. This phase is characterized by a distinct and coordinated release of individual bacterial cells resulting in a restructuring of the emerging biofilm. This process happens approximately 6 hours after the start of the multiplication phase. The exodus phase is initiated by the degradation of eDNA through nuclease that is produced and secreted by a subpopulation of *S. aureus* cells. In consequence, a majority of the accumulated biofilm population becomes detached. Additionally, the composition of EPS embedding the *S. aureus* cells becomes more complex, and individual matrix components as eDNA, polysaccharide intercellular adhesin, and proteins interact more intensively. Even though the biological role of the exodus stage is not yet fully understood, this process is thought to be essential for the formation of three-dimensional microcolonies [37].

## Maturation

The maturation phase describes how accumulated bacteria cells that have resisted the exodus stage, expand to microcolonies and form a three-dimensional structure. This enhanced structure increases the surface area to facilitate nutrient supply and removal of metabolites. In addition, bacterial cells can disseminate to more distal regions, where they are better protected from environmental influences such as shear stress or killing agents [52, 53]. This process is frequently accompanied by a transition to a dormant state of the bacteria, enhancing the diversity of the biofilm through coordinated gene expression patterns [54, 55]. In fundamental terms, maturation phase is characterized by the strong proliferation of *S. aureus* cells and their formation in resilient aggregations. The transfer of nutrients to the deeper layers of the biofilm is realized by fluid-filled channels [56]. However, the exact mechanisms of maturation are not yet fully understood. Several research groups assume that *S. aureus* grow in thick cell layers, from which some cells disperse and form new microcolonies in surrounding areas [57, 58]. However, other groups support the theory that microcolonies are derived exclusively from cells of the basal cell layer that have survived the exodus phase [37].

## Dispersal

Once a biofilm has reached a certain size, it starts to disperse. The release of mature cells can be induced by environmental factors such as shear stresses, pH alterations, accumulation of metabolic products, or nutrient deficiency [59]. Several studies suggest that the dispersal of *S. aureus* biofilms is controlled by Agr quorum sensing, a communication mechanism of bacterial cells to sense and react to alterations in population density by gene regulation [58, 60]. As other quorum sensing systems, it is highly dependent on cell density and the accumulation of signal molecules. Accordingly, the biofilm is stimulated to disperse when the density of cells or signal molecules reach a certain threshold. This correlation was further confirmed by a study showing that Agr-deficient strains form more robust biofilms than their wild-type counterparts [61].

*S. aureus* cells that have been dispersed by the mature biofilm are released to the environment and have the chance to attach to another surface that might provide better conditions for survival [62].



### 2.1.3 Influence of flow conditions on bacteria

The influence of mechanical properties on bacterial adhesion and biofilm formation has been neglected in research for many years. Classical laboratory methods such as agar plate and broth cultures exclusively investigate the influence of the chemical environment. Only in recent decades the focus has shifted to the evaluation of mechanical influences, which has led to the development of numerous flow models. Studies with these new platforms not only have demonstrated that adhesion and biofilm formation are highly influenced by mechanical effects, such as WSS in blood flow, but also that bacteria can adapt to these conditions [63, 64].

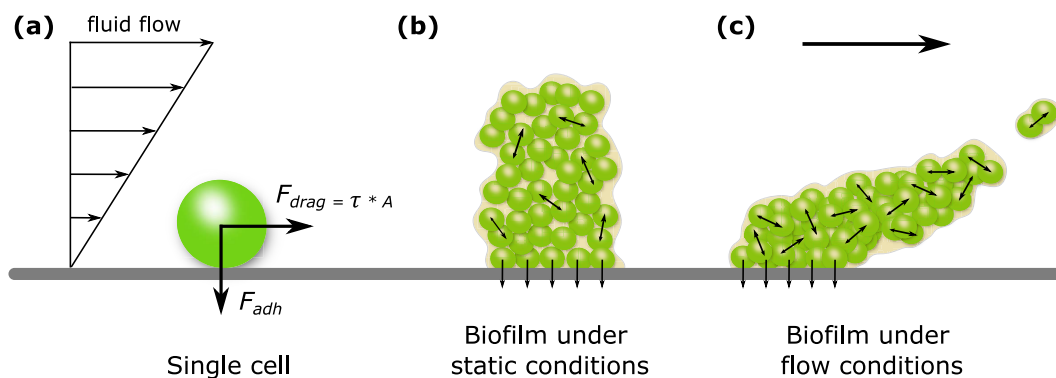


**Figure 2.3:** Single bacteria and biofilms under the influence of flow conditions: (a) Forces acting on single bacteria cell when placed under fluid flow, (b) Biofilm grown under static conditions; arrows indicating adhesion forces to the surfaces and interactions between single cells and EPS, (c) Biofilm grown under flow conditions; increased mass density and strong interactions between EPS components are indicated by the high cell density and number of arrows; derived from [63] and [64].

As shown in Chapter 2.1.2, bacteria tend to attach to surfaces in order to improve their chances of survival. Once attached to a surface, the mechanical environment changes enormously compared to the planktonic state. Generally, bacteria are held to the surface by an adhesive force. This adhesive force ( $F_{adh}$ ) acts normal to the surface and is influenced by physicochemical parameters such as hydrophobic or electrostatic interactions and by adhesive structures of the bacteria such as flagella, pili, or extracellular matrix components. Under the influence of fluid flow, the adhesion force of a single bacteria cell needs to exceed the drag force caused by the fluid flow in order to stay attached. This drag force ( $F_{drag}$ ) acts tangential to the surface and is calculated from the product of WSS ( $\tau$ ) and exposed surface area ( $A$ ) (Figure 2.3 a) [63]. Once this drag force exceeds the adhesion force, bacteria “slide and roll” over the surface, and may be detached [65, 66].

When bacteria are aggregated into biofilms, this equation becomes more complex. Through the formation of EPS, the bacteria stabilize each other and are stronger anchored to the surface. Here, numerous adhesion and cohesion forces act between the individual components. This biofilm can be described as a viscoelastic material. It reacts dynamically to the influence of shear forces by deformation and can thus prevent detachment from the surface to a certain degree [64, 65]. However, if the drag force becomes too strong, individual bacteria or subpopulations of the biofilm will detach (Figure 2.3 b,c) [67].

In addition, shear forces have a high influence on the morphology and composition of biofilms. It was observed that a high fluid flow increases mass transport and diffusion of solutes, which in turn promotes metabolism and thus bacterial growth [68]. At the same time, biofilm viability decreases, which has been attributed to an accumulation of waste products within the biofilm [69]. Since bacteria and subpopulations with insufficient adhesive forces can be carried away, biofilm maturation slows down and a young biofilm is maintained [70]. In consequence, mass density of biofilm increases and the biofilm gets thicker [64, 71]. The biofilm becomes more elastic and rigid, allowing it to resist mechanical failure and detachment to a greater extent. This phenomenon can be explained by the fact that alignment and interactions between individual EPS components become stronger, resulting in higher adhesion and cohesion forces [72, 73]. However, even though much progress has been made in understanding the mechanical effects on biofilms, many processes are not yet fully understood.

#### **2.1.4 Host defense to bacterial invasion**

When bacteria invade an organism, the host's immune system is immediately activated and attempts to eliminate the intruders. The innate immune system is the first to react. It is non-specific and able to eliminate the majority of pathogens just within a few minutes or hours [74]. However, for those that are able to overcome the innate defense mechanism, the support of the adaptive immune system is required. In contrast to the innate system, the adaptive response is highly specific to the pathogen that induced it. Beyond that, it can develop a memory to allow a quick response in case of a re-invasion of the same pathogens. In addition to the innate and adaptive immune systems, the coagulation system also plays an important role in defending the host against invading microorganisms. This function includes the prevention of pathogen spreading, as well as the support of killing mechanisms and tissue repair [75].

However, the invading microorganisms are not defenseless and have developed their own strategies to overcome the host's immune system. These include the release

of proteins interfering with the complement system and antibody opsonization, the evasion of neutrophil recruitment and activation, as well as the production of toxins [76]. Furthermore, bacteria are able to aggregate and enclose themselves in a protective layer of EPS making it difficult for components of the immune system to attack them. This biofilm formation occurs particularly on surfaces of medical devices. If the colonized device is not removed and the immune system is continuously stimulated, there is the risk of a systemic inflammatory response syndrome, the so-called sepsis [77, 78].

### **Innate immune system**

The first line defense of the innate immune system are physical barriers such as the skin, tears, mucus, and cilia. These components prevent bacteria from reaching potential infection sites within the organism. However, the insertion of medical devices often requires the penetration of these physical barriers, thus opening an entry port for invading microorganisms. Once bacteria manage to intrude the organism, components of the humoral immune response become active. These include several types of soluble molecules found in extracellular fluid, blood, and epithelial secretions that can kill a pathogen immediately or attenuate its effects. Antimicrobial enzymes and peptides as well as components of the complement system either destroy the bacterial cell membrane directly or opsonize them for subsequent phagocytosis by macrophages [74, 78].

In the next step, the cellular response by non-specific immune cells, such as macrophages, PMNs, and natural killer cells commences. These cells possess several pattern recognition receptors (PRRs) that are able to detect bacteria by their pathogen-associated molecular patterns (PAMPs). PRRs include receptors such as the transmembrane toll-like receptor (TLR) 2 that recognizes lipoteichoic acid of the cell walls of Gram-positive staphylococci and TLR 4 that recognizes lipopolysaccharides (LPS) of the outer cell membrane of Gram-negative bacteria. If these receptors are stimulated, they mediate further immune defense by the release of inflammatory cytokines and initiating the antigen-specific adaptive immune response [78].

### **Adaptive immune response**

The adaptive immune system becomes active when the innate immune system fails to eliminate all bacteria. As mentioned above, it is activated by an increased cytokine level as well as by the presentation of bacterial antigens on antigen-presenting cells. The main tasks of the adaptive immune response include the recognition of foreign

antigens, the elimination of pathogens or pathogen-infected cells, and the formation of an immunological memory that enables immediate reaction in case of a new infection. The main actors of these processes are B- and T- cells. The antigen-specific T-cells bind to the foreign antigens, are thereby activated to proliferate, and either kill bacterial cells directly or attract other phagocytes. In contrast, B-cells differentiate to plasma cells that produce antigen-specific antibodies, which in turn opsonize the pathogens for subsequent phagocytosis. Both B- and T-cells are able to produce memory cells that become active in case of a new infection with the same pathogen [79, 80].

### Coagulation system

The coagulation system is part of the hemostatic system that describes all physiological processes that aim to stop bleeding after a blood vessel injury. In addition to blood coagulation, these processes also include vasoconstriction as well as platelet adhesion, activation, and aggregation. Blood coagulation can be activated by two different pathways: the intrinsic pathway that is triggered by clotting factors present in the blood and the extrinsic pathway that is triggered by factors released from the injured tissue. Both pathways are activated separately, but combine during activation of factor (F)X to FXa. The subsequent joint pathway involves the conversion of prothrombin to thrombin that in turn converts fibrinogen to fibrin. In a last step, fibrin monomers undergo spontaneous polymerization and form a network, that is stabilized and crosslinked by FXIIIa (Figure 2.4) [81].

However, coagulation is not only activated by bleeding in blood vessels, but also by the presence of bacteria. This process aims to limit the dissemination of bacteria in the system, for example by trapping bacteria in the fibrin network, and can be initiated by multiple factors. The intrinsic pathway is activated when FXII binds to negatively charged structures, such as teichoic acids of *S. aureus* [82, 83]. Beyond that, PAMPs on bacterial cells can induce the expression of tissue factor on monocytes and macrophages, resulting in the initiation of the extrinsic coagulation pathway [84, 85]. Generally, the innate immune response and blood coagulation are closely connected, as cellular and protein modulators are often involved in both processes [86]. One of those interconnected mechanism is the formation of neutrophil extracellular traps (NETs) by neutrophilic granulocytes. These structures are composed of decondensed DNA, histones, and enzymes and aim to trap foreign objects such as bacteria. In addition to their antibacterial function, they also enhance coagulation by their negative charge [75, 87, 88].

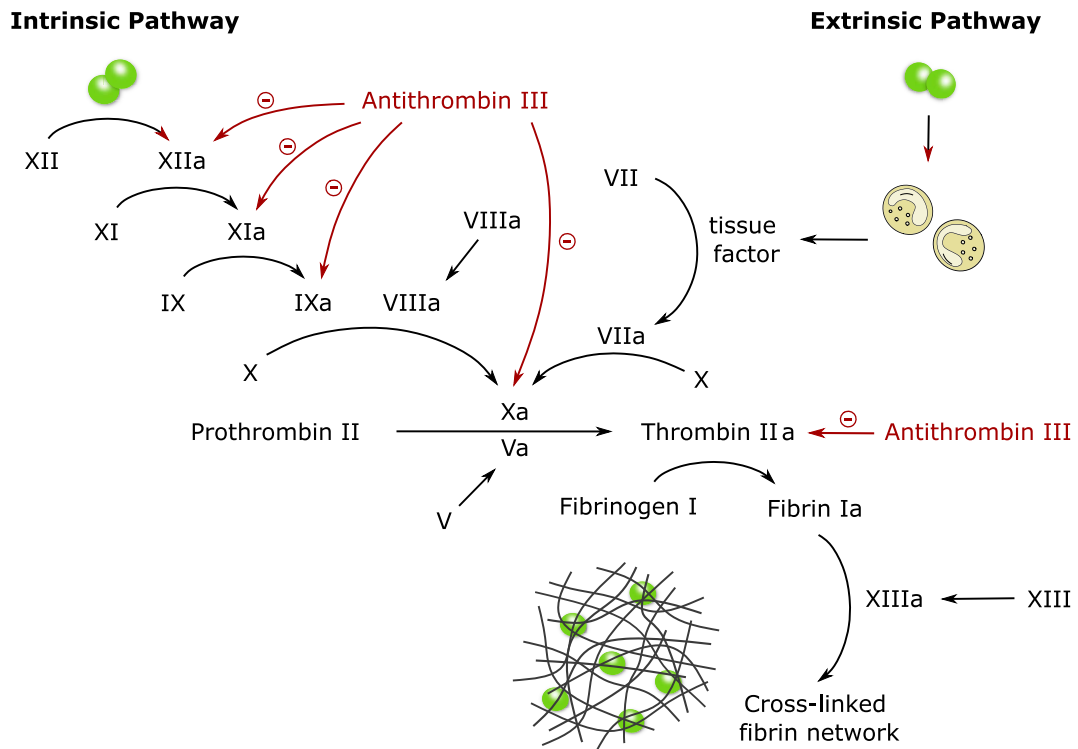


**Figure 2.4:** Simplified illustration of the intrinsic and extrinsic pathways of coagulation cascade, triggered by the presence of bacteria.

### Adaption strategies of bacteria

Bacteria have developed various strategies to evade the host's immune defense mechanism. Those protection mechanism depend strongly on the bacterial strain. While many bacteria protect themselves by hiding in thick capsules, *S. aureus* are specialized in defense by protein secretion [76]. Those secreted proteins have various functionalities. Among others, they can target antibody opsonization or phagocytosis. For instance, staphylococcal protein A binds to Immunoglobulin G in the wrong orientation, thus blocking the Fc receptor-mediated phagocytosis [89, 90]. Beyond that, extracellular adherence protein [91], extracellular complement-binding protein [92] or staphylococcal complement inhibitor [93] can prevent complement activation and subsequent opsonization. Other secreted proteins (e.g. SSL3, CHIPS) prevent priming and activation of PMNs by blocking the interactions of their receptors with chemoattractants [94, 95]. In addition, *S. aureus* processes various strategies to withstand the immune cells' killing mechanism. These include the secretion of protease inhibitors, nucleases, and enzymes as well as the alteration of the cell wall charge. Furthermore, *S. aureus* produce several proteins that can kill immune cells directly by disrupting their cell membrane [76].

Another evasion strategy of *S. aureus* and other bacteria is the aggregation in biofilms, as presented in Chapter 2.1.2. The secreted EPS provide mechanical protection against phagocytosis by connecting single cells with each other. This agglomeration of cells can result in “frustrated phagocytosis” as PMNs are only able to phagocytose cells that are smaller than themselves ( $\sim 10\text{ }\mu\text{m}$ ) [96]. In addition, positively charged components of EPS are able to protect against both positively and negatively charged antimicrobial peptides, either by repelling or sequestering them [97]. Other protective effects of EPS are based on its function as a shield for immune recognition as well as decoy for opsonization [76].

With regard to blood coagulation, *S. aureus* possess a very special adaption strategy. The *S. aureus* cells do not only evade this aspect of the immune response, but actively exploit it. The production of staphylococcal clumping factors such as canonical coagulase and von Willebrand factor binding protein promotes the conversion of prothrombin to thrombin, thus stimulating the formation of fibrin networks. By embedding themselves within a fibrin network, *S. aureus* cells experience two major advantages. First, the fibrin coating shields them from the host’s immune cells, and second, their aggregation in clots protects them from phagocytosis due to their increase in size [98, 99].

## 2.2 Prevention of bacterial colonization on medical devices

### 2.2.1 Antimicrobial materials

Once a biofilm has formed on the surface of a medical device, it usually requires the removal of the colonized device. To avoid this and prevent biofilm formation from the outset, numerous antimicrobial materials have been developed in recent decades. In most cases, these materials cannot completely prevent bacterial colonization of medical devices [100]. However, they slow down the process, giving the immune system’s defense mechanisms or administered antibiotics more time to react before bacteria settle into protective biofilms. The efficacy of antimicrobial materials to reduce bacterial colonization on medical devices was demonstrated in various clinical trials [101–103]. A meta-analysis of 23 studies evaluating antimicrobial-coated CVCs revealed that both bacterial colonization and occurrence of device-related bloodstream infection per 1,000 catheter-days were reduced by approximately 35 % compared to untreated devices [104].

In general, antimicrobial materials can be divided into three distinct categories: anti-adhesive materials that prevent bacterial adhesion through repulsion, release-based materials that deliver bactericidal agents to the surroundings, and contact-killing materials that kill adherent bacteria through coupled biocides (see Figure 2.5).

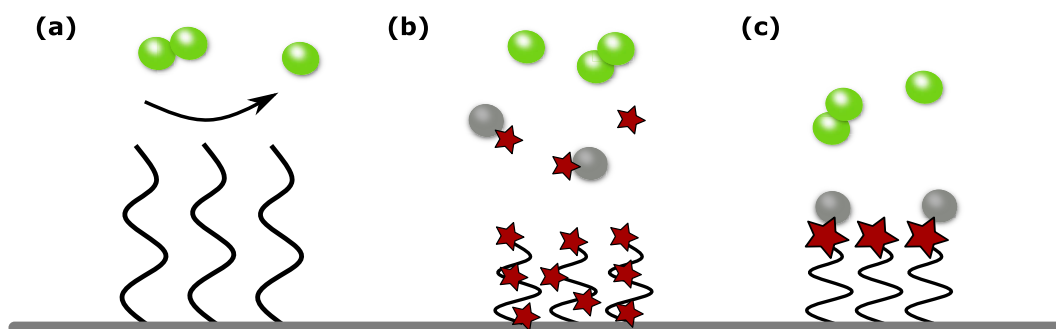


**Figure 2.5:** Categories of antimicrobial coatings commonly applied in medical devices: (a) Anti-adhesive materials, (b) Contact-killing materials, (c) Release-based materials.

### Anti-adhesive materials

The repellent properties of anti-adhesive materials are usually realized by either hydrophilic or superhydrophobic surfaces. Hydrophilic polymers obtain their anti-adhesive behavior through a combination of hydration and steric hindrance. A thin water layer forming on the surface creates a physical and energetic barrier that makes bacterial adhesion thermodynamically unfavorable. In addition, hydrogen bonds of hydrophilic polymers interact with approaching bacteria, leading to a compression of polymer chains and release of bound water molecules, thus provoking osmotic pressure and steric repulsion [105, 106]. The most common hydrophilic polymer is PEG, frequently considered as the gold standard of anti-adhesive polymers for medical devices [105, 107]. Its repulsive strength is mainly dependent on molecular weight, packing density, film thickness, and chain conformation [105, 108].

In contrast, superhydrophobic materials aim to reduce surface interactions due to low surface energy. This concept is biologically inspired by the anti-adhesive properties of lotus leaves or dragonfly wings. Artificial superhydrophobic surfaces can be manufactured by different techniques, including the adaption of material composition (e.g. fluorinated compounds), or by altering the surface structure (e.g. nanopatterning) [108, 109].

### Release-based materials

Another strategy to prevent bacterial colonization on medical devices is the application of materials that actively release antibacterial agents. This way, planktonic bacteria in the surroundings can already be eliminated before they have the chance to attach to the biomaterial. However, a major drawback of release-based materials is the inevitable loss of activity once all compounds have been released. In addition, the release of sublethal biocide concentrations does not only accelerate the development of drug resistance [110, 111], but also the formation of biofilms [112, 113].

Antibacterial agents can be brought to biomaterials by impregnation, physical adsorption, conjugation, or complexation. These include, among others, antibiotics (e.g. gentamicin, ciprofloxacin), antiseptics (e.g. chlorhexetidine), or other agents with biocidal activity (e.g. silver, nitric oxide) [106, 108]. In most applications, release is facilitated by either diffusion or erosion, although novel approaches also include pH-triggered release [114, 115] or enzymatic cleavage of covalent bonds [116, 117]. Approved medical products applying the release-mechanism include CVCs impregnated with minocycline and rifampin (Cook Spectrum<sup>®</sup>, Cook Medical, Bloomington, USA) or chlorhexidine and silver sulfadiazine (Arrowg+ard Blue Plus<sup>®</sup> Protection, Teleflex, Wayne, USA).

### Contact-killing materials

Contact-killing materials are mostly polymers in which either bioactive molecules are copolymerized with a second monomer or covalently bound to the polymer matrix, or the entire macromolecule is bioactive. In consequence, they are chemically stable and non-volatile, thus killing of bacteria only occurs if they attach to the surface. As their antimicrobial agents cannot deplete, they have a longer life time than release-based materials and minimize the risk of antibiotic resistance and environmental issues [108, 118].

The efficacy of most contact-killing materials is based on cationic compounds. Due to their positive charge, they bind to the bacterial cell wall and react with lipids or proteins of the cell membrane, leading to membrane disassembly and subsequent destruction [119, 120]. Examples for contact-killing polymers, where the entire polymer matrix is bioactive, are the naturally occurring polymer chitosan, the synthetic polymer polyethylenimine, as well as cationic silicones and acrylic polymers [108, 118]. However, both positively and negatively charged surface are not recommended for blood contact due to their high activation of blood coagulation [121, 122]. Covalently bound bactericidal agents include chlorhexidine [123, 124], quaternary ammonium



compounds [125, 126], as well as antibiotics such as ciprofloxacin [127] and gentamicin [128]. However, the immobilization of antibacterial agents to the polymer matrix always bears the risk of efficacy loss [108].

### 2.2.2 Host reaction to biomaterials

When vascular devices are inserted into the organism, they invariably trigger an immune response. The processes that occur are similar to those after bacterial invasion (see 2.1.4) and are mainly initiated by the innate immune system and the coagulation system. Both systems are strongly intertwined and influence each other [129]. The adaptive immune system, on the other hand, only plays a minor role, as artificial materials do not carry activating antigens. However, it is becoming increasingly relevant as more and more biomaterials are functionalized with proteins, peptides, and other biomolecules [130]. Since this is not the case for the materials investigated in this work, that aspect will be neglected here.

To date, no single material is known that can completely suppress this process, even though advances in biomaterials research have led to a significant reduction in occurring inflammatory reactions. This is particularly problematic with blood-contacting materials, as the activation products are distributed throughout the organism via the bloodstream and are not limited locally. When inserting vascular devices, it is usually aimed to keep the immune response as low as possible. This can either be achieved by modifying the used materials to improve their hemocompatibility or by the administration of supplementary medication that helps to control the immune response [129].

#### **Innate immune system**

When foreign materials come into contact with blood, numerous plasma proteins adsorb to the artificial surface just within a few seconds. In this process, proteins with a high mobility (e.g. fibrinogen) adsorb first and are gradually replaced by proteins with a higher affinity to the material surface (e.g. kininogen, FXII). This process is commonly known as the Vroman effect [131, 132]. The composition of the final protein layer is strongly influenced by the physicochemical properties of the material and further affects the subsequent immune response. The adsorption of plasma proteins is often accompanied by denaturation or conformational change, which in turn attracts proteins of the complement system. These complement proteins attempt to opsonize the foreign body for phagocytosis, analogous to how it occurs for pathogens or abnormal cells [122]. The activation of the complement cascade

by artificial surfaces is either initiated by the classical or the alternative pathway. Kallikrein plays a major role in this process as it is able to activate both pathways, either by activating C1 by cleavage of FXII, or by directly activating C3 and C5 [133, 134]. The resulting C3a and C5a in turn attract leukocytes to the surface and trigger their activation, which directs the further immune response. Upon activation, leukocytes undergo an internal cell reorganization that results in the presentation of CD11b and other adhesion ligands. This reorganization does not only enable cell adherence and interaction with other immune cells, but also triggers further strategies of the innate immune system such as the release of soluble factors, microparticles, and the formation of NETs [135].

### **Coagulation system**

As mentioned before, coagulation system and innate immune system strongly interact with each other. Accordingly, both mechanisms are driven by similar processes such as protein and cell adsorption. As an example, the adsorption of FXII to artificial surfaces does not only initiate complement activation, but also triggers the intrinsic pathway of coagulation that leads to the formation of blood clots by enclosing platelets and other adherent cells in fibrin networks [129, 135]. Here, the course of the coagulation cascade is comparable to that after bacterial invasion (Figure 2.4). In addition to protein-driven coagulation, adherent platelets also play a major role in the formation of blood clots. The activation of these platelets causes an increased production of thrombin, that in turn leads to a further amplification of the coagulation cascade [136]. Even though blood coagulation is a necessary process after blood vessel injuries to prevent excessive bleeding, it carries a high risk of life-threatening thrombosis when occurring at inserted biomaterials. For this reason, biomaterials research is working ambitiously on the development of materials that can limit both inflammation and coagulation processes.

### **Strategies to reduce host reaction**

Inflammatory and coagulation responses due to biomaterials can be limited by several approaches. A frequently used method is the administration of antithrombogenic pharmaceuticals, a strategy particularly applied with cardiac devices such as artificial heart valves or stents. There are two different categories of antithrombogenic drugs: anticoagulants (e.g. heparin, warfarin) that directly or indirectly inhibit enzymes involved in coagulation, and antiplatelet drugs (e.g. aspirin, clopidogrel) that inhibit biomaterial-induced activation via different mechanisms [129]. In many cases, these antithrombogenic drugs must be taken for the rest of the patient's life. Another

drawback of antithrombogenic treatment is the high risk of adverse drug events, such as increased bleeding [137–139].

Further strategies to reduce inflammatory and coagulation reactions on biomaterials are passive and active modification of the material surface. Passive surfaces are designed to minimize the interactions with the immune and coagulation system, mostly by suppressing protein adsorption [140]. This can be achieved by the application of hydrophilic brushes [141, 142], hydrogels [143, 144], or super-hydrophobic surfaces [145, 146]. This type of modification has the positive side effect that it often prevents bacterial adhesion at the same time. In contrast, active surface modifications aim to prevent or counteract activation processes by coupling anticoagulant or fibrinolytic agents to the surface. For this purpose, several agents such as nitric oxide [147, 148], thrombomodulin [149, 150], and plasminogen activators [151, 152] are under investigation. However, to date, only heparin-functionalized active surfaces have received approval for clinical use [153].

Another strategy to prevent a host reaction is the endothelialization of the surfaces, aiming to mimic the natural environment of the vessel walls. Despite great advances in research, this approach still struggles with activation of adherent endothelial cells, biological reactions to degradation products, as well as undesired growth of other cell types [140].

## **2.3 Approval of medical devices**

### **2.3.1 The evolution of an idea to a medical product**

When developing antimicrobial coatings for medical devices, it is a long way from the initial idea to the market launch of the final product. The entire development process must comply with strict regulations in order to demonstrate the safety and effectiveness of the product. Since May 2017, the requirements for market approval within the European Union are specified in the Regulation (EU) 2017/745 [154], also called Medical Device Regulation (MDR). After a transition period of three years, this regulation replaced the previously applicable Council Directive 93/42/EEC [155], shortly called Medical Device Directive (MDD). The MDR represents the first regulation that applies directly in all European Union countries and does not require prior transposition into national laws.

The process of medical device development can be divided into four phases (Figure 2.6). The first phase includes the identification of the product idea and its translation into a final concept. According to the type of the planned device and its intended

use, the product has to be assigned to one of four risk classes (I, IIa, IIb, or III). Subsequently, basic requirements that are placed on the manufacturing processes and the device must be identified. The requirements placed on the product are strongly dependent on the device type and its risk classification. However, the implementation of a quality (ISO 13485) and risk management system (ISO 14971) are mandatory for all medical devices.

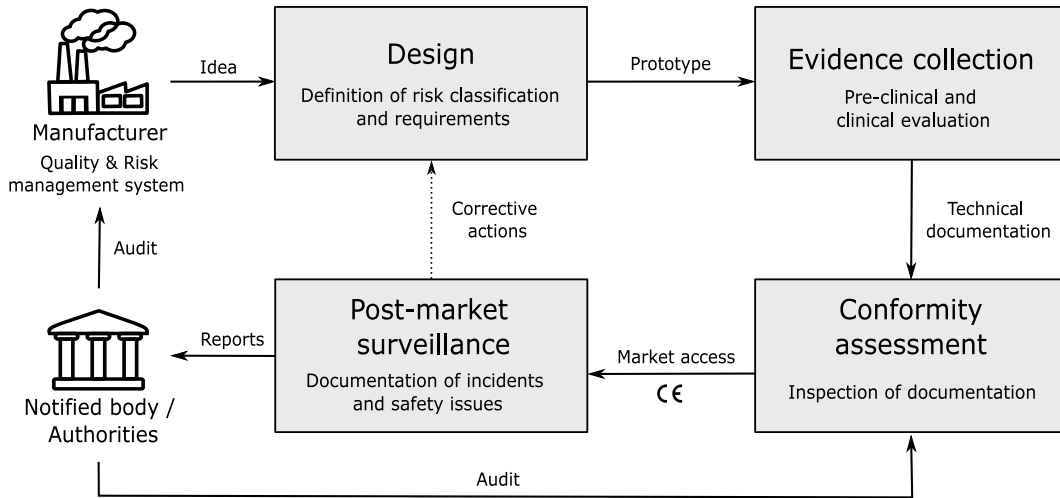


**Figure 2.6:** Procedure of medical device development in accordance to Medical Device Regulation including design, evidence collection, conformity assessment, and post-market surveillance.

The second phase of medical product development involves prototyping and evidence collection. A technical documentation is compiled to specify all incorporated materials and components and whether they meet the previously defined requirements. This can be verified by relevant scientific literature, comparison to existing devices or standard-compliant tests (e.g. ISO 10993 for biological evaluation). In addition, the finished prototype must undergo various laboratory tests to ensure the safety of the device. For implantable and risk class III devices, this clinical evaluation must be supplemented by a clinical investigation.

The third phase comprises the conformity assessment of the medical product. Here, risk and quality management system as well as technical documentation of the product are assessed by a notified body. The scope of the evaluation depends on the risk classification of the product. If passed, the medical device manufacturers can issue a declaration of conformity. With this declaration, the manufacturer can finally register the medical device and place it on the market. To demonstrate its compliance, the medical device shall bear the CE marking of conformity.

The last phase of medical device development involves post-market surveillance and vigilance. All incidents related to the product have to be documented and evaluated in a post-market surveillance report (class I) or periodic safety update report (class IIa, IIb, and III), serious incidents require immediate reporting to the appropriate authorities. Any safety concerns that arise have to be addressed by field safety corrective actions from the manufacturer, which in turn must be approved by the competent authorities.

### 2.3.2 Evaluation according to harmonized standards

When developing novel antimicrobial materials, the first two phases of medical device approval become relevant. Once structure and functional principle of the materials are defined, they need to undergo extensive characterization and testing to demonstrate conformity with the general safety and performance requirements. Whenever possible, these tests should be carried out in accordance with harmonized standards. If the conducted examinations attest conformity with the harmonized standards, conformity with the requirements of the MDR can be presumed as well.

Since this thesis focuses on the evaluation of antimicrobial coatings for blood-contacting devices, the following sections explain whether and how testing procedures for hemocompatibility and antimicrobial coating have been included in harmonized standards.

#### Hemocompatibility

The harmonized standard ISO 10993-4 (Biological evaluation of medical devices - Part 4: Selection of tests for interactions with blood) [156] specifies the requirements for hemocompatibility testing of blood-contacting devices. The required tests strongly depend on the character and length of blood interactions and can be divided into the categories hemolysis (material-induced, mechanically induced) and thrombosis (coagulation, platelet activation, complement, and hematology). The need for *in vivo* tests is also dependent on the type of the device and especially required for implantable devices. Taking the example of an intravascular catheter, it can be seen that material-induced hemolysis as well as coagulation, platelet activation and hematology need to be examined. However, the manufacturer can decide for himself whether the parameters of thrombosis should be investigated *in vivo* or whether selected *in vitro* tests are appropriate.

Even though the ISO standard specifies various test categories and parameters, it does not determine specific methods to evaluate them. This lack of standardization has

been widely criticized for decades [157, 158], but not yet been remedied. The current version of the ISO 10993-4 (2017) neither proposes a specific incubation system nor a reference material, incubation time or anticoagulant. However, this absence of standardization has led to the development of numerous static and dynamic *in vitro* models, each with its own advantages and disadvantages. Accordingly, it is now at the judgement of the manufacturer or accredited test facility to select a test method suitable for the device under investigation.

### **Antimicrobial Activity**

In contrast to hemocompatibility assessment, there is no harmonized standard to evaluate the antimicrobial activity of materials for medical devices. Available industrial standards mostly refer to the testing of non-medical products such as textile products (ISO 20743, ISO 20645), chemical disinfectants and antiseptics (EN 13697), or plastic surfaces (ISO 22196). However, those standards vary greatly and do not even employ a uniform definition of the term “antibacterial”. While ISO 20743 [159] defines antibacterial activity as the “activity of an antibacterial finish used to prevent or mitigate the growth of bacteria, to reduce the number of bacteria or to kill bacteria”, ISO 22196 [160] describes antibacterial effectiveness as “ability of an antibacterial agent to inhibit the growth of bacteria on the surface of materials treated with an antibacterial agent”. Thus, it is unclear whether only the growth inhibition or also the killing process of the bacteria should be considered.

Besides, industrial standards often do not distinguish between the modes of action of antimicrobial materials (anti-adhesive, contact-kill, or release-based). As a result, many of the available standard tests have been modified in recent decades, multiplying the number of tests available in the literature. These include agar zone of inhibition methods, suspension methods, methods comprising a high area to volume ratio, adhesion-based methods, and biofilm-based methods. Sjollem *et al.* [100] provide a comprehensive overview that presents individual methods and indicates for which mode of action they are suitable. However, none of those methods reflect the interactions of surface and bacteria with blood as they occur *in vivo*.

## 3 Coating evaluation

### 3.1 Objective

Although medical devices have revolutionized the treatment of a wide range of diseases, they always carry the risk of causing device-related bloodstream infections. To inhibit bacterial adhesion and subsequent biofilm formation on the material surfaces, numerous antimicrobial materials and coatings have been developed in recent decades. One of these novel antimicrobial coating strategies, the so-called anchor polymer (AP) coatings, has been recently established by our research group. These are amphiphilic styrene-maleic acid copolymers that attach to various polymer surfaces through hydrophobic interactions. While coupled PEG chains provide an anti-adhesive effect, further bioactive functionalization can enable an additional contact-killing effect. Conceptual design, synthesis and basic characterization of the AP coatings were realized in a parallel dissertation by André Ruland and published in [18].

The scope of this thesis was to evaluate the AP coatings in terms of their applicability as antimicrobial coatings in blood-contacting devices. For this purpose, five different anti-adhesive APs were selected and tested with regard to their adsorption and stability on two relevant polymer substrates, their biological safety and their antimicrobial efficacy. Evaluation was performed with established *in vitro* laboratory tests. The coating with the most promising results was then functionalized with the biocidal agent hexetidine. Further tests determined to which extent hexetidine functionalization influenced biological safety and antimicrobial activity compared to the anti-adhesive variant. Subsequently, it was discussed whether the AP coatings meet the demands of pre-clinical *in vitro* evaluation and should be considered for further *in vivo* testing to pursue subsequent certification for medical devices.

The objective of this part was the evaluation of AP coatings concerning their applicability as antimicrobial coating in blood-contacting devices. Established laboratory tests were performed to investigate adsorption characteristics, stability, biological safety, and antimicrobial efficacy of the coatings.

## 3.2 Background

### 3.2.1 Anchor polymer coatings

As mentioned above, the detailed concept and synthesis strategy of the AP technology has been previously described by Ruland *et al.* [18]. For a better understanding of the project, the basic principle is briefly summarized here.

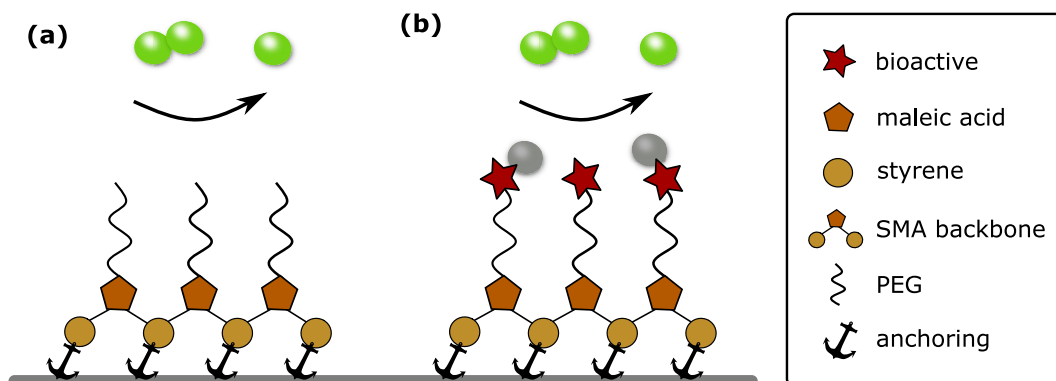


**Figure 3.1:** Scheme of compositional and functional features of anchor polymer (AP) coatings: **(a)** Physisorption of AP coatings is based on hydrophobic interactions between the styrene molecules of the styrene-maleic acid (SMA) backbone and the polymer substrate (illustrated by the anchor); anti-adhesive properties are realized by functionalization of maleic acid with poly(ethylene) glycol, **(b)** Further functionalization with bioactives (e.g. hexetidine) provides an additional bactericidal effect.

As shown in Figure 3.1, APs are based on styrene-maleic acid (SMA) copolymers (hydrophobic backbone) that are functionalized with PEG chains of different sizes (hydrophilic side chains). The well-balanced amphiphilicity ensures high water solubility of the polymers and a strong binding affinity towards various polymer surfaces. The main driving forces for physisorption are hydrophobic interactions between the styrene molecules of the SMA backbone and the hydrophobic polymer substrate. As a consequence, the backbone aligns to the substrate, while the PEG chains stretch into the hydrophilic environment and form brush-like structures. Thanks to the hydrophilic PEG brushes, APs exhibit strong anti-adhesive properties. To realize additional functionalities, further bioactives can be coupled to the PEG side chains. These include adhesion ligands such as RGDSP and SIRT, and - as relevant in this project - biocidal agents such as hexetidine. These biocidal agents provide an additional bactericidal effect, creating a contact-killing surface (Figure 3.1 b).

The properties of the AP coatings strongly depend on the chemical structure of the SMA backbone and PEG side chains. Accordingly, the combination of various SMA



copolymers and PEG chains results in a large library of possible APs. Each of them is labeled with the following nomenclature, revealing the average molecular weight of the SMA backbone in kDa ( $MW_{bb}$ ), the percentage of maleic acid groups within the SMA copolymer (MA %), the number of PEG monomer units per number of styrene monomer units (PEG/S), and the average molecular weight of the PEG chain in kDa ( $MW_{PEG}$ ).

$$MW_{bb} - MA\% - PEG/S - MW_{PEG}$$

To include the full range of possible molecular architecture in this study, five different APs were selected: 10-30-16-2, 120-30-13-2, 10-10-6-2, 10-30-8-2, and 10-30-165-20. As presented in Table 3.1, each of them represents either a low or high value of the defined molecular characteristics.

**Table 3.1:** Range of molecular characteristics of selected AP coatings.

| Molecular characteristic | low        | high         |
|--------------------------|------------|--------------|
| $MW_{bb}$                | 10-30-16-2 | 120-30-13-2  |
| MA %                     | 10-10-6-2  | 10-30-16-2   |
| PEG/S                    | 10-30-8-2  | 10-30-16-2   |
| $MW_{PEG}$               | 10-30-16-2 | 10-30-165-20 |

### 3.2.2 Polymer substrates

The applicability of AP coatings was tested on two medically relevant polymer substrates: thermoplastic polyurethane (TPU) and polycarbonate (PC). Both polymers are of great relevance in blood-contacting medical devices due to their high hemocompatibility and favorable mechanical properties.

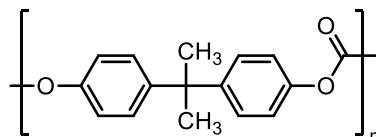


**Figure 3.2:** Chemical structure of polycarbonate (PC) including aromatic hydroxy compounds.

The selected PC (Makrofol® DE 1-1 000000) is an amorphous thermoplastic polymer that is produced by polycondensation of phosgene and hydroxy compound bisphenol A (Figure 3.2). It is characterized by a high mechanical strength and chemical resistance

[161]. Applications in the medical field include intravenous connectors, disposable needles, surgical instruments, and stents.

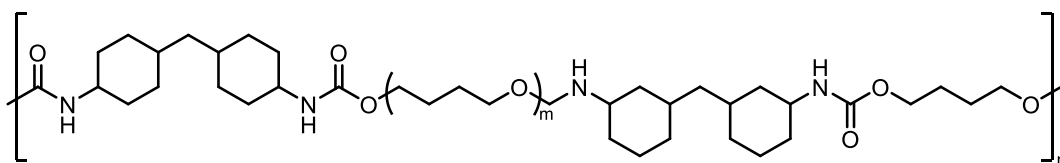


**Figure 3.3:** Chemical structure of aliphatic polyether-based thermoplastic polyurethane (TPU).

The selected medical-grade TPU (Tecoflex™ SG-80A) is an aliphatic polyether-based thermoplastic polyurethane (Figure 3.3). The linear segmented block copolymer consists of soft polar and rigid nonpolar segments, which accounts for the high flexibility of the polymer. In contrast to the polyester-based variant, polyether-based TPU is characterized by an excellent resistance against hydrolysis and microbial colonization [162, 163], making it ideal for medical applications. Due to its high flexibility, TPU is widely employed in various types of catheters. Further applications include scaffolds, wound dressings, and infusion systems.

### 3.3 Characterization of anti-adhesive coatings

#### 3.3.1 Quartz crystal microbalance

Quartz crystal microbalance (QCM) measurements were performed to analyze adsorption and retention of the selected anti-adhesive APs on both polymer substrates PC and TPU. For this purpose, AP solutions were pumped over the model substrates prepared on QCM crystals. The thickness of the adsorbed polymer layer was determined when reaching a frequency plateau after initial adsorption and after a subsequent rinsing step with PBS. Layer thicknesses presented in Figure 3.4 show the obtained values after rinsing, i.e. after removal of loosely bound polymer chains. Retention indicates the ratio of the two values, presenting the percentage of the layer thickness that was retained after the rinsing process.

The performed QCM measurements demonstrated that all investigated APs adsorbed to both PC and TPU and formed adsorbate layers with thicknesses ranging from 2.3 to 6.5 nm. Retention values were above 50 % in all measurements, indicating a good and stable anchorage of the coatings on both model surfaces.

However, when comparing the obtained values, it is noticeable that the adsorbed polymer layers on TPU displayed a higher layer thickness, but lower retention than on PC. This correlation might be explained by the dual structure of TPU with polar and nonpolar segments. In addition to the attraction between the styrene backbone of the AP and the hydrophobic segments of the polymer substrate by hydrophobic interactions, there may also be additional attachment of the hydrophilic PEG chains to the hydrophilic segments of the TPU. According to the characteristic “train-loop-tail” structure of physical adsorbed polymers [164, 165], more molecules might thereby be present in non-adsorbed segments, so-called “loops”. These loops are known to increase the overall thickness of the resulting polymer layer, which could explain the high layer thicknesses on TPU compared to PC.

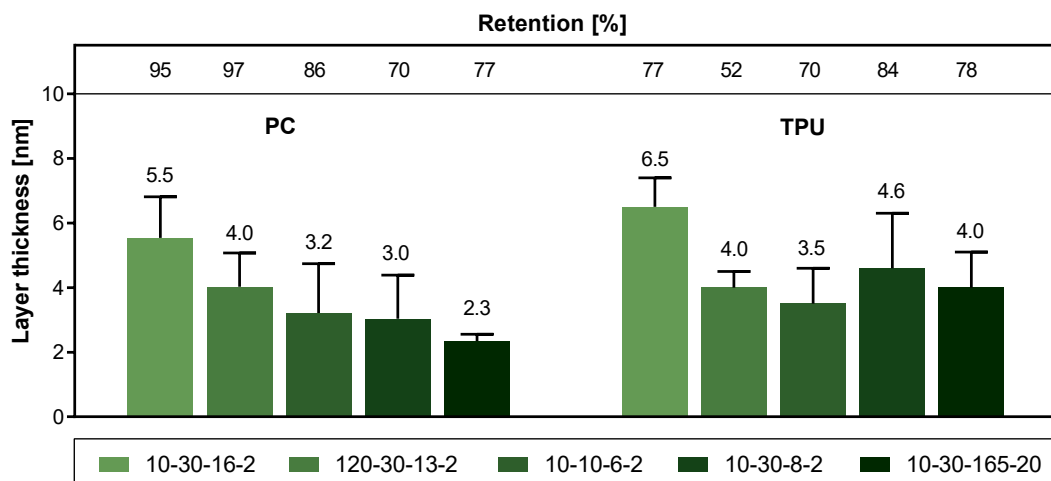


**Figure 3.4:** QCM-based measurements displaying adsorption and retention properties of selected anti-adhesive APs on polymer substrates PC and TPU,  $n = 6$ .

Low retention values of APs on TPU might also be explained by the dual structure of TPU. It is commonly known that physically adsorbed polymer molecules do not remain fixed in one place, but move on the surface [164]. When they reach the hydrophilic segments of TPU, the molecules therefore desorb more easily. In consequence, desorption of initially adsorbed molecules lead to low retention values. Moreover, it can be assumed that potentially adsorbed PEG side chains are easily displaced either by repulsion of neighboring hydrophobic segments or by replacement through competing styrene molecules of the AP backbone. Beyond that, high retention values on PC suggest that the stability of AP layers is further enhanced by  $\pi$ - $\pi$ -stacking between the aromatic units of PC and the styrene units of the AP backbone. Similar effects could also be observed on polymer substrates polystyrene (PS) and polyethersulfone (PES) [18].

When comparing the APs with each other, a large difference in layer thickness between 10-30-16-2 and 10-30-165-2 was particularly striking. The reduced layer thickness with increasing  $MW_{\text{PEG}}$  and therefore higher PEG/S ratio might be related to the overall higher hydrophilic fraction of the AP. As a result, the APs have a higher tendency to remain in solution instead of being adsorbed to the surface. This assumption is supported by an approach of Sartori *et al.* [166] describing adsorption characteristics of amphiphilic comb polymers with an adsorbing backbone and hydrophilic side chains to hydrophobic surfaces. According to their theory, swollen polymers do not reach stable adsorption if the number of non-adsorbing side chain units ( $N_{\text{PEG}}$ ) exceeds the number of adsorbing backbone units ( $N_{\text{S}}$ ) to the power of  $11/6$  ( $N_{\text{PEG}} \geq N_{\text{S}}^{11/6}$ ). Calculating this ratio, AP 10-30-165-20 is indeed above this adsorption threshold, while 10-30-16-2 remains within it.

QCM measurements confirmed that all investigated APs formed stable polymer layers on both model surfaces PC and TPU. Although adsorption on TPU tended to result in higher layer thicknesses, these were subject to greater desorption, resulting in comparatively low retention values. Overall, the AP 10-30-16-2 showed the highest layer thickness on both PC and TPU as well as high retention, indicating a particularly stable adsorbate layer.

### 3.3.2 Contact angle

To further characterize the resulting AP coatings on PC and TPU, contact angle measurements were performed to provide information on wettability. A contact angle is defined as the angle between a dispensed water droplet and the material surface. In general, it rises with increasing hydrophobicity of the material surface. Dynamic measurements, as carried out in this study, further differentiate between advancing and receding contact angle, displaying the highest and lowest possible values that occur during dispense and re-dispense of the droplet. Hysteresis was calculated as the difference between these two values.

Figure 3.5 displays the measured contact angles of all five investigated APs in comparison to the native polymer substrates PC and TPU, respectively. In particular, AP coatings applied on PC have led to a considerable change of wettability. Both advancing and receding contact angles decreased with the coating, indicating successful hydrophilization of the surfaces. Furthermore, contact angle hysteresis increased after application of AP coatings, which is typically a sign of high surface heterogeneity [167, 168]. However, previous investigations of APs on PS and PES [18] have shown that the application of APs increase surface roughness only marginally. For this

reason, it is assumed that the high hysteresis differences were caused by swelling processes. During the measurement of the advancing contact angle, the drop spread on the surface and the previously dried AP layer absorbed the water. This swelling process can increase wettability, thus leading to a reduced receding contact angle.

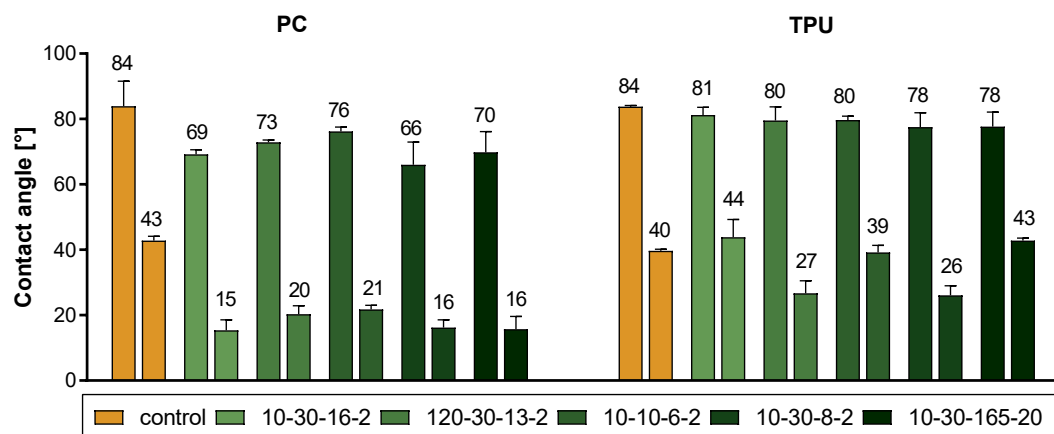


**Figure 3.5:** Dynamic contact angle of AP coated and uncoated (control) polymer substrates PC and TPU, two bars for each sample display advancing (left) and receding (right) contact angle,  $n = 4$ .

On TPU, wettability was much less affected by the application of AP coatings. In particular, APs 10-30-16-2, 10-10-6-2, and 10-30-165-20 only showed marginal differences. One reason for this observation might be the previously described attachment of the hydrophilic PEG chains to the hydrophilic segments of the TPU (see Chapter 3.3.1). The resulting polymer arrangement with more loop segments might have exposed more hydrophobic styrene molecules, thus leading to a lower degree of hydrophilization. Additionally, the stronger AP desorption on TPU compared to PC might also explain the low alteration of contact angles.

In contrast, differences between the individual APs were only minimal on both polymer substrates PC and TPU. The slight deviations that were observed should be considered with caution, as wettability could have been influenced by roughness and heterogeneity of the native polymer substrates.

The reduced contact angles after application of the APs demonstrated successful hydrophilization of the surfaces. Observed effects were considerably stronger on PC than on TPU. The molecular architecture of the APs had no considerable effect on wettability.

### 3.3.3 Protein adsorption

To further analyze the characteristics of the AP coatings, protein adsorption on AP layers was measured after 1, 4, and 24 hours. Therefore, AP coated substrates were incubated in a solution containing fluorescence-labeled proteins and then imaged with a confocal microscope to determine the fluorescence intensity of the adsorbed proteins. On one side, these measurements served as indirect evidence of the AP layers' existence. Beyond that, they provided information about the anti-adhesive properties of the polymers and how effectively they can prevent adsorption of proteins present in the blood, as these can be a mediator for subsequent adhesion of bacteria and platelets. Blood proteins bovine serum albumin (BSA) and fibrinogen (FGN) were selected for this analysis. The investigation was carried out with the APs 10-30-16-2 and 10-30-165-20, as the length of the PEG chains was assumed to be the greatest influencing factor. Figure 3.6 presents the relative fluorescence intensity of the surfaces normalized to the reference surface PC or TPU, respectively.

The study showed that AP coatings reduced initial protein adsorption for almost all samples. In particular, BSA adsorption was strongly reduced on both polymer substrates. After 1 hour of incubation, only  $22.1\% \pm 1.2\%$  (PC) and  $16.9\% \pm 1.1\%$  (TPU) had been deposited on AP 10-30-16-2 compared to the respective bare substrates. Protein adsorption on 10-30-165-20 was only marginally higher at this time. However, the amount of adsorbed proteins increased strongly with increasing incubation time. While BSA adsorption on AP coated PC substrate was still reduced by at least 30% after 24 hours, BSA adsorption on AP coated TPU surfaces was comparable to the control. The different results between TPU and PC could be related to a lower stability of the AP coatings on TPU, as already discussed in the chapters on QCM (see 3.3.1) and contact angle (see 3.3.2) measurements. As a consequence, the surfaces lose their anti-adhesive properties and the proteins can adsorb more easily to the surface.

Increased protein adsorption with advancing time can also be explained by the displacement of AP molecules by the added proteins. Analogous to the exchange of different proteins (Vroman effect), physically adsorbed polymers can also be displaced by competing molecules. For a more detailed investigation of these effects, the long-term stability of the AP coatings was tested under the influence of various physiological media.

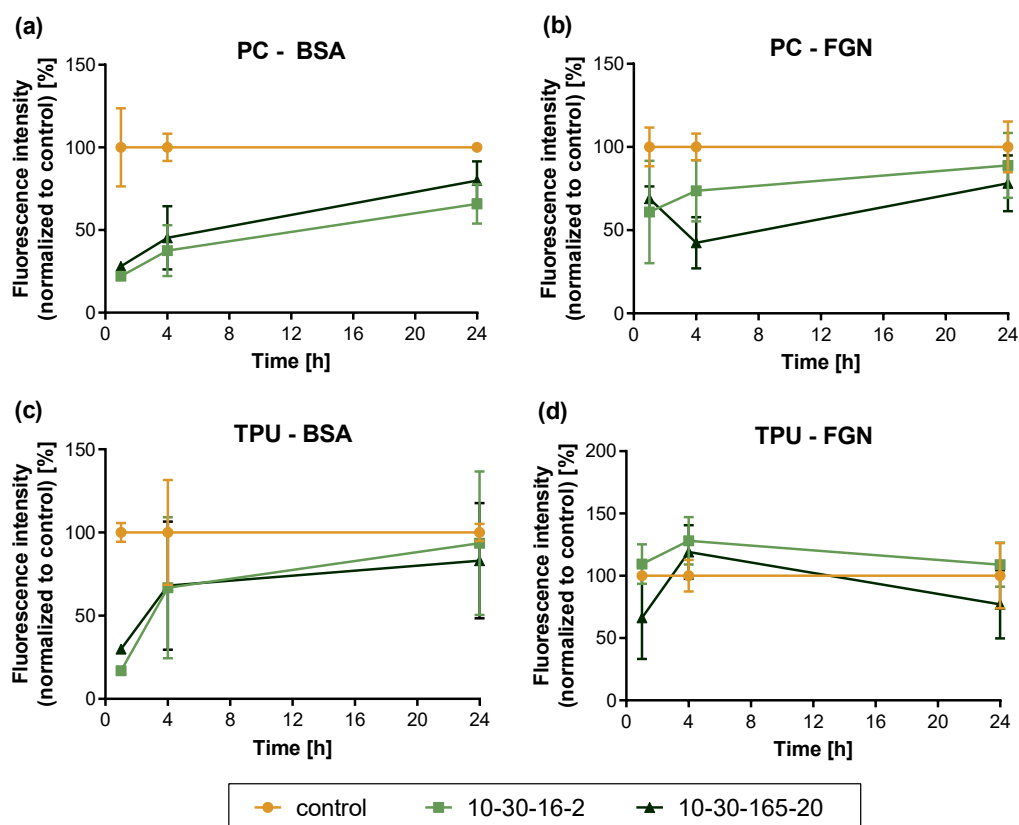


**Figure 3.6:** Adsorption of fluorescence-labeled bovine serum albumin (BSA) and fibrinogen (FGN) solution ( $c = 100 \mu\text{g mL}^{-1}$ ) on AP coatings applied on polymer substrates PC and TPU, determined by confocal fluorescence microscopy, normalized to the bare substrate,  $n = 4$ ; **(a)** BSA solution incubated on PC and AP-coated PC surfaces, **(b)** FGN solution incubated on PC and AP-coated PC surfaces, **(c)** BSA solution incubated on TPU and AP-coated TPU surfaces, **(d)** FGN solution incubated on TPU and AP-coated TPU surfaces.

The study of protein adsorption served as further indirect evidence of the existence of the AP coatings. In addition, it showed that the amount of adsorbed proteins could be reduced by the application of the AP polymer coatings. This effect was very strong at the beginning of the incubation, but decreased with advancing incubation time.

### 3.3.4 Long-term stability

To predict the long-term stability of AP coatings on blood-contacting devices, they were challenged by exposure to various physiologically relevant solutions for 14 days at 37 °C. PBS, buffered BSA ( $c = 40 \text{ mg mL}^{-1}$ ), and citrated blood plasma were applied for this purpose. Tween 20, which has previously been shown to reliably displace adsorbed AP layers [18], was used as a negative control. Measurements focused on the AP 10-30-16-2, as it showed the most promising results in prior experiments with high layer thickness and retention. Furthermore, previously performed measurements on PS and PES already confirmed the superior stability of this AP compared to APs with varying molecular architecture [18]. To allow detection of the adsorbate layer desorption over time, the AP was labeled with fluorescent dye Atto 647N before applying the coating. Reduction in normalized fluorescence intensity (compared to the initial value) was interpreted as removal of the adsorbed AP layer. Obtained results are presented in Figure 3.7.

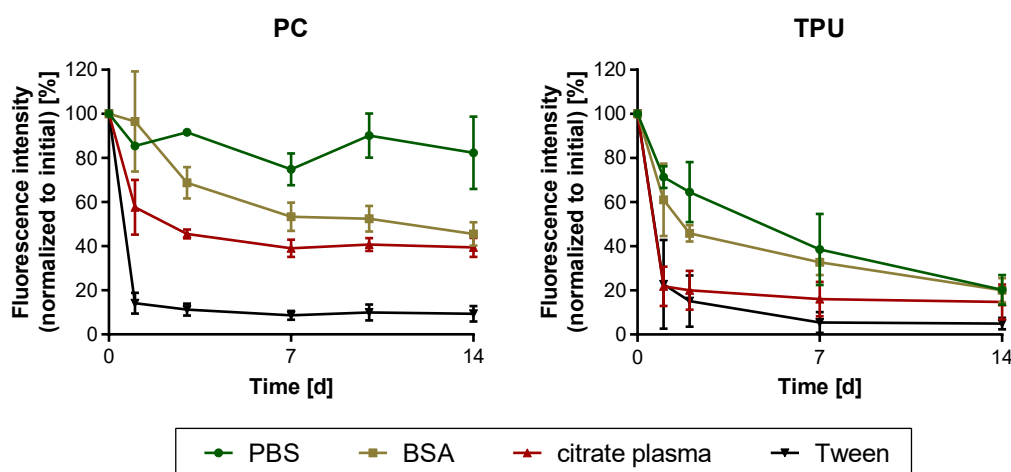


**Figure 3.7:** Long-term stability of AP 10-30-16-2 under physiological conditions; adsorbate layer was incubated in PBS, buffered BSA ( $40 \text{ mg mL}^{-1}$ ), citrate plasma, and Tween 20 for 14 days at 37 °C under constant agitation,  $n = 4$ ; (a) AP adsorbed on polymer substrate PC, (b) AP adsorbed on polymer substrate PC.

All analyzed samples showed a reduction in fluorescence intensity after the first days of incubation. A loss of fluorescence intensity due to bleaching has been excluded in preliminary experiments. Thus, it was concluded that loosely bound polymer chains, which resisted the initial washing step, must have been detached here. When comparing the two polymer substrates, it became obvious that long-term stability on PC is clearly superior. While  $82.4\% \pm 16.4\%$  of the initial AP layer was still present



on PC after 14 days of incubation in PBS, only  $26.6 \% \pm 12.6 \%$  remained on TPU. This observation is consistent to the previously discussed results of QCM, contact angle, and protein adsorption measurements. The higher stability on PC is mainly attributed to additional stabilizing interactions between the aromatic units of the styrene units and the aromatic units of the PC substrate via  $\pi$ - $\pi$ -stacking. In contrast, hydrophilic units in the TPU structure hinder the hydrophobic interactions, which are considered to be the main factor for the attraction between AP and polymer substrates.

Comparing the influence of the different physiological solutions with each other, it is noticeable that the coating was most stable in PBS. With the addition of BSA and citrated plasma, the AP layer desorbed considerably and was reduced to  $45.6 \% \pm 5.4 \%$  and  $39.4 \% \pm 4.3 \%$ , respectively (after 14 days, PC). On TPU, the coatings were also the most stable in PBS and desorbed more strongly under the influence of BSA and citrated plasma. This correlation can be attributed to the displacement of AP molecules by proteins present in BSA solution and citrated plasma. The previously mentioned Vroman effect, describing the displacement of small proteins by large ones, also applies to macromolecular adsorption [164]. While BSA molecules have a molecular weight of 66 kDa, the size of plasma proteins range from 66 kDa to 1.3 MDa. This makes them at least twice as large as the examined AP 10-30-16-2. Even though such a comparison is difficult due to the different structure of APs and proteins, it can be assumed that loosely bound AP molecules got displaced by the blood proteins, whereas the most effectively immobilized ones withstood displacement. After approximately 7 days, a plateau was reached, indicating excellent long-term stability of the remaining adsorbate layer.

The long-term stability measurements revealed superior stability of the AP layers on PC compared to TPU. Here, competing plasma proteins displaced the adsorbed layers only to a limited extent. However, after desorption of insufficiently anchored AP molecules, the remaining AP layer adhered stably to the surface, indicating an excellent long-term stability.

### 3.3.5 Hemocompatibility

To analyze whether the different APs would provoke a strong immune response when applied on blood-contacting devices, they were subjected to a hemocompatibility assessment. Therefore, well-established quasi-static blood incubation chambers were employed, in which the coatings were incubated in freshly drawn blood for 2 hours [169]. Subsequently, material surfaces and blood samples were analyzed for various inflammation and hemostasis parameters. Due to the higher stability of the coatings on PC compared to TPU, measurements were carried out exclusively on PC. The obtained results are presented in Figure 3.8 as well as in the Appendix in Figure A.1.

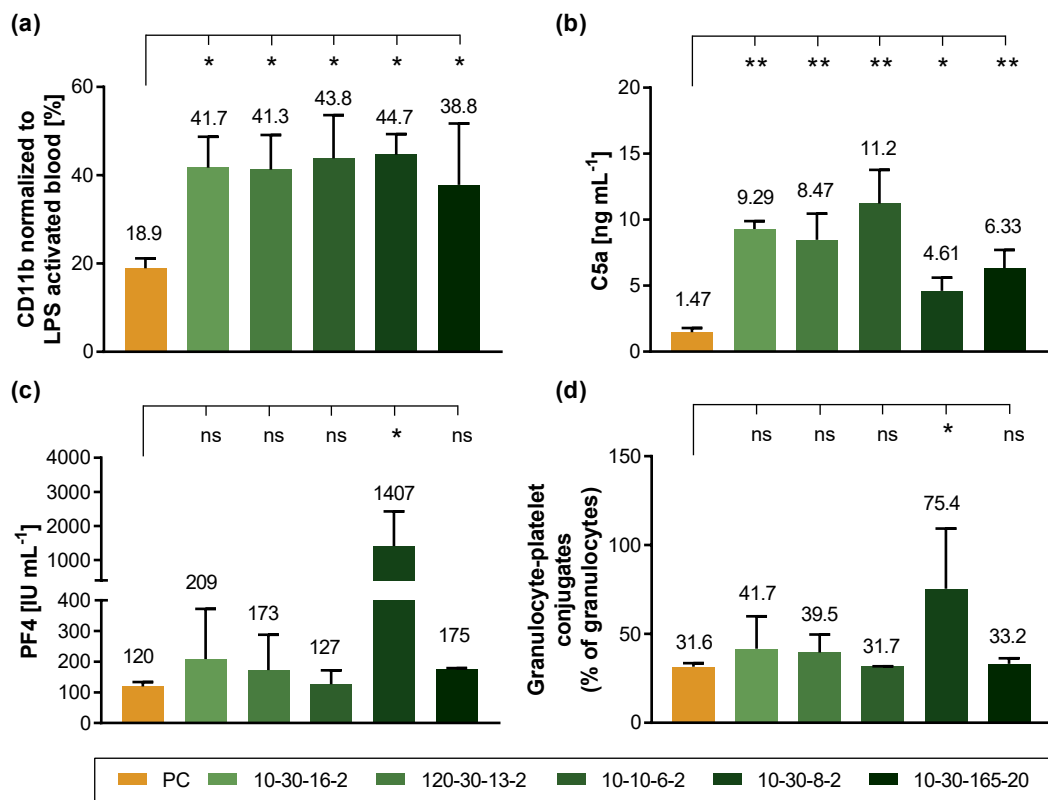


**Figure 3.8:** Static hemocompatibility assessment of anti-adhesive AP coatings in comparison to untreated polymer substrate PC; statistical significance was determined in comparison to the control surface PC using ANOVA and Holm-Sidak's multiple comparisons test (\*  $p < 0.05$ , \*\*  $p < 0.01$ , ns: not significant),  $n = 9$ ; (a) Expression of inflammation parameter CD11b on granulocytes, normalized to LPS activated blood, (b) Expression of complement factor C5a, (c) Release of platelet factor 4 (PF4) as parameter for platelet activation, (d) Granulocyte-platelet-conjugates normalized to total granulocytes.

While there were only few differences between most of the investigated coatings, the AP 10-30-8-2 clearly stood out. It did not only cause comparatively high hemolysis (see Figure A.1 b), but also an increased hemostasis response. The blood sample taken after the experiment formed visible blood clots and showed strongly elevated levels of platelet activation, measured as the release of platelet factor 4 (PF4) and formation of platelet-granulocyte conjugates, as well as an increased activation of the coagulation system, measured as the release of prothrombin fragment 1+2 (F1+2). The structure of the AP 10-30-8-2 is similar to that of AP 10-30-16-2 (same SMA backbone), however, the PEGylation degree is only 50 % instead of 100 %. Accordingly, remaining anhydrides can be hydrolyzed upon contact with water, forming carboxylic acids with negatively charged carboxyl groups. As it is well known that negatively charged surfaces induce a strong hemostasis response [122], this reaction is considered to be the cause for the increased coagulation and platelet activation. All other investigated APs showed a very low hemostasis response, which was comparable to the control surface PC.

However, the inflammation response was considerably influenced by the AP coatings. Complement activation, measured as the formation of the complement fragment C5a, showed significantly increased values for all investigated APs. However, this strong activation of the complement system only triggered moderate leukocytes activation, as CD11b activation (cellular inflammatory response) was below 50 % compared to the LPS control for all investigated APs. Also, granulocyte count was hardly affected by incubation with the APs. Similarly, SEM and fluorescence microscopy images showed little alterations in adhesion and morphology of blood cells on the tested surfaces. Differences between the individual AP surfaces were minimal.

Hemocompatibility assessment revealed that a 100 % PEGylation of the SMA backbone is mandatory to avoid triggering increased hemolysis and blood clotting. Apart from that, all investigated AP showed similar hemostasis activation compared to the control surface PC. Inflammation, in particular complement activation, was significantly increased compared to PC. However, as cellular inflammation response did not exceed 50 % of the LPS activated control, they were considered as acceptable.

### 3.3.6 Antimicrobial activity

A static bacterial adhesion test was conducted to investigate whether the molecular architecture of the AP coatings had an impact on their antimicrobial activity. Therefore, AP coated substrates were pre-seeded with *S. aureus* and incubated at 37°C under constant shaking. A low-nutrient M9\* medium was utilized to limit the proliferation rate of *S. aureus*, thus allowing a better discrimination between the examined materials. After an incubation period of 24 hours, each surface was imaged at five randomly selected locations. Bacterial surface coverage was determined as the mean surface colonization of the acquired image sections (100 % coverage corresponds to a completely covered surface).

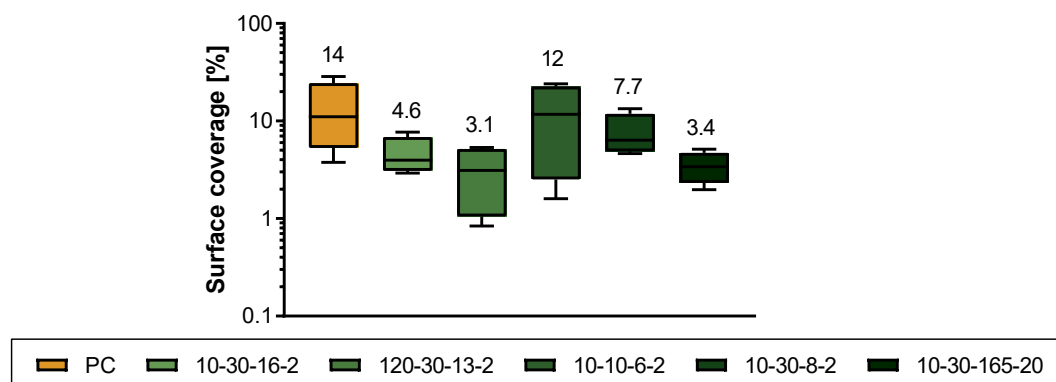


**Figure 3.9:** Antimicrobial activity of the investigated AP coatings compared to reference surface PC: Bacterial coverage on pre-seeded surfaces after 24 hours incubation in M9\* media at 37 °C; no statistically significant differences detected when comparing APs to PC control surface using ANOVA and Holm-Sidak's multiple comparisons test ( $p < 0.05$ ),  $n = 4$ .

The obtained data are presented in Figure 3.9. Even though differences were not significant according to the statistical analysis performed, clear disparities can be observed. The lack of significance might be explained by the strong clustering of bacteria. As *S. aureus* grow in microcolonies that are not evenly distributed on the surface, one section of the surface might be completely covered while another is free of bacteria. Therefore, in further experiments, sample size was increased and at least 10 images were acquired per sample. However, the values obtained in this study were considered sufficient to estimate the influence of the molecular architecture on their performance to prevent bacterial colonization.

While a considerable decrease in bacterial coverage was observed for all APs with a high number of PEG side chains (10-30-16-2, 120-30-13-2, and 10-30-165-20), the reduction was much lower for APs with a lower percentage of PEG (10-10-6-2 and

10-30-8-2). PEG is known to have anti-adhesive characteristics, which is why it is frequently suggested for antimicrobial coatings [105, 107]. The anti-adhesive properties are based on a combination of hydration and steric hindrance, making bacterial adhesion thermodynamically unfavorable [106]. Both APs 10-10-6-2 and 10-30-8-2 possess a significantly lower number of PEG chains than the other three investigated APs. With a maleic acid percentage (MA %) of 10, AP 10-10-6-2 has only one third of PEG binding sites available compared to the other APs. This structure also results in a reduced PEG/S-ratio. In contrast, AP 10-30-8-2 has the same number of maleic acid molecules as 10-30-16-2, but only 50% of them are PEGylated. Accordingly, it is assumed that a reduction in bacterial colonization correlates with the density of PEG chains.

APs 10-30-16-2 and 10-30-165-20 were compared to explore whether the molecular weight of the PEG chains also affected bacterial coverage. However, only minimal differences were detected between a molecular weight of 2 kDa (10-30-16-2) and 20 kDa (10-30-165-20). This observation is consistent with data from literature. Even though it is described that the anti-adhesive effect of PEG increases with increasing  $MW_{\text{PEG}}$ , the maximum activity is reached at a threshold value of approx. 2 kDa [170, 171]. This value corresponds to the lowest  $MW_{\text{PEG}}$  used in the study, thus explaining the minimal differences.

The examination of bacterial colonization on the different AP coatings demonstrated their anti-adhesive effect. Bacterial coverage was considerably affected by the molecular architecture of the AP coatings, revealing a high positive correlation of PEG density and antimicrobial activity. In contrast, molecular weight of PEG only had a minor effect on bacterial colonization.

### 3.4 Characterization of contact-killing coatings

To further enhance the antimicrobial efficacy of the AP coatings, they can be functionalized with a biocidal agent. This way, a contact-killing effect can be added to the anti-adhesive effect. Here, the decision was made in favor of the antiseptic agent hexetidine, which is known to be very effective against Gram-positive bacteria, which are the most common cause of device-related bloodstream infections [27, 28]. It is approved for the use in mucous membranes (e.g. in mouthwashes and vaginal antiseptics) [172, 173], but has not yet been deployed in any blood-contacting applications. However, preliminary tests confirmed a low blood activation by pure hexetidine at relevant concentrations, thus demonstrating its potential for blood-contacting materials. AP 10-30-16-2 was selected for functionalization as it showed the most promising performance in the previous experiments with a high layer thickness, low desorption tendency and strong anti-adhesive properties. To test whether the functionalization affected hemocompatibility and actually provided an additional antimicrobial effect, the two polymers and the reference surface PC were compared to each other regarding hemocompatibility and antimicrobial activity.

#### 3.4.1 Hemocompatibility

To investigate the influence of hexetidine functionalization (AP 10-30-16-2-Hex) on the blood compatibility of the APs, further hemocompatibility measurements were carried out. In addition to the unfunctionalized AP 10-30-16-2 and the uncoated PC surface, three well-characterized materials were included as additional control surfaces: (1) hydrophilic glass as activating control due to its high hemostasis response [87, 174], (2) Teflon AF as bio-inert and non-thrombogenic control [140], and (3) TPU as clinically approved reference material. As the additional control surfaces are only intended to serve as an orientation, they were not included in the statistical evaluation. Results of the hemocompatibility assessment are presented in Figure 3.10 as well as in the Appendix in Figure A.2.

No hemolysis occurred with any of the materials tested. Furthermore, blood gases and pH remained stable during the whole incubation process. As in the study of anti-adhesive APs (see Chapter 3.3.5), significantly increased C5a levels were also detected for AP 10-30-16-2-Hex. Again, this complement activation triggered the cellular immune response (CD11b activation of granulocytes) only moderately. Activation of granulocytes by both polymers was around 50 % of the activating LPS control or below. Therefore, it is elevated to the PC control, but in a similar range as the clinically approved TPU. In contrast, the loss of granulocytes due to surface adhesion

or various forms of cell death during incubation was comparable for both antimicrobial coatings and the control surfaces; as a trend, granulocyte count was the highest on 10-30-16-2-Hex coated surfaces.

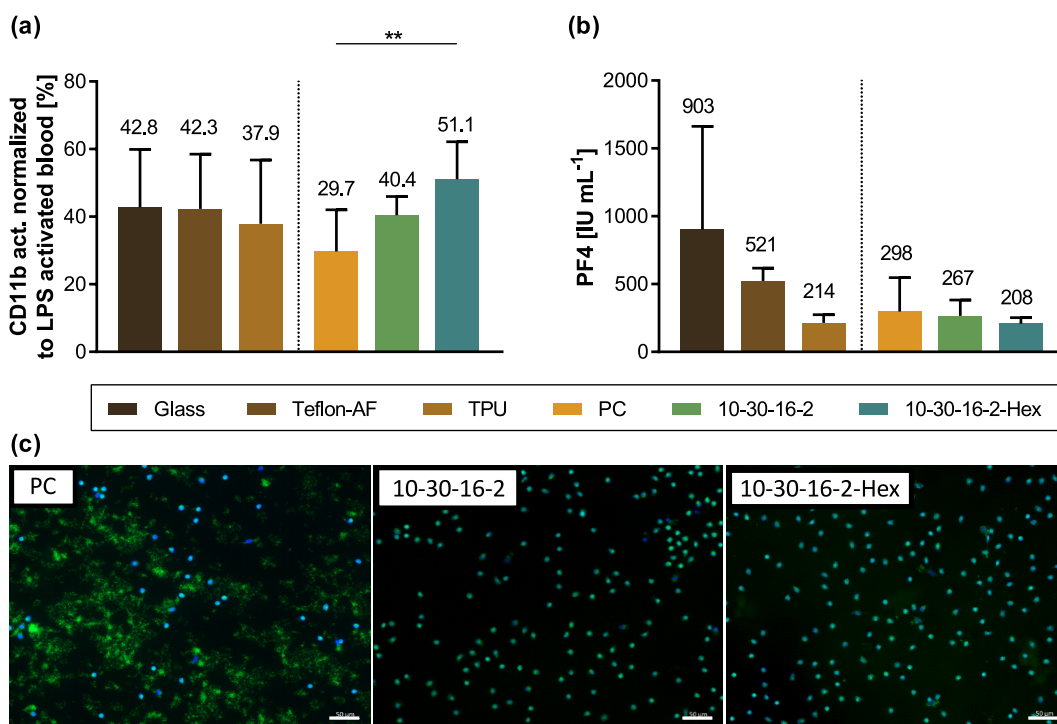


**Figure 3.10:** Static hemocompatibility assessment of AP 10-30-16-2 and 10-30-16-2-Hex in comparison to control surfaces: glass, Teflon AF, TPU, and PC; statistical significance between PC, 10-30-16-2, and 10-30-16-2-Hex was determined using ANOVA and Holm-Sidak's multiple comparisons test (\*  $p < 0.05$ , \*\*  $p < 0.01$ ),  $n=9$ ; **(a)** Expression of inflammation parameter CD11b on granulocytes, normalized to LPS activated blood, **(b)** PF4 release as parameter for platelet activation, **(c)** Fluorescence images of blood cell adhesion on test surfaces after blood contact stained with DAPI and DiCO<sub>6</sub>; scale bar: 50 μm.

Hexetidine functionalization also had only little effect on the hemostasis response of the APs. In fact, tendencies towards lower hemostasis were observed for both investigated APs compared to the control surface PC. Differences in platelet activation, measured as release of PF4, were not significant, but showed a tendency towards lower activation on PEGylated AP surfaces. Beyond that, platelet adhesion, detected via fluorescence microscopy, was considerably reduced on both investigated AP surfaces compared to the PC control (Figure 3.10 b). This observation points to an inhibitory effect of the anti-adhesive AP layers on platelet activation and adhesion. This correlation is consistent with findings from literature about PEGylated surfaces. Functionalization with PEG has been reported to reduce the adsorption of plasma

proteins such as fibrinogen, fibronectin, and von Willebrand factor [175, 176]. As these plasma proteins mediate platelet adhesion, this effect leads to a reduction in adsorbed platelets on AP surface and other PEGylated surfaces. The fact that this correlation was not observed during hemocompatibility assessment of the various anti-adhesive APs (see Chapter 3.3.5) might be explained by an insufficient sample size.

The evaluation of hemocompatibility revealed that functionalization with hexetidine did not significantly affect inflammation and hemostasis response of the AP coatings. Comparable to the unfunctionalized variants, an increased inflammatory response was also observed here. In contrast, both anti-adhesive and contact-killing AP coatings managed to inhibit a hemostasis response, as platelet adhesion and activation were slightly reduced compared to the PC control.

### 3.4.2 Antimicrobial activity

In order to quantify the additional antimicrobial effect of the biocide functionalization, another static bacterial adhesion assay was carried out examining bacterial colonization on the anti-adhesive AP 10-30-16-2, the hexetidine-functionalized AP 10-30-16-2-Hex, and the control surface PC. As in the study of anti-adhesive APs (see Chapter 3.3.6), the surfaces were pre-colonized with *S. aureus* and then incubated for 24 hours in M9\* media at 37°C. The surfaces were imaged initially (0h) and after 4 and 24 hours at ten randomly selected spots and analyzed for surface coverage. The results of the analysis are presented in Figure 3.11 a.

Significant differences between the three materials were already detected after pre-seeding of bacteria (0h). While 3.8% of the PC surface were initially colonized, only 1.7% of the anti-adhesive surface (coated with AP 10-30-16-2) was covered with bacteria. This corresponds to a two-fold reduction. On hexetidine-functionalized AP 10-30-16-2-Hex, bacterial colonization was reduced to 0.2%, corresponding to a 8-fold reduction compared to the anti-adhesive AP surface and a 20-fold reduction compared to the untreated PC surface. During the 24-hour incubation period, bacteria continued to proliferate on the PC surface, resulting in a bacterial coverage of 10.4% after 24 hours of incubation. In comparison, bacterial colonization on 10-30-16-2 and 10-30-16-2-Hex remained almost unchanged over the entire period. Therefore, differences between the antimicrobial surfaces and the control surface PC increased over time, resulting in an overall 5-fold bacterial reduction on anti-adhesive 10-30-16-2 and an approximately 100-fold reduction on contact-killing 10-30-16-2-Hex coatings.



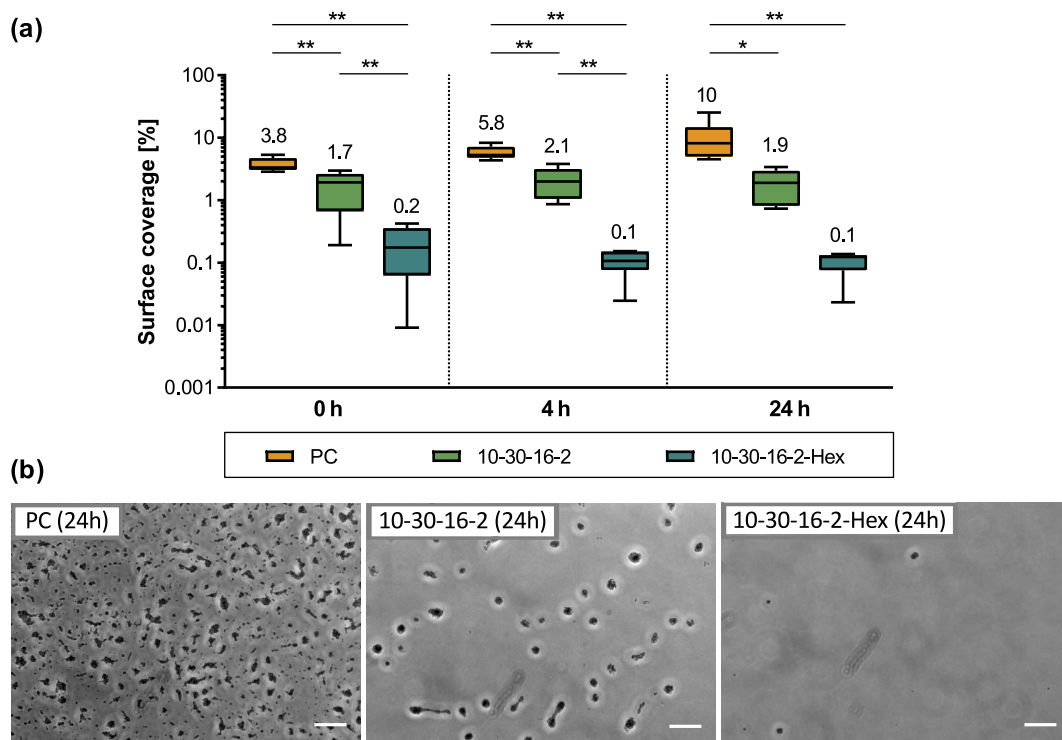


**Figure 3.11:** Analysis of antimicrobial activity on the examined surfaces PC, 10-30-16-2, and 10-30-16-2-Hex after static incubation in M9\* media at 37 °C; statistical significance was determined using ANOVA and Holm-Sidak's multiple comparisons test (\*  $p < 0.05$ , \*\*  $p < 0.01$ ),  $n = 6$ ; (a) Surface coverage measured after 0, 4, and 24 hours incubation time, (b) Exemplary phase-contrast microscopy images taken after 24 hours incubation time, scale bar: 20  $\mu\text{m}$ .

Figure 3.11 b shows representative phase-contrast images of control (PC) and both antimicrobial coatings after 24 hours of incubation time. It was observed that bacteria proliferated in microcolonies that reached a similar size after 24 hours incubation time for all surfaces. However, the number of present microcolonies varied depending on the coating. Most colonies were on the control surface PC, while the fewest formed on the hexetidine-functionalized AP 10-30-16-2. This ratio was already reflected in the initially adhered bacteria after 0 hours (Figure A.3).

Considering the AP 10-30-16-2, initial reduction in bacterial coverage can be related to the anti-adhesive properties of the PEG chains that prevent bacteria from adhering to the material surface. However, PEGylation does not impede bacterial proliferation after successful adhesion. Therefore, the minor changes in colonization over time are thought to be due to growing colonies detaching more easily once they reach a certain size. This effect has been frequently reported for *S. aureus* and other species in various biofilm studies [37, 177]. Comparing the anti-adhesive AP 10-30-16-2 and the

contact-killing AP 10-30-16-2-Hex, it becomes evident that biocide functionalization indeed further reduced bacterial coverage. It is suspected that hydrophobic alkyl-side chains and positively charged regions of the hexetidine interact with lipid-rich parts of the bacterial cell wall and negatively charged cell-wall components, respectively. These interactions can lead to cell wall disruption, thus providing an antibacterial effect of the agent [178, 179]. In regard to this study, it is assumed that the conjugated hexetidine acted on those bacteria that had overcome the anti-adhesive properties of the PEG chains, thus providing an additional antimicrobial effect.

The performed bacterial assay showed that both tested AP coatings led to a significant reduction in bacterial colonization. In addition to the anti-adhesive effects of the PEG layer active in both APs, a further antimicrobial effect was achieved by biocide functionalization with hexetidine.

### 3.5 Discussion

This part of the work was aimed to evaluate whether the recently developed AP technology is feasible for the application in blood-contacting devices. These PEGylated styrene-maleic acid copolymers are intended to be used as antimicrobial coatings on devices with short-term exposure, such as vascular catheters. In order to receive market approval of products that contain novel materials, they must meet general safety and performance requirements. Accordingly, AP coatings were subjected to various laboratory tests to verify compliance with these requirements. Subsequent evaluation of the results was divided into four distinct categories: First, it was checked whether the APs adsorb to medically relevant polymer substrates and if the formed polymer layers are stable under physiological conditions. Second, the efficacy of the coatings was investigated, i.e. whether they are able to inhibit bacterial colonization on the surfaces. Third, the safety of the anchor polymers was evaluated, focusing on the blood activation triggered by the materials. The forth and last point of discussion focused on the general applicability of the materials.

#### Adsorption & Stability

Five different APs were selected for the study of adsorption and stability properties, reflecting the wide range of different molecular architectures. The selected APs were applied to two different polymer substrates: PC and TPU. Both materials are

commonly used in blood-contacting products such as surgical instruments, connectors and catheters, which are considered common entry points for bacteria.

Performed QCM measurements have shown that all investigated APs adsorbed to both PC and TPU, forming adsorbate layers with thicknesses between 2.3 and 6.5 nm. The increase in wettability further indicated a successful hydrophilization of the surfaces. However, the stability of the adsorbate layers is clearly superior on PC compared to TPU, which can be attributed to the chemical structure of the polymers. Strong desorption of the AP molecules on TPU might be explained by hydrophilic segments in the polymer substrate that impede attracting hydrophobic interactions. On the other side, aromatic units within the structure of PC enhance the attractive forces through  $\pi$ - $\pi$ -stacking, which acts in addition to the hydrophobic interactions. The strong desorption of the AP coatings on TPU makes a potential application as antimicrobial coating difficult. One possibility would be the application on devices with only transient contact time. The analysis of protein adsorption on the surfaces showed that AP coatings on TPU can certainly minimize initial adsorption of proteins. As these proteins mediate subsequent bacterial adhesion, this could give an advantage over uncoated surfaces. Furthermore, an application as “sacrificial layers” could be considered. Controlled desorption of the layers could either release specific active substances or impede bacterial colonization of the surface. Furthermore, by adjusting the chemistry of either TPU or AP structure, desorption could possibly be minimized, thus increasing long-term stability. However, all these approaches require further research.

To evaluate whether AP coatings withstand the challenging conditions in blood contact, their long-term stability was tested under *in vivo* like conditions. For this purpose, they were exposed to different physiological solutions, specifically a buffered saline solution (PBS), a Tris-buffered BSA solution, and citrated plasma. The selected BSA concentration of 40 mg mL<sup>-1</sup> is based on the albumin concentration in whole blood [180], while citrated plasma contains all relevant plasma proteins in the corresponding concentration. During the 14-day incubation period, it was found that competing proteins displace parts of the adsorbed AP molecules. However, approx. 40 – 50 % remained attached to the polymer substrate PC. As desorption only took place during the first days of protein exposure, it is assumed that the remaining adsorbate layer stays stable in the long term. To ensure that the coatings retain their stability even at body temperature, all long-term stability measurements were performed at 37 °C. As QCM measurements were carried out under flow conditions, they also confirmed that the anchoring of the coatings can withstand applied shear forces. Further investigations are recommended to examine whether this stability is compromised above a certain shear stress limit.

### Antimicrobial efficacy

To investigate the efficacy of the AP coatings, antimicrobial activity was assessed using a static adhesion test. For this purpose, five selected anti-adhesive APs of varying molecular structure were investigated first. A subsequent test further evaluated the effect of additional drug functionalization with hexetidine.

The study showed that all investigated AP coatings were able to reduce the bacterial colonization of the surfaces. This effect can be attributed to the PEG side chains, which are known for their anti-adhesive properties and are therefore often suggested for anti-adhesive coatings for blood-contacting devices. Comparing the five different APs, it became apparent that the density of the PEG chains had the strongest impact on bacterial colonization of the material. One of the most promising APs, 10-30-16-2, was able to reduce bacterial colonization by factor 5 (after 24 hours). Additional biocide functionalization of the PEG chains, creating a contact-killing surface, led to a further reduction of bacterial colonization by factor 20 compared to the anti-adhesive variant. Accordingly, it reduced bacterial coverage by a factor of 100 compared to the native PC control.

Despite this strong reduction, bacterial colonization could not be completely prevented on any of the surfaces examined. However, it is well known that neither anti-adhesive nor contact-killing surfaces can entirely prevent bacterial colonization. For this reason, the long-term risk of biofilm formation cannot be eliminated completely by any material [100]. However, the reduced bacterial load gives more time for antibiotic treatment before a mature, more resistant biofilm can develop [66, 178].

In general, it is very difficult to find comparative values in literature, since incubation and test methods vary greatly between the respective studies. This lack of standardization for the evaluation of antimicrobial activity has already been elucidated in Chapter 2.3.2. However, both the 5-fold reduction (AP 10-30-16-2) and the 100-fold reduction (AP 10-30-16-2-Hex) in bacterial coverage can be considered very promising. For a more accurate prediction of the antimicrobial efficacy in clinical use, further tests are required. However, these should be performed under more physiological conditions and take into account the flow conditions as they occur *in vivo*.

### Biological safety

To ensure the biological safety of medical devices, they must be evaluated in accordance with the harmonized standard ISO 10993 (Biological evaluation of medical devices). One of its most important parts for the evaluation of blood-contacting materials is ISO 10993-Part 4 (Selection of tests for interactions with blood).

For an investigation of hemocompatibility according to this standard, an established quasi-static incubation setup [169] was applied. Here, the material samples were incubated with whole blood for 2 hours in an incubation chamber. Subsequently, both surfaces and blood samples were analyzed for various parameters of hemolysis, inflammation and hemostasis. Thereby, most of the investigated APs showed satisfying results. Regarding the molecular architecture of the coatings, it was found that 100 % PEGylation of the SMA backbone is mandatory to avoid increased hemolysis and blood clotting. However, all APs with 100 % PEGylation as well as the hexetidine-functionalized AP showed neither hemolysis nor increased hemostasis. In fact, both platelet adhesion and activation could be minimized by the AP coatings. This anti-thrombogenic effect is attributed to the anti-adhesive properties of the PEG chains. However, evaluation of inflammation parameters showed slightly elevated values for all investigated APs. In particular, complement activation, measured as formation of C5a, showed significantly increased values. As this activation of complement only had a limited effect on leukocyte activation, the impact on inflammation was considered acceptable.

Another part of the evaluation of biological safety concerns the identification and quantification of degradation products from polymeric medical devices, as well as the determination of permissible limits for substances that can be leached out (ISO 10993 - Part 13 & 17). In this regard, it is necessary to consider the displacement of AP molecules by blood proteins. Even though the results of the long-term stability tests showed that about 50 % of the AP coating was removed within the first days after protein exposure, the remaining AP layer appeared to be stable. This observation suggests that adsorbed AP layers should be exposed to competing proteins prior to blood contact. Thus, loosely bound AP molecules can be removed prior to use and would not be released into the bloodstream. Such an approach is also recommended for further testing.

Another aspect in the assessment of biological safety is the evaluation of cytotoxicity (ISO 10993 - Part 5: Tests for *in vitro* cytotoxicity). In a parallel dissertation project by Melissa Sikosana [181], a standard-compliant assay was performed showing that fibroblast cells (cell line L929) cultured on AP 10-30-16-2 and AP 10-30-16-2-Hex for 24 hours retained viability of approximately 99 % and 92 %, respectively. In addition, the study by Ruland *et al.* [18] confirmed the viability of human umbilical vein endothelial cells (HUVECs) and human induced pluripotent stem cells (cell line CRTD3) cultured on AP coatings with different molecular architecture and biofunctionalization.

## Applicability

In order to have a chance on market launch, newly developed materials and products must not only be safe and effective, but also economically feasible and easy-to-handle. These include, among others, an uncomplicated manufacturing process, cost-effective procurement and production, as well as the possibility of sterilization. This section focuses on selected aspects related to the applicability of AP coatings.

One major advantage of AP technology is certainly its water solubility. This enables quick and easy application of the coatings from an aqueous solution. Moreover, this application procedure avoids the use of hazardous solvents that would require time-consuming and costly subsequent washing steps. The physical reversible adsorption of AP on the polymer substrates also opens up various application areas. Ruland *et al.* [18] demonstrated that AP adsorbate layers can be detached and replaced as often as desired, introducing the idea of renewable coatings. Even though this methodology is not an option for a large proportion of medical devices, as these are sterile single-use products, it could be relevant for reusable equipment in hospitals (e.g. endoscopes). As single-use surgical instruments and other disposable products are often criticized for their lack of sustainability [182], this re-coating strategy could be a future-oriented concept.

Another advantage of the AP technology is its versatility. It was demonstrated that the adaption of the APs' molecular architecture allows the simple adjustment of its properties. This provides a large range of different AP coatings, each with its individual characteristics. Functionalization with bioactives to realize additional functionalities further enhances this library. This diversity can also be an advantage for market approval of the AP coatings. Even though each variation of materials and active ingredients has to be approved individually, data from existing products can be referred to in future processes. In consequence, the approval of one AP coating would facilitate the market launch of other variations.

Considering the economical feasibility, the AP technology provides another advantageous characteristic. Ruland *et al.* [18] have demonstrated that the concentration of AP solutions can be significantly downscaled. It was shown that an AP solution with a concentration of  $300 \mu\text{g L}^{-1}$  formed adsorbate layers with only slightly reduced layer thickness compared to a concentration of  $1 \text{ g L}^{-1}$  (as applied in this study). This possibility of a 3,000-fold dilution promises an enormous financial benefit in a potential commercial application.

Another aspect to be considered when converting the concept into a medical product is its suitability for sterilization. Pre-tests have shown that the AP coatings are not suitable for autoclaving as the hot steam destroys the chemical structure of

the coatings. However, other sterilization procedures such as Gamma and Ethylene oxid sterilization are considered harmless. In particular, Ethylene oxid sterilization has already demonstrated its suitability on polymers with a comparable chemical structure [183]. Further studies are recommended to verify these assumptions.

## Conclusion

The investigation of adsorption behavior, stability, antimicrobial efficacy and biological safety confirmed the high potential of AP coatings for a future application in blood-contacting devices. However, further testing is required for a more profound consideration. This includes a more realistic assessment of antimicrobial performance that also considers the influence of an immune response as well as the flow conditions encountered. Typically, this kind of information are obtained by the performance of animal studies during pre-clinical evaluation. However, the need of expensive, time-consuming and controversial animal studies might be reduced if more realistic *in vitro* models were available. The development of such an *in vitro* model was the objective of the second part of this thesis.

## 4 Model development

### 4.1 Objective

The strict regulatory requirements for the approval of new antimicrobial materials strongly demands the development of realistic *in vitro* models. These models are meant to evaluate materials under physiological conditions to reduce, if not completely replace, the need for subsequent animal testing. However, established laboratory tests and *in vitro* models often do not adequately represent *in vivo* conditions. This leads to a high discrepancy between pre-clinical *in vitro* tests and both pre-clinical and clinical *in vivo* studies. Criticisms of available *in vitro* models exist particularly with respect to the choice of microorganisms, culture medium, and flow conditions, as well as to the lack of an immune response [9].

The objective of this work was to address these aspects and develop an *in vitro* model that simulates *in vivo* conditions more realistically. In order to be used for the evaluation of antimicrobial materials, two performance requirements were set. First, the model should be able to differentiate various antimicrobial surfaces; and second, it should represent the well-documented dependence between flow conditions and bacterial colonization. Moreover, to better predict the clinical performance of the materials, the model was expected to provide information about the antimicrobial efficacy of the materials that cannot be obtained by established laboratory methods.

To validate these objectives, one anti-adhesive and one contact-killing AP coating were evaluated with the developed *in vitro* model, and data were compared with those obtained in the first part of this thesis (see Chapter 3).

The objective of the planned *in vitro* model was the evaluation of anti-adhesive and contact-killing materials under realistic conditions. To fulfill this task, the model should be able to differentiate various antimicrobial surfaces, represent the well-documented dependence between flow conditions and bacterial colonization, and provide information about the efficacy of the materials that cannot be obtained by established laboratory methods according to the state of the art.



## 4.2 Requirements

### General requirements

To adequately reflect the influence of the immune system on the performance of antimicrobial materials, the *in vitro* model must be operated with human blood. Here, simultaneous incubation of blood, bacteria and material surface is required to incorporate the mutual influence of the three parameters. Whole blood influences bacterial proliferation and protein adsorption on the test surface, whereas bacteria affect blood activation and colonization of the material. On the other hand, the test surfaces have a high impact on bacterial adhesion and proliferation as well as on blood activation.

### Incubation conditions

Incubation of the test materials must take place under physiological conditions. Therefore, it was aimed to incubate the test surfaces with freshly drawn human blood at a temperature of 37 °C (body temperature). Additionally, the test surfaces should be exposed to realistic shear conditions as they occur in vascular devices. This requirement consequently necessitated the implementation of a dynamic flow model.

### Pumping conditions

To realize a dynamic flow model, blood must be pumped over the test sample. Here, various requirements are demanded of a suitable pumping mechanism. Most importantly, the process must not provoke any hemolysis or excessive blood activation - thus ensuring the hemocompatibility of the system. In addition, a steady movement of the whole blood must be maintained to prevent the sedimentation of blood cells. Furthermore, the pumping system must be designed in a way that avoids the accumulation of activation products (e.g. dead bacterial cells) that may influence the analysis of blood activation parameters.

### Analysis

In order to analyze the mutual influence of blood, bacteria, and test surface, the model must allow the analysis of blood activation (affected by bacterial colonization and test surface) as well as bacterial colonization on the test surface (affected by whole blood incubation and test surface).

## 4.3 Design rationale

At the beginning of model development, numerous design decisions had to be made. The following section describes selected challenges and explains how they were addressed during the development process.

### 4.3.1 Selection of an incubation system

In order to decide on a suitable incubation system for the evaluation of antimicrobial coatings, several available dynamic incubation and pumping systems were analyzed. Static incubation systems were excluded from the outset, as the realization of relevant shear conditions was one of the main requirements. All considered incubation systems were checked whether they can fulfill the defined requirements for pumping conditions: 1) hemocompatibility, 2) no sedimentation of blood cells, and 3) no accumulation of activation products.

#### Chandler loop

The Chandler loop was first described by A. B. Chandler [184] in 1958 as a technique to produce a thrombus and was later modified for dynamic hemocompatibility assessment of biomaterials. Thanks to its simple design and handling, it is considered an attractive test platform and has been employed in numerous studies evaluating the blood compatibility of stents [185, 186], heparin surface coatings [187], and other materials and devices [188, 189]. The setup of the modified Chandler loop is relatively simple: Polymer tubes are connected to form closed loops and partly filled with whole blood. The test material can be either the tube itself or a sample placed inside the tube. Rotation of the closed loops in a temperature-controlled environment is then supposed to simulate arterial flow conditions. One disadvantage of the Chandler loop system is the air-blood interface, which can lead to the formation of air locks on the sample surface interfering with both platelet aggregation and complement activation [190, 191]. Another drawback of the system is provoked by the special sample geometry, which can complicate their microscopic analysis. In addition, the lack of blood exchange throughout the incubation period can lead to an accumulation of activation products, which should be avoided in particular when working with bacteria (see Chapter 4.3.3).

Based on these considerations, the Chandler loop was excluded as a potential incubation system after initial trials.

### **Syringe pump**

The implementation of a blood flow through a syringe pump is not as common as the Chandler loop system, but also occasionally applied [192]. Here, blood can be transported either unidirectionally or back and forth between two syringes. The main advantages of syringe pumps are the simple setup as well as the gentle pumping process, which does not provoke hemolysis or elevated blood activation. Furthermore - in contrast to the Chandler loop - there is no air-blood interface that could impair the analysis. However, the sedimentation of blood cells in the syringe represents a greater challenge. One way to reduce sedimentation would be the forth- and back-pumping of the same blood volume in contrast to a unidirectional blood flow. However, this procedure would lead to an accumulation of activation products analogous to the Chandler loop system. Also, a reduction of the incubation time does not appear to be a reasonable option to prevent sedimentation, since bacteria need a certain time to adapt to a new environment and start to proliferate (see Chapter 4.3.5). Another approach to prevent cell sedimentation would be the overhead rotation of the blood-filled syringes. However, this would be impracticable to implement due to the high weight of a the syringe pumps.

On the basis of these considerations, the syringe pump was also discarded as a possible incubation system for the evaluation of antimicrobial coatings.

### **Anti-sedimentation pump by Biophysical Tools**

After both Chandler loop and syringe pump were excluded, potential commercial solutions were investigated. A market research of available options drew the attention to the company Biophysical Tools, who specialize on ultra-precise and -fast flow control of fluids. At that time (January 2020), they were working on a further development of their established pump system (P<sup>2</sup>CS, Biophysical Tools, Leipzig, Germany) to include an anti-sedimentation function. The functionality of the pumping system is based on pressure control: by creating over- or underpressure in the reservoir, the liquid is drawn from the reservoir into the connecting tubes or vice versa. Sedimentation of the cells is meant to be prevented by small magnetic stirrers in the reservoir, which constantly mix the blood. After consultation, the company allowed to test the system concerning its applicability to pump blood. To assess the basic blood compatibility of the system, a simple hemolysis test was performed. Here, it was differentiated between the influence of the pumping process (without previous stirring) and of the stirring process (with a small and a large magnetic stirrer, without pumping). The results of the hemolysis test are presented in Figure 4.1.

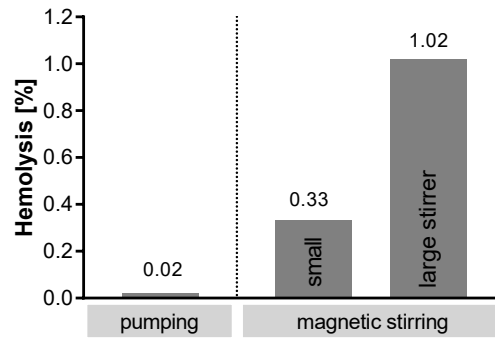


**Figure 4.1:** Hemolysis caused by the anti-sedimentation prototype of the commercial pumping system from Biophysical Tools,  $n=1$ .

After a short incubation time of 10 minutes, no hemolysis was caused by the pumping process. However, the magnetic stirring severely damaged the blood cells. It was assumed that the blood cells are squeezed between the stirrer and the wall of the blood reservoir. This effect naturally occurs more strongly with the larger stirrer than with the small one, thus explaining the stronger hemolysis. However, the hemolysis caused by the small stirrer would already be critical for the planned *in vitro* flow model. Beyond that, sedimentation could only be sufficiently prevented with the large stirrer, but not with the smaller one.

Due to these results, the pump system from Biophysical Tools also had to be excluded for the application in the planned *in vitro* model.

### Modular pumping system by Fraunhofer IWS

Another contemplable incubation system was the “modular plug and play construction kit” of the Fraunhofer IWS that offers the possibility to manufacture customized microfluidic pump systems [193]. It was already successfully applied in various biomedical research projects, such as studies on aortic valve tissue [194], maturation of stem cell-derived cardiomyocytes [195], and pressure-dependent filtration at an artificial glomerular kidney barrier [196]. The customized systems contain different functional and miniaturized modules like micro pumps, oxygenators, reservoirs and cell culture compartments.

For the planned *in vitro* model, the research group of Fraunhofer IWS suggested a setup based on a triple-pump-chip and a customized test chip. The triple-pump-chip (see Figure 4.2) is a pneumatic pumping module composed of thin membranes separating the fluidic and pneumatic parts. It consists of three parallel, fluidically independent channels, each having an inlet valve, a pump chamber and an outlet

valve. Frequent membrane deflection by compressed air loads and unloads the pump chambers with fluid, thus initializing a directed pulsatile volume flow. The frequency of this process is regulated by the pneumatic control unit “MPScntrl”, whereas the “MPShemodyn” module adjusts the hemodynamic pumping behavior (velocity curves, WSS). The customized test chip would then contain the test surface.

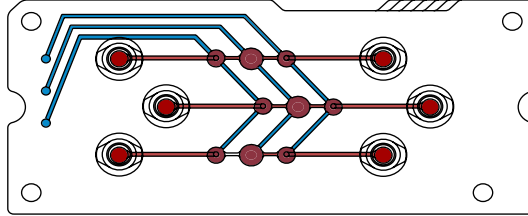


**Figure 4.2:** Schematic topview of the triple-pump-chip by Fraunhofer IWS with fluidic parts in red and pneumatic parts in blue; adapted from [193].

The pumping system had not been tested with whole blood before. However, the selection of biocompatible materials and the gentle pumping procedure gave reason to be optimistic that a blood-friendly pumping process would be possible. Another uncertain factor was the sedimentation of blood cells. This could not be prevented by the pumping system directly, however, the modular setup would allow the implementation of an external system to enable over-head rotation of the blood reservoir (see Chapter 4.3.4). Furthermore, the adaptability of the modular system allows both the pumping in circuits as well as the implementation of a single-pass flow from a reservoir to avoid the accumulation of activation products (see Chapter 4.3.3).

Even though the “modular plug and play construction kit” of the Fraunhofer IWS did not initially meet all stated requirements, it was the most promising concept for the development of an *in vitro* blood flow model. For this reason, it was decided to develop a new setup that is based on this modular pumping system.

### 4.3.2 Incubation of the test surface

Another challenge has been the exposure of antimicrobial test surfaces to the pumped blood. In consultation with the research group of Fraunhofer IWS, it was decided to pump blood through a customized chip after it has passed the triple-pump-chip. This new so-called microchannel chip had to meet a number of different requirements. First and foremost, it had to offer three independent channels - analogous to the triple-pump-chip. The shape of these channels should allow a homogeneous fluid flow and avoid the occurrence of turbulences. Further requirements were the possibility of microscopic examination of bacterial colonization on the test surface, as well as hemocompatibility of the entire chip.

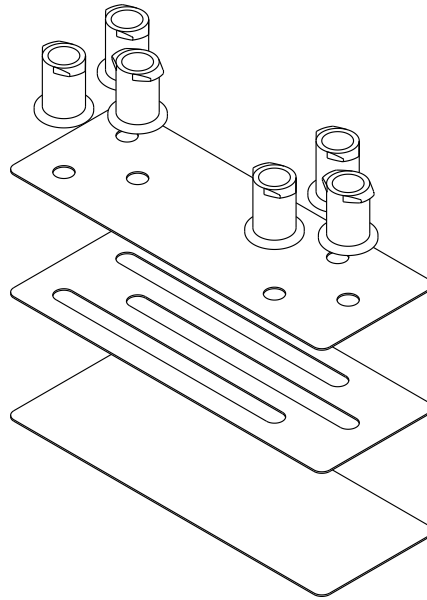


**Figure 4.3:** Exploded view of microchannel chip design, composed of three layers: (1) Top layer with Luer Lock connections, (2) Intermediate layer determining the channel design, and (3) Bottom layer with customizable test material.

A first draft of a microchannel chip is presented in Figure 4.3. It is made of three single layers: (1) the top layer with Luer Lock connections for in- and outlet, (2) the intermediate layer determining the channel design, and (3) the bottom layer with customizable test material. Three parallel rectangular channels were chosen as channel geometry. The simple shape and a relatively large length-to-width ratio shall enable a uniform flow and prevent the formation of turbulences [197]. The Luer Lock connections provide an air-tight in- and outlet for the pumped blood. Furthermore, they facilitate easy application of AP solution and bacterial suspension to the test surface via standardized syringes. All applied test materials are transparent and

flat-shaped in order to facilitate microscopic analysis for the quantification of bacterial colonization. Additionally, the chip design avoids sharp edges and constrictions that could affect blood compatibility. All applied materials passed hemocompatibility assessment before they were incorporated in the microchannel chip (see Figure A.5).

However, the exact geometry and material composition of the chip could not be finalized at this stage, as it still required further fine-tuning. The optimization steps to achieve optimal hemocompatibility and flow conditions are presented in Chapter 4.4.2.

The construction of microchannel chips must allow a defined exposure of the test surface to the pumped blood. The chosen design promises a uniform blood flow without excessive blood activation and with defined flow conditions, as well as the possibility to quantify bacterial colonization on the test surfaces.

### 4.3.3 Accumulation of activation products

When bacteria overcome the body's physical barriers and invade the organism, they elicit an immune response within minutes or hours. In particular, macrophages and neutrophil granulocytes recognize the pathogens and coordinate the immune reaction by releasing inflammatory mediators and cytokines. The recognition of bacteria is based on its differing chemical structure of cell wall and proteins, such as lipopolysaccharides (Gram-negative bacteria), and peptidoglycan or lipoteichoic acids (Gram-positive bacteria). Once the bacterial invasion is successfully controlled by the host's immune system (or with the help of antibiotics), all bacterial cells and their debris are removed by phagocytosis. Inflammatory mediators and cytokines will be downregulated and the inflammation subsides.

Unfortunately, emulation of this process is not possible within an *in vitro* system. Destroyed bacterial cells and apoptotic phagocytes remain in the system and continue to trigger the immune response. As a result, it is difficult to detect whether present bacteria are alive or have been killed. In both cases, inflammatory markers would be elevated. In consequence, an *in vitro* model designed for the evaluation of antimicrobial properties of coatings will have difficulties to fulfill its purpose.

To avoid this accumulation of activation products, it was decided to implement a single-pass flow system. In this way, blood is pumped unidirectionally from a reservoir and collected for analysis immediately after passing the colonized test surface. Consequently, no cell debris will accumulate in the blood and thus falsify the analysis of the blood parameters. Another advantage of this incubation method is

the kinetic analysis of inflammation and hemostasis processes by periodic collection of blood samples.

A single-pass flow system was implemented to avoid the accumulation of cell debris and other activation products. Here, blood was collected directly after it has passed the test surface - thus contamination of the blood reservoir can be prevented.

#### 4.3.4 Sedimentation of blood cells

The Fraunhofer IWS “modular plug and play construction kit” allowed blood to be pumped from any reservoir. Here, the decision was made in favor of a blood bag in order to avoid the formation of a blood-air interface. The most practical and gentle way to prevent sedimentation of cells in a blood bag is overhead-rotation. Unfortunately, a market research for the acquisition of a suitable rotation device remained unsuccessful. For this reason, it was decided to design and build such a rotation device within the scope of this project.

The concept was to connect a holder for the blood bag to an electric motor and rotate it 180° back and forth in regular intervals. That way, the overhead rotation could be ensured without connection tubes getting entangled. The desired rotation was realized with the help of a micro-controller. Figure 4.4 presents the circuit diagram designed for this purpose.

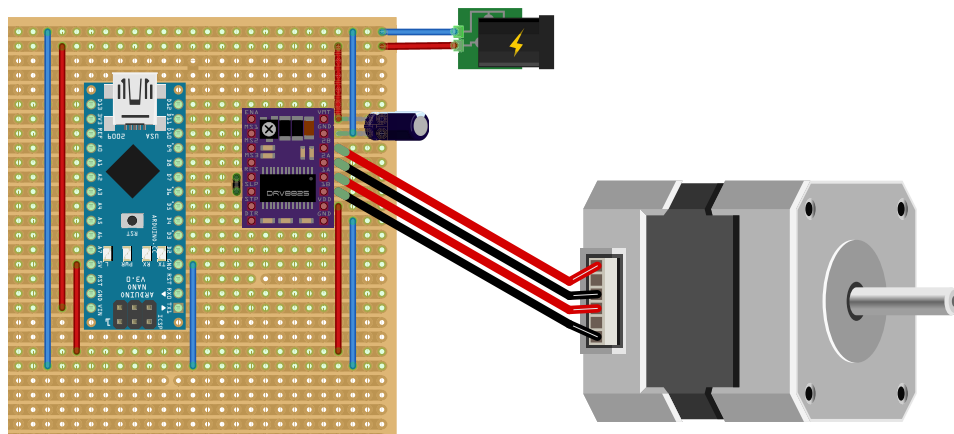


**Figure 4.4:** Circuit diagram for a rotation device with micro-controller, motor driver carrier, and stepper motor (from left to right).

The three main components are the micro-controller, the motor driver carrier, and the stepper motor. The micro-controller and the stepper motor were connected to a



wall plug transformer providing a voltage of 12 V, the motor driver was powered by the micro-controller via a 5 V connection.

The software describing the planned motor movement was uploaded to the micro-controller (see Listing A.1). It included the definition of pins connected to the motor driver carrier, as well as a description of the motion sequence. A regular step of the stepper motor executed a turn of  $1.8^\circ$ , thus 100 steps were necessary for a half turn. Since such an implementation turned out to be very noisy, the individual  $1.8^\circ$  steps were divided into another 32 microsteps. This allowed a smoother movement with a lower noise level. Thus, the software described a loop that demands 3200 microsteps in one direction, one second waiting time, and 3200 microsteps in the opposite direction. After waiting another second, the process started again. The software running on the micro-controller performed the aforementioned algorithm and transmitted the corresponding rectangular function to the motor driver. There, each pulse of the function triggered a step of the motor.

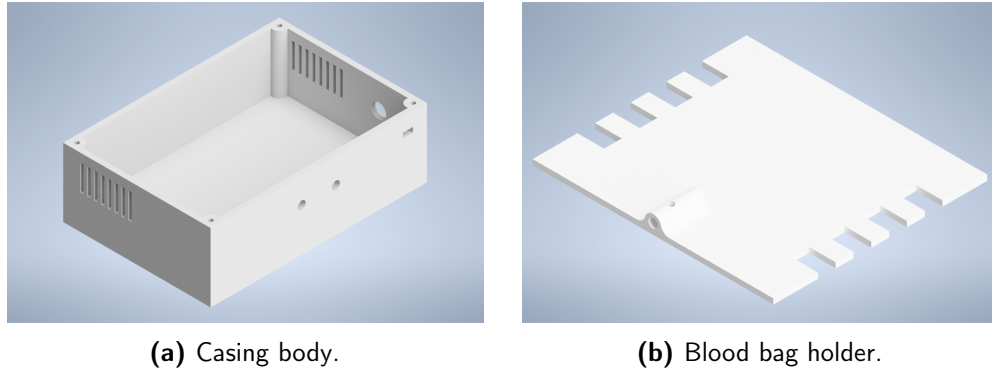


**Figure 4.5:** Models for 3D printing of casing and holder for rotation device.

After all connections were soldered and the motor successfully performed the desired movement, a holder for the blood bag and a case for dust and splash water protection were required. A corresponding design was created using computer-aided design (CAD) software. The casing consists of two parts: the main body (Figure 4.5 a) and a cover. Its shape was designed to fit exactly the assembled circuit board. Slots in the body were intended for fixation and as outlet for power and motor connections, the built-in ventilation slots should provide sufficient air exchange when the board heats up. The corresponding technical drawings of both parts can be found in Figures A.9 and A.10. The blood bag holder (Figure 4.5 b) was meant to be screwed directly to the shaft of the stepper motor in order to transmit its movement. Protrusions on each side help to fix the blood bag with a rubber band. The corresponding technical drawing can be found in Figure A.11.

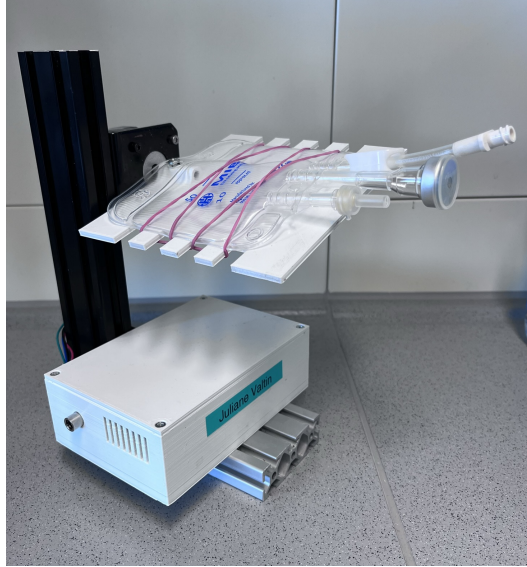


**Figure 4.6:** Photograph of final rotation device.

The designed models were manufactured by 3D printing. Subsequently, the rotation device was finalized by attaching the motor and the casing containing the circuit board to aluminium struts. Figure 4.6 presents a photograph of the completed rotation device. A detailed list of components and software applied for construction of the rotation device can be found in Chapter 6.4.1.

The constructed rotation device succeeded in preventing cell sedimentation when storing whole blood in blood bags. Further measurements confirmed that the gentle overhead rotation did not affect blood activation.

#### 4.3.5 Incubation time

The determination of an appropriate incubation time was quite challenging. The handling with whole blood and bacteria had some conflicting needs that both had to be reconciled. On the one hand, bacteria need a certain period of adaptation before they start proliferating when they are introduced to a new environment. This lag phase usually lasts about 2 hours for *S. aureus* laboratory strains [198]. For this reason, the aim was to enable the longest possible incubation period. On the other hand, the function of blood cells and proteins are strongly influenced by storage time. Blood activation starts directly after blood collection and therefore affects biomarkers that need to be quantified for hemocompatibility assessment. Consequently, it is recommended to limit the incubation time to a maximum of 4 hours in order to avoid inaccurate results [199, 200]. To minimize the time between blood collection and

incubation, it was decided to apply freshly drawn human blood rather than blood from a donation center. As a result, the available blood volume became another limiting factor. The implementation of a single-pass flow system naturally requires a significantly larger volume of blood than steady-pool systems with circulating blood. This need increases proportionally to the incubation time. According to the obligations of the ethics committee, we are only allowed to collect a blood volume of 40 mL of each donors (80 mL total). Therefore the incubation time was limited to approximately 4 hours.

The three factors 1) blood activation, 2) bacterial lag phase, and 3) limited blood volume equally contributed towards the decision to set the incubation time to 4 hours.

#### 4.3.6 Detection of bacteria after blood contact

One of the major challenges during model development has been the detection of bacteria after whole blood incubation. Here, the focus was on the quantification of surface colonization to enable the evaluation and comparison of different antimicrobial coatings. In order to select a suitable method, various techniques have been considered.

##### Clinical practice

In everyday clinical practice or clinical studies, bacterial colonization is mostly examined indirectly. This can be done either by analysis of a blood sample or by detachment of bacteria from the material surface and subsequent CFU counting [201–203]. Here, bacterial detachment can be realized by rolling the colonized material on an agar plate (implemented by Maki *et al.* [204]), by sonication (implemented by Sheretz *et al.* [205]), or by flushing the lumen of the material (implemented by Cleri *et al.* [206]). However, none of these methods is particularly practical for the application on the microchannel chip. Furthermore, a direct quantification method was preferred for the *in vitro* blood flow model. Therefore, other options were taken into consideration.

##### “Classical” microscopy

In laboratory practice, only a few methods are applicable for the detection of bacteria after blood contact. Phase-contrast microscopy (as applied for bacterial detection

after incubation with growth media) cannot be used, as bacterial cells are barely visible between large blood cells. Even after washing the sample, numerous blood cells still adhere to the material. On the other hand, classical staining with fluorescent dyes is also difficult. Most common dyes target either nucleic acid or cell membranes and are not specific for a particular cell type. As a result, both bacteria and blood cells are stained after incubation with whole blood. Even in Gram staining, which is commonly applied in clinical practice to identify bacteria, white blood cells and macrophages receive a Gram-negative stain, analogously to Gram-negative bacteria [207]. Although bacteria and blood cells can be clearly distinguished by their size, this is only useful for studying the shape of bacteria, but not for quantification. This is especially true when microcolonies form and individual bacteria can no longer be distinguished from one another.

### **Fluorescence *in situ* hybridization**

Another technique that was taken into consideration is Fluorescence *in situ* hybridization (FISH) - a macromolecular recognition technique that is widely used for the identification, visualization, and quantification of specific DNA sequences on chromosomes and plasmids. The technology was first described by Langer-Safer *et al.* [208] and is based on the complementary nature of DNA or DNA/RNA double strands. Selected oligonucleotides with incorporated fluorophores are used as probes to hybridize onto the complementary sequences in tested cells, thus making them visible by fluorescence microscopy. In microbiological research, this technique is regularly used to detect bacteria [209–211]. Thanks to the highly specific staining, differentiation to blood cells is also guaranteed. However, one drawback is the rather complex procedure, which requires numerous washing steps to remove unbound dye. These washing steps can lead to incalculable WSS within the microchannel chip, thus provoking the detachment of bacteria. Since one of the main requirements of the *in vitro* flow model was the implementation of realistic WSS, this disadvantage could not be disregarded.

### **Fluorescence-expressing bacteria**

Additionally, the use of fluorescence-expressing bacteria was considered. This has become a popular technique in microbiological research to facilitate studies of bacterial growth, biofilm formation, and bacterial behavior in complex environments [212]. Various mechanisms were introduced to deliver fluorescent protein genes into bacterial cells, for example the incorporation of plasmids [213, 214] and the chromosomal insertion of fluorescent markers into the bacterial genome [215, 216]. A major

advantage of this strategy is the fact that the fluorescence signal is passed on over generations. Consequently, surfaces can be imaged directly after incubation without additional time-consuming staining procedures. In addition, bacterial growth can be easily observed over a longer period of time.

To evaluate the suitability of fluorescence-expressing bacteria for the newly developed flow model, the visualization of bacteria after blood contact was investigated. Gram-positive *S. aureus* (RN4220) and Gram-negative *Escherichia coli* (*E. coli*) (MG 1655), both expressing green fluorescent protein (GFP), were selected for this purpose. Here, both bacterial strains were pre-seeded on PC surfaces, subsequently incubated in whole blood and imaged at regular intervals. Even though the signal of the GFP *E. coli* could initially be observed through whole blood, it was no longer detectable after 30 minutes. It was assumed that *E. coli* were eradicated by the immune response of the whole blood. This assumption is supported by another experiment demonstrating that the utilized *E. coli* cells are also no longer cultivable on agar plates after 30 minutes of blood contact. In contrast, the GFP signal of *S. aureus* was detectable for at least 4 hours after blood incubation. The clear signal allowed quantification of surface coverage by the image-processing software Fiji [217] (Figure 4.7).

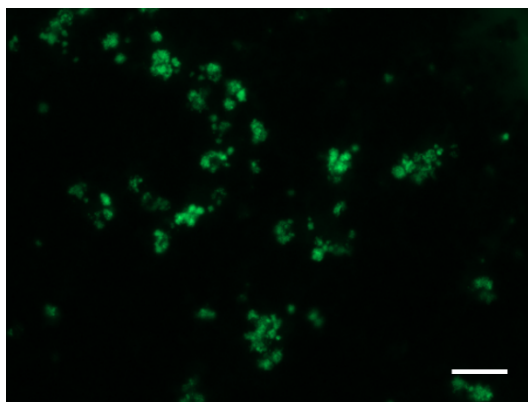


**Figure 4.7:** Exemplary image of GFP-expressing *S. aureus* on PC after 4 hours blood incubation, surface coverage = 7.8%, scale bar: 50  $\mu\text{m}$ .

Due to the excellent detectability after blood contact and the practical handling, it was decided to use fluorescence-expressing *S. aureus* in the *in vitro* blood model. This choice allowed the testing of antimicrobial materials with one of the most relevant pathogens in device-related bloodstream infections.

## 4.4 Model setup

After addressing initial challenges and considerations, it was finally possible to define the final model setup and begin with fine-tuning of the *in vitro* flow model. The following sections will first show the basic setup of the model, then explain how incubation and pumping parameters as well as the design of the microchannel chips were optimized, and finally present the occurring flow conditions that can be adjusted with this model setup.

### 4.4.1 Overview

The general setup of the *in vitro* blood flow model (Figure 4.8) was divided into two separate units: the pumping unit and the blood stream unit.

The pumping unit consisted of the control unit “MPSControl” (1), the damper “MPShemodyn” (2), and the triple-pump-chip (4). As described in Chapter 4.3.1, the triple-pump-chip directed the blood through loading and unloading of the pump chambers by frequent membrane deflection. This mechanism was initiated by the application of compressed air or vacuum, respectively. The frequency of this membrane deflection and thus the pumping speed were regulated by the pneumatic control unit “MPSControl”. Between the control unit and the triple-pump-chip, there was a damper (“MPShemodyn”). This device contained air chambers of various sizes that dampened the pressure of the compressed air and the vacuum. By applying a large damping volume, the pumping process got smoother as the pump chambers opened and closed with less pressure. This effect also led to a decrease in shear stresses within the microchannel chip that was inserted downstream. Details on occurring WSS in dependence on the pumping cycle are presented in Chapter 4.4.3.

On the other side, there was the blood stream unit, which consisted of the rotated blood reservoir (3), the triple-pump-chip (4), the microchannel-chip (5), and the collection tubes (6). The main component of this unit was the microchannel chip as it contained the test surface. Before integrating the microchannel chip in the pumping circuit, the test surfaces had been pre-treated with AP coating and bacterial suspension. For this purpose, the fluids were successively filled into syringes and applied to the channels via Luer lock connections of the microchannel chip. Preparation and incubation of AP solution and bacterial suspension were carried out analogously to the methods of static measurement. After pre-treatment of the microchannel chip, all components of the blood stream unit were interconnected with Luer Lock connection tubes. Right after the blood reservoir, the blood flow was divided by three-way stopcocks into independent streams, one for each microchannel

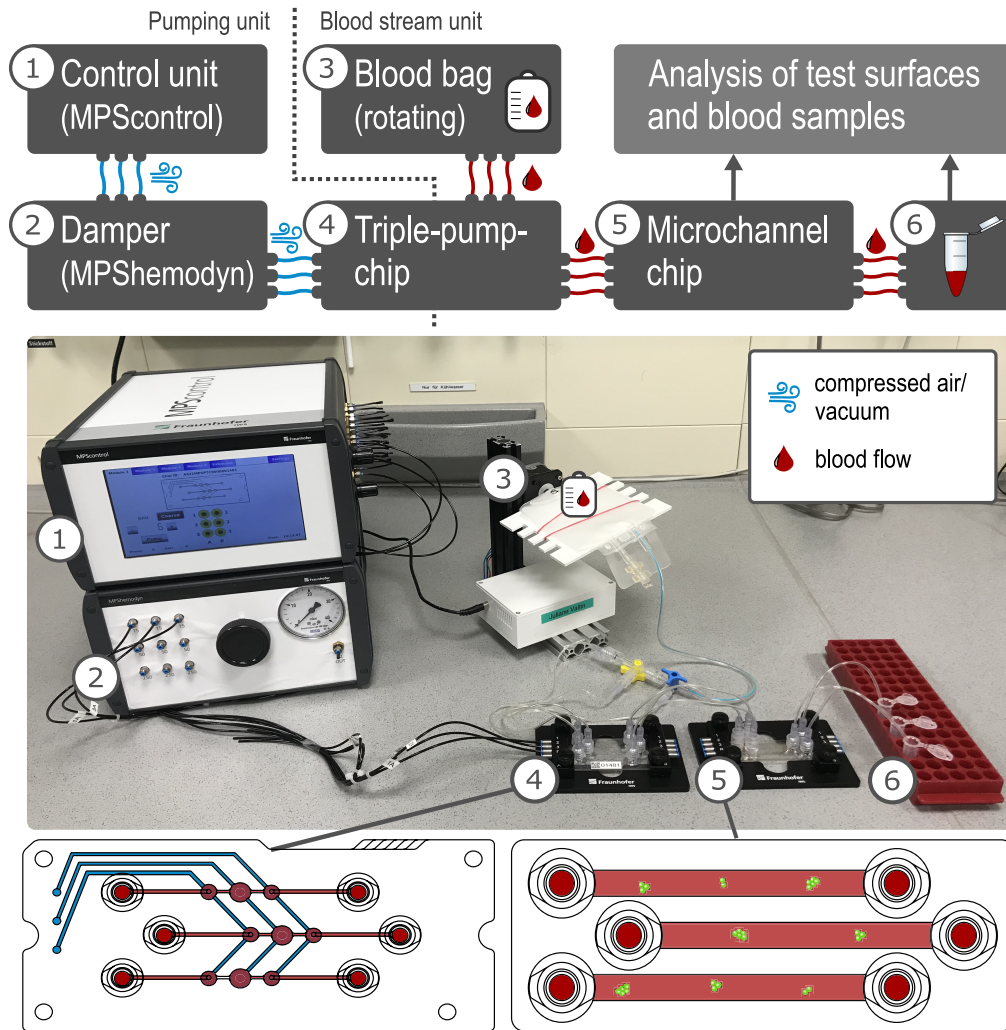


**Figure 4.8:** General setup of the *in vitro* flow model: 1) Control unit “MPScontrol”, 2) Damper “MPShemodyn”, 3) Blood reservoir and rotation device; 4) Triple-pump-chip; 5) Microchannel chip; 6) Eppendorf tubes for blood collection; adapted from [218].

to be examined. To maintain physiological temperature and stability of blood gases and pH, the entire bloodstream unit was placed into an incubator set to 37 °C and 5 % CO<sub>2</sub>. When starting the pumping process, the triple-pump chip drew the blood from the reservoir and passed it on to the microchannel chip. Here, interactions between pre-colonized bacteria, pumped whole blood and test material took place. To evaluate the mutual influences, blood was collected in 5 mL Eppendorf tubes after it had passed the microchannel chip and was subsequently analyzed. In addition, bacterial colonization on the test surface was quantified by fluorescence microscopy. A detailed description of all utilized components and the workflow of the experiment are provided in Chapter 6.4.2 and 6.4.4.

### 4.4.2 Optimization

The previous chapter described the basic setup of the *in vitro* blood flow model. However, initial test runs indicated that fine-tuning of some parameters was required to optimize the hemocompatibility of the flow model. These adjustments related in particular to pumping speed, structure of the microchannel chip, and anticoagulation of the blood. The following chapter elucidates the individual factors and their adjustments. Some of these optimizations were carried out in parallel and are therefore not necessarily shown in chronological order.

#### Anticoagulation

Initially, blood was anticoagulated with  $1.5 \text{ IU mL}^{-1}$  heparin, analogously to static hemocompatibility assessment. However, in first trials, blood flow often stagnated after 1-2 hours. It was suspected that blood clots had formed in the channel constrictions, and therefore impeded the blood flow. This assumption was confirmed after washing the microchannel chips right after blood incubation. Particularly in the area of in- and outlets, the coagulated blood residues could not be removed despite intensive rinsing; in some cases, complete blood clots were found (see Figure 4.9).



**Figure 4.9:** Effects of blood incubation with heparin-anticoagulated blood in microchannel chip.

For that reason, the application of another anticoagulant was considered. Here, the decision was made in favor of hirudin (Refludan, Celgene, Munich, Germany), a highly specific direct thrombin inhibitor. Its anticoagulant effect is based on the binding and inactivation of active thrombin, which prevents the conversion of fibrinogen into fibrin and thus the formation of fibrin networks [219, 220]. In contrast, heparin inhibits blood clotting by enhancing the anticoagulant antithrombin III. When binding to each other, antithrombin III undergoes a conformational change that enormously accelerates its binding capability to thrombin, FXa, FXIa, and FXIIa, thus inhibiting their coagulant effect [219, 221]. However, by inhibiting various steps of the coagulation cascade, heparin also affects the complement cascade, blood cells,



and several mediators - thus making it difficult to analyze complement activation and cellular processes. On the contrary, hirudin only acts at the very end of the coagulation cascade, which makes it very suitable for *in vitro* inflammation studies [222]. Moreover, it is considered very powerful due to its direct mode of action [223]. Consequently, it might be more suitable than heparin in preventing the blood clot formation within the microchannel chip.

To investigate the suitability of hirudin for the *in vitro* model, a test run was performed with 5  $\mu\text{M}$  hirudin - a concentration comparable or even lower to those applied in other hemocompatibility studies [220, 222]. The test trial confirmed the applicability of hirudin as anticoagulant. Blood could be pumped for 4 hours without interruptions, and no residues of clotted blood remained within the microchannel chip.

Due to the more effective anticoagulation effect, all further experiments were carried out with 5  $\mu\text{M}$  hirudin. The application of hirudin had the positive side effect that the coagulation cascade was less affected compared to anticoagulation with heparin, thus enabling a more realistic analysis of inflammation processes.

### Pumping speed

The control unit “MPScontrol” allows to set pumping frequencies between 1 and 150 beats per minute (bpm), corresponding to pumping speeds from 5.4 to 600  $\mu\text{L min}^{-1}$ . When deciding on an ideal pumping speed for the *in vitro* flow model, various factors needed to be considered. If the pump speed is set too high, the blood volume might not be sufficient for the entire incubation period. As already mentioned in Chapter 4.3.5, the available volume of freshly drawn blood is limited due to restrictions by the ethics committee. On the other hand, a very low pumping speed might lead to sedimentation of blood cells. Even though the rotation device prevents blood sedimentation within the blood reservoir, this does not apply to the connecting tubes, as you can see in Figure 4.10. However, first trials have shown that this sedimentation is enormously reduced when applying a pumping frequency of 6 bpm or higher.



**Figure 4.10:** Exemplary photo showing sedimentation of blood cells within the connection tubes.

According to trials and calculations, a pump setting of 6 bpm (corresponding to  $32.4 \mu\text{L min}^{-1}$ ) has shown to be ideal. This pumping speed prevents the sedimentation of blood cells and ensures that a blood volume of 80 mL is sufficient to pump blood for up to 4 hours over two microchannel chips.

### Luer Locks

During initial tests, it was noticed that most blood clotting occurred in the area of the Luer Locks connectors. In this regard, two potential causes were identified: the hemocompatibility of the adhesive that was applied to fix the connectors on the microchannel chip and the geometry of the in- and outlet.

In the first step, the adhesive for the Luer Locks was examined more closely. A selection of suitable adhesives was provided by Fraunhofer IWS and examined via quasi-static hemocompatibility assessment. Hereby, the adhesive Loctite<sup>®</sup> EA M-31 CL was found to be the one with the best hemocompatibility. This 2-component liquid epoxy adhesive is characterized by its high impact resistance and minimal shrinkage, and is ISO 10993 certified for medical applications. The results of hemocompatibility assessment are presented in Figure A.5, along with the other blood-contacting materials within the microchannel chip.

The second step was to take a closer look at the shape of the Luer Lock connectors. As shown in Figure 4.11, the access at the bottom of the connector narrows to a diameter of only 1.3 mm. As the microchannel itself has a width of 3 mm, this leads to an unnecessary bottleneck, which could negatively influence flow dynamics. For

this reason, it was decided to enhance the diameter to 3 mm by drilling the access and therefore providing a smooth transfer of blood to the microchannels.

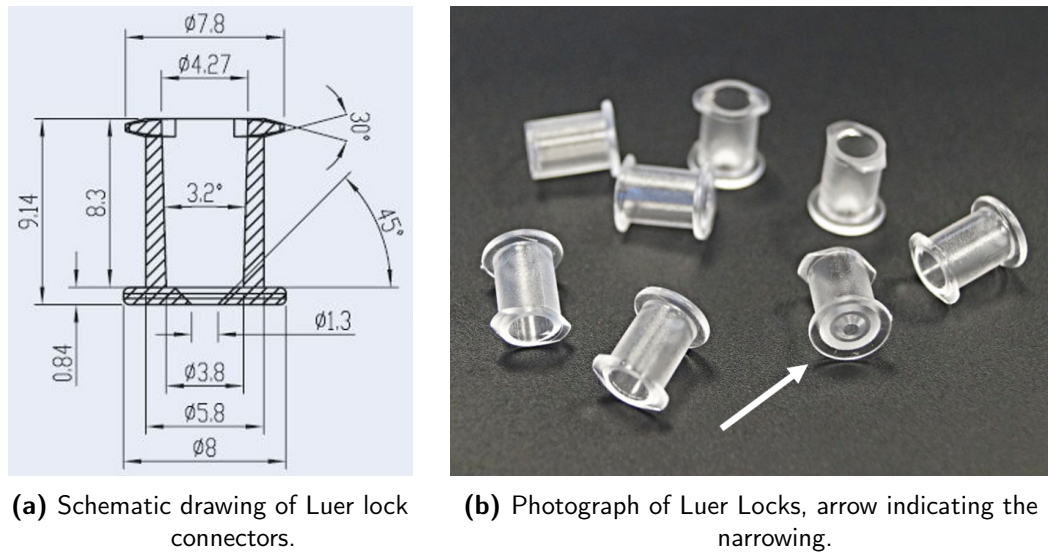


**Figure 4.11:** Female Luer Lock connectors, before enlarging the diameter.

The usage of the adhesive Loctite® EA M-31 CL as well as the drilling of the connectors to widen the access to the microchannels greatly improved hemocompatibility in the area of the Luer Locks connectors. In future tests, these areas were free of blood residues after incubation, and blood activation was further reduced.

### Blood reservoir

Further optimization was required concerning the selection of a suitable blood bag. Since standard-sized blood bags (volume = 500 mL) are too large for the available blood volume, another option had to be found. Most important requirements were the hemocompatibility of the bag material as well as the possibility to connect the bag via Luer Locks. The initial decision was made in favor of an infusion bag (MiXi® mixing and infusion bags, 50 mL, Hemedis, Weissenborn, Germany), made of ethylene-vinyl acetate (EVA). The blood compatibility of the bag material was tested by quasi-static hemocompatibility assessment (see Figure A.5). Blood activation was comparable to control surfaces PC and TPU, also no hemolysis or pH shift was observed. However, during the initial trials with the *in vitro* flow model, elevated hemolysis of the blood samples was detected, increasing steadily with incubation time. Initially, typical causes of hemolysis such as sharp edges and constrictions were suspected as possible

causes. However, after excluding these error sources, the blood bag was identified as the cause for hemolysis. This was demonstrated by comparing the blood samples after passing the whole setup with samples taken directly from the blood reservoir. To avoid such a source of error for future experiments, from now on, a blood sample was always taken from the reservoir and analyzed as control.

After further research for a suitable blood bag, the decision was made in favor of a blood bag for veterinary medicine (feline blood collection bag, Alvedia) that holds up to 100 mL. This blood bag is made of polyvinyl chloride (PVC), a material commonly used for commercial blood cell containers and blood bags. Its low tendency to provoke hemolysis is explained by the use of the plasticizer di-2-ethylhexyl phthalate (DEHP), which is known to improve the morphology, deformability, and osmotic fragility of red blood cells [224–226]. Even though DEHP is often criticized due to its toxic potential, it is still widely used for blood storage as the advantages outweigh the disadvantages [227, 228].

The first trials with the veterinary PVC blood bag confirmed its suitability as blood reservoir. After 4 hours of incubation, hemolysis level was below 0.1 %. Inflammation and hemostasis were also considerably less activated compared to the collected samples, demonstrating the gentle storage in the blood bag. (see Figure A.4).

The veterinary blood collection bag of Alvedia was selected as blood reservoir for the *in vitro* flow model due to its low blood activation and hemolysis, as well as its possibility to easily connect to the rest of the blood stream unit by Luer Lock connections.

### Channel height

One of the first approaches to regulate WSS within microchannel chips was to adjust the channel height. To determine if this would affect hemocompatibility, initial experiments were conducted in this regard. Therefore, three independent channels with heights of 50, 100, and 250  $\mu\text{m}$ , respectively, were analyzed according to their influence on blood activation. The pumping speed was kept constant at 6 bpm. Within the 50  $\mu\text{m}$  channel, blood flow already stopped after approximately 1 hour incubation time. This could be explained by the fact that the channel is more easily blocked by aggregating blood cells. In contrast, blood incubation has worked consistently at channel heights of 100 and 250  $\mu\text{m}$ . Analysis of blood parameters revealed a tendency to higher blood inflammation for the smaller channel height after both examined time points at 2 and 4 hours, as presented in Figure 4.12. However, it is not clear whether

these differences are due to the higher WSS or due to the squeezing of blood cells. Therefore, it was decided to perform all experiments with the same channel height and to adjust shear stresses only by varying the damping behavior (see Chapter 4.4.3).

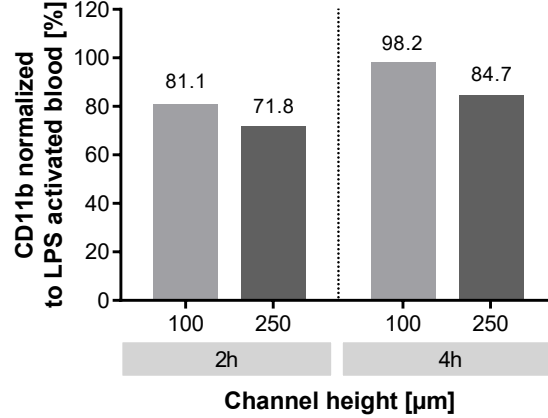


**Figure 4.12:** Blood activation in dependence of channel height: Expression of inflammation parameter CD11b on granulocytes, normalized to LPS activated blood,  $n=1$ .

As a channel height of 250  $\mu\text{m}$  seems to have the least impact on blood activation, this height was chosen for the construction of the microchannel chips. By manufacturing all chips with the same geometry and only using damping to adjust occurring WSS, it could also be excluded that channel height is an influencing factor on blood activation.

#### 4.4.3 Hemodynamic pumping behavior

*Experimental design and data evaluation on hemodynamic pumping behavior was done in cooperation with the Fraunhofer IWS. The acquisition of experimental data was carried out by Stephan Behrens (Fraunhofer IWS).*

To determine the hemodynamic behavior in the microchannel chips, micro-particle image velocimetry (micro-PIV) measurements were performed. For this purpose, the model was operated with a suspension of latex beads, water, glycerin and xanthan gum that exhibits similar shear thinning behavior as blood. The movement of the latex beads was tracked and analyzed to calculate the volume flow in dependence of the membrane deflection in the triple-pump-chip. Based on these data, the corresponding WSS was calculated using Equation 6.3 (see Chapter 6.4.3). Measurements were

performed with a pumping frequency of 6 bpm and for damping adjustments of 0, 15, and 50 mL.

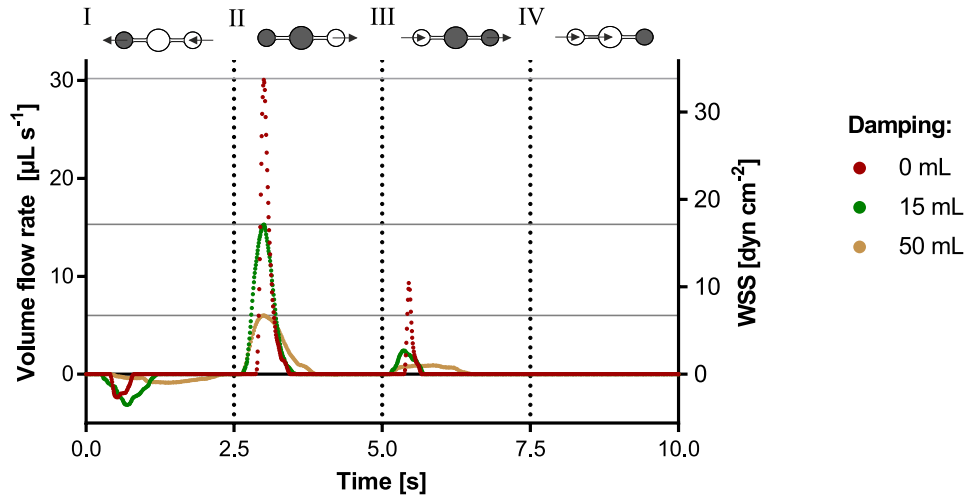


**Figure 4.13:** Volume flow and corresponding WSS in the microchannel chip measured by micro-PIV at 0, 15, and 50 mL pneumatic damping; (I) – (IV): Behavior of the pump deflection with charged (white) and discharged (grey) pump chambers,  $n=3$ ; data acquired by Stephan Behrens (Fraunhofer IWS), adapted from [218].

The results of the micro-PIV measurements are presented in Figure 4.13. At a pumping frequency of 6 bpm, each pumping cycle has a duration of 10 s with a shift of the pump chambers every 2.5 s. The peaks of volume flow and WSS differ according to the damping volume, adjusted by “MPShemodyn”. This connection demonstrates the possibility to independently vary flow conditions within the system and mimic hemodynamic shear stresses as they occur in different vascular devices. The three damping volumes applied in this study demonstrate maximum WSS of 7  $\text{dyn cm}^{-2}$  (50 mL), 17  $\text{dyn cm}^{-2}$  (15 mL), and 33  $\text{dyn cm}^{-2}$  (0 mL). These values closely reflect the WSS that actually occur in vascular devices. As comparison, numerical simulations estimated WSS of 3 to 10  $\text{dyn cm}^{-2}$  in central venous catheters for hemolysis [229] and 20 to 24  $\text{dyn cm}^{-2}$  in coronary stents [230]

The adaptable damping settings of the pump system allow the adjustment of maximum WSS in the range from 6 to 33  $\text{dyn cm}^{-2}$  in the *in vitro* model. Comparison with data from literature showed that these values realistically reflect shear conditions occurring in various vascular devices.

## 4.5 Verification

To ensure compliance with quality standards, a verification process is required when developing new systems. According to EN ISO 9000-2015 [231], verification is defined as “confirmation, through the provision of objective evidence, that specified requirements have been fulfilled”. Therefore, the requirements for the *in vitro* model specified in Chapter 4.2 were reviewed at this point.

### General requirements

*The model must realize a simultaneous incubation of blood, bacteria, and test surface.*

As demonstrated in Chapter 4.4, the newly developed *in vitro* flow model enabled simultaneous incubation of blood, bacteria, and test surface. Here, the test surface in the microchannel chip was first pre-colonized with bacteria and subsequently brought into contact with whole blood. This procedure is supposed to reflect the colonization of material surfaces with microorganisms from the environment (e.g. skin) during insertion of medical devices - one of the most prevalent entry routes for bacteria on catheters and other medical devices [25, 232]. Thus, the requirement can be considered as fulfilled.

### Incubation conditions

*The incubation of test surfaces must take place under physiological conditions.*

The realization of physiological conditions was divided into three aspects: the application of freshly drawn human blood, the incubation at body temperature (37°C), and the adjustment of relevant shear conditions. The first two aspects have been directly implemented during model design, as described in Chapter 4.4. In contrast, the adjustment of shear stresses was a more complex aspect. The hemodynamic pumping behavior of the *in vitro* flow model was regulated by the damper “MPShemodyn”. This unit contains air chambers of various sizes that dampen the compressed air and vacuum responsible for the membrane deflection within the triple-pump-chip. By increasing the damping volume, the pump chambers opened and closed with less pressure, resulting in lower WSS on the test surface. Chapter 4.4.3 presents the maximum WSS in dependence of the adjusted damping volume, ranging from 7 to 33 dyn cm<sup>-2</sup>. These values reflect the actual WSS occurring in various vascular devices [229, 230, 233]. Thus, this requirement can also be considered as fulfilled.

### Pumping conditions

*The pumping process must not provoke any hemolysis or excessive blood activation to ensure hemocompatibility of the system.*

After all blood-contacting materials of the microchannel chip had been tested individually (Figure A.5) and thus been excluded as a potential source for excessive blood activation, the pumping system was investigated concerning its blood compatibility. As described in Chapter 4.4.2, individual parameters of the model setup were already optimized in this regard. For a final evaluation of hemocompatibility, the pump system was tested without pre-colonization of bacteria in order to exclude these as a possible cause for blood activation. Instead, three microchannel chips with different test surfaces (glass, TPU, and Teflon AF) were applied in the model setup for 2 hours. Collected blood samples revealed that occurring hemolysis was negligible ( $<0.1\%$ ), also blood gases and pH remained within the expected range. Inflammation, measured by granulocyte CD11b expression, was comparable to incubation in the established quasi-static incubation chamber ( $\sim 40\%$  in relation to LPS-activated blood). Based on these data, it can be concluded that the pumping procedure of the flow chamber is quite gentle and does not provoke excessive blood activation. The detailed results of this study were presented at the 55th Annual Conference of the German Society for Biomedical Engineering and published in [218].

*The pumping system must prevent the sedimentation of blood cells.*

The rotation device presented in Chapter 4.3.4 ensured constant mixing of blood within the reservoir and thus enabled blood storage without cell sedimentation. A pump speed that was sufficiently high was also able to prevent subsequent sedimentation within the connection tubes and the chips. Consequently, this condition can be considered fulfilled.

*The incubation must avoid the accumulation of activation products.*

The presented *in vitro* model allowed blood to be pumped from a reservoir via a microchannel chip with the test surface into collection tubes. In this way, the blood came into contact with the pre-colonized microchannel chip only once and bacteria could not enter the blood reservoir. This so-called single-pass flow model consequently prevented the accumulation of activation products such as dead bacteria. Therefore, this requirement can be considered as fulfilled.



## Analysis

*The model must allow the analysis of blood activation.*

The previously presented study regarding the hemocompatibility of the pump system [218] confirmed that blood parameters can be measured very well after blood has passed the system and that the results differ depending on the material surface of the test system. For the investigation of bacterial colonization on the test surface, the inflammation parameter CD11b and platelet activation factor PF4 proved to be particularly suitable, as these were strongly affected by the presence of GFP *S. aureus* (see Figure A.6).

*The model must allow the analysis of bacterial colonization on the test surface.*

The application of GFP-expressing *S. aureus* allowed the detection of surface colonization after whole blood contact (see Chapter 4.3.6). The bacterial coverage could be quantified via fluorescence microscopy and thus be compared between different test surfaces. In consequence, this condition can be considered fulfilled.

Verification of the *in vitro* model confirmed that all requirements specified for model development were met.

## 4.6 Validation

In addition to verification, the new model system also has to undergo a validation process. According to EN ISO 9000-2015 [231], validation is defined as “confirmation, through the provision of objective evidence, that the requirements for a specific intended use or application have been fulfilled”. As specified in Chapter 4.1, the intended use of the flow model was the evaluation of antimicrobial coatings for a potential use in blood-contacting devices.

In order to check whether the model can fulfill this intended purpose, the validation was divided into two distinct steps. In a first step, the control surface PC and the APs 10-30-16-2 and 10-30-16-2-Hex presented in the first part of the work were tested with the *in vitro* flow model and results were compared with each other to determine if the model is able to distinguish the different surfaces. Here, both bacterial colonization of the surfaces and blood activation were taken into account. In a second step, experiments were conducted at different flow conditions to determine whether it is able to represent the well-documented dependence between occurring WSS and bacterial colonization.

#### 4.6.1 Differentiation of antimicrobial surfaces

As an initial step of validation, it was checked whether the *in vitro* flow model was able to distinguish blood-surface-bacteria interactions between the reference material PC and the two antimicrobial coatings. As the model only allows the testing of two materials in parallel, PC was first tested against the anti-adhesive AP 10-30-16-2 and then both APs 10-30-16-2 and 10-30-16-2-Hex were compared with each other to see whether the *in vitro* flow model is able to detect the additional antimicrobial effect of hexetidine. Thereby, the focus was set on examining the influence of the anti-adhesive and contact-killing coatings on *S. aureus* adhesion and growth in blood contact, as well as the influence of bacterial colonization on inflammation and hemostasis of whole blood.

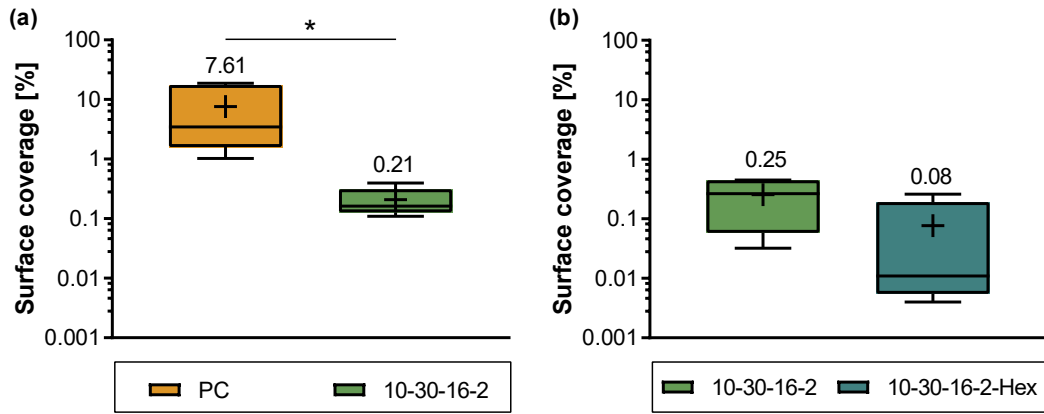


**Figure 4.14:** Validation of the *in vitro* flow model: Bacterial coverage on microchannel chips after 4h whole blood incubation (WSS of  $17 \text{ dyn cm}^{-1}$ ); statistical significance was determined using an unpaired, two-tailed t-test (\*  $p < 0.05$ , \*\*  $p < 0.01$ ),  $n = 6$ ; (a) Comparison of PC vs. AP 10-30-16-2, (b) Comparison of AP 10-30-16-2 vs. AP 10-30-16-2-Hex.

For this purpose, the *in vitro* flow model was operated as described in Chapter 6.4.4. In brief, microchannel chips were first pre-treated with the respective AP coating, then incubated in bacterial suspension, and subsequently connected to the pumping setup. Freshly drawn whole blood was pumped over the microchannel chip at a maximum WSS of  $17 \text{ dyn cm}^{-2}$  (15 mL damping volume) and then collected in Eppendorf tubes. After a 4-hour incubation at  $37^\circ\text{C}$ , the microchannel chip was imaged to analyze bacterial coverage at the bottom of the chip. Blood activation of the collected blood samples was examined after each hour (1 - 4 hours total).

Figure 4.14 presents bacterial coverage that was detected at the bottom of the microchannel chips after 4-hour incubation in whole blood. Comparing PC and

AP 10-30-16-2 with each other, it becomes obvious that the anti-adhesive coating significantly reduced bacterial colonization. While 7.61 % of the PC surface was colonized by bacteria, only 0.21 % were covered on AP 10-30-16-2, corresponding to a reduction by factor 36. Hexetidine-functionalized AP 10-30-16-2-Hex further reduced bacterial coverage by a factor of 3.

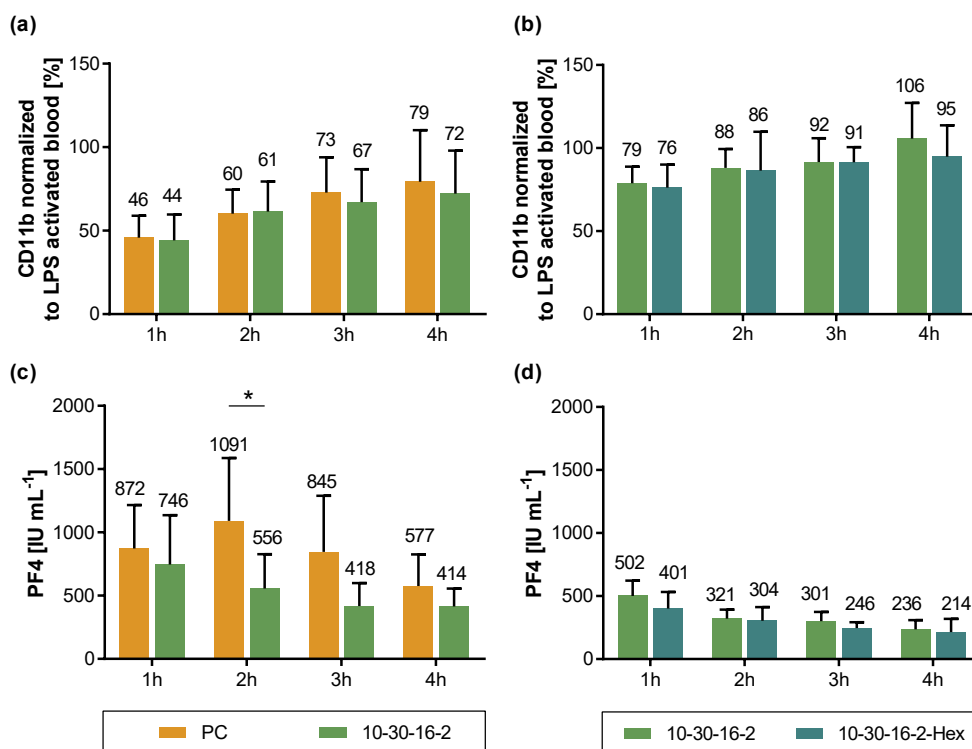


**Figure 4.15:** Validation of the *in vitro* flow model: Activation of blood samples collected after every hour during 4 hours incubation time; statistical significance was determined using unpaired, two-tailed t-tests for each time point (\*  $p < 0.05$ , \*\*  $p < 0.01$ ),  $n = 6$ ; (a) Expression of inflammation parameter CD11b on granulocytes after incubation on PC and AP 10-30-16-2, (b) Expression of inflammation parameter CD11b on granulocytes after incubation on AP 10-30-16-2 and AP 10-30-16-2-Hex, (c) PF4 release as a parameter for platelet activation after incubation on PC and AP 10-30-16-2, (d) PF4 release as a parameter for platelet activation after incubation on AP 10-30-16-2 and AP 10-30-16-2-Hex.

Analysis of the collected blood samples (Figure 4.15) after every hour revealed slightly reduced inflammation (CD11b) and platelet activation (PF4) for the surfaces coated with AP 10-30-16-2, and AP 10-30-16-2-Hex, respectively. These tendencies positively correlated with the results of bacterial coverage (Figure A.8). The same trend was observed for the formation of granulocyte-platelet conjugates (Figure A.7). However, the data showed a clear time-dependence. The influence of bacterial colonization

on cellular inflammation (CD11b expression) was first detected after an incubation period of 3 hours. In contrast, impact on platelet activation, measured as PF4 release, was detectable from the beginning, showing increased activation for the samples with high bacterial coverage at each time point. However, absolute levels of PF4 decreased over time, indicating a reduced platelet activation with advancing incubation time.

Increased PF4 release as a consequence of bacterial colonization has already been observed in previous studies [234, 235]. It is assumed that PF4 bind to the surface of *S. aureus*, provoking a conformational change in PF4 that cause them to express neoepitopes. These neoepitopes are known to bind anti-PF4/H antibodies, that in turn promote platelet activation [234]. Accordingly, it was shown that the model is able to represent this correlation between platelet activation and bacterial colonization. The decrease in PF4 release with advancing incubation time could be explained by various factors. On the one hand, bacteria embed themselves in protective EPS layers, preventing PF4 from binding to the surface of *S. aureus*. Beyond that, it is known that *S. aureus* actively exploit blood coagulation to protect themselves from elimination by the immune system (see Chapter 2.1.4). Accordingly, it is assumed that platelet activation particularly occurs in the first hours after initial blood contact before the protective layer has been formed.

Similar to platelet activation, the slightly elevated cellular inflammatory response (CD11b activation) can also be attributed to the increased bacterial colonization. Presumably, this effect is related to the rapid opsonization of bacteria with immunoglobulins and complement factors upon contact with blood, making them recognizable to neutrophil granulocytes. As a result, the neutrophils are activated (CD11b expression) and enabled to phagocytose and subsequently kill the bacteria [236, 237]. Here, differences between the coatings were only detectable after about 3 hours of blood incubation. This time delay might be accounted for the lag-phase behaviour of *S. aureus* cells that must adapt to the more challenging environment before starting to proliferate. Accordingly, differences in bacterial colonization might be too small to detect its effect on CD11b expression.

The first step of validation confirmed the ability of the *in vitro flow* model to differentiate blood-surface-bacteria interactions between the tested antimicrobial coatings. Blood activation correlated slightly with bacterial coverage, which in turn was strongly dependent on the investigated material surface.

#### 4.6.2 Influence of wall shear stress

It is commonly known that bacterial adhesion and growth on surfaces are highly dependent on the prevailing flow conditions (see chapter 2.1.3). Accordingly, it is of great importance to evaluate novel antimicrobial materials under the influence of realistic WSS. The introduced *in vitro* model addressed this challenge and allowed for the adjustment of flow conditions within a physiological range. Thus, the model did not only enable evaluation under flow, but also allowed application-specific testing, as occurring shear conditions vary greatly between different medical devices.

Accordingly, the second validation step aimed to investigate whether this well-documented dependence of bacterial colonization and WSS can actually be represented with the flow model. Therefore, the model was operated with two different damping adjustments (50 and 15 mL damping volume), evoking maximum WSS of 7 and 17  $\text{dyn cm}^{-2}$ , respectively. These flow settings were selected as they reflect actual occurring WSS in various vascular devices. As an example, WSS on central venous catheters for hemodialysis were estimated in a range of 3 to 10  $\text{dyn cm}^{-2}$  [229], whereas WSS in coronary stents have shown WSS between 20 and 24  $\text{dyn cm}^{-2}$  [230]. The evaluation was performed with control surface PC and anti-adhesive AP 10-30-16-2.

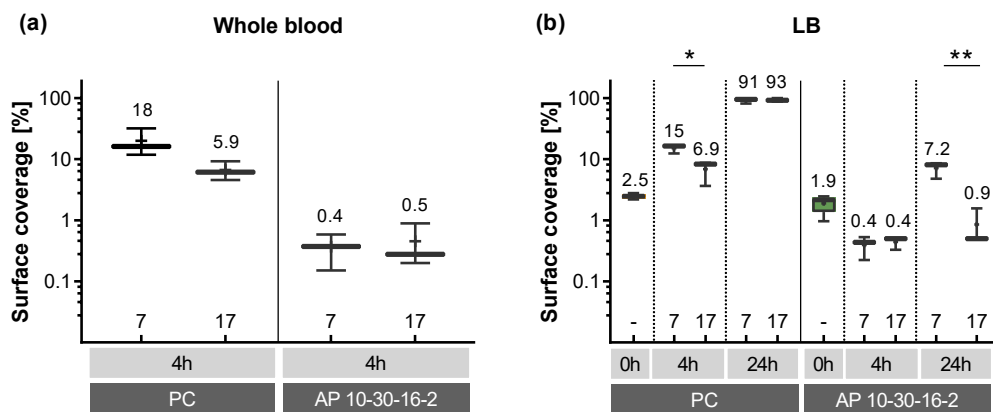


**Figure 4.16:** Validation of the *in vitro* flow model: Bacterial coverage in dependence of occurring maximum WSS (7  $\text{dyn cm}^{-2}$  and 17  $\text{dyn cm}^{-2}$ ) on PC and AP 10-30-6-2; statistical significance was determined using unpaired, two-tailed t-tests for each time point (\*  $p < 0.05$ , \*\*  $p < 0.01$ ),  $n = 3$ ; **(a)** *In vitro* flow model was operated with whole blood; **(b)** *In vitro* flow model was operated with LB medium.

First, the two surfaces were tested for 4 hours under the influence of whole blood (Figure 4.16 a). Here, the impact of varying WSS was clearly detectable for PC surfaces. Surfaces that were exposed to a WSS of  $17 \text{ dyn cm}^{-2}$  showed considerably lower bacterial coverage (3-fold reduction) than those exposed to lower WSS of  $7 \text{ dyn cm}^{-2}$ . In contrast, no differences were detected for anti-adhesive AP surfaces.

To investigate whether this relation changes with increasing incubation time, the flow model was additionally operated for a duration of 24 hours. Here, a medium change from whole blood to LB medium was necessary as (1) the available blood volume was only sufficient for single-pass pumping of maximum 4 hours and (2) blood becomes increasingly activated with advancing time, thus making measurements inaccurate (see Chapter 4.3.5). Like whole blood, LB medium contains many nutrients that promote bacterial proliferation. However, due to the absence of blood cells, the influence of an immune response was not considered.

Bacterial coverage was evaluated after 0, 4, and 24 hours for both shear stress settings (Figure 4.16 b). After 4 hours of incubation, the obtained values were similar to those of whole blood incubation. Bacterial coverage on PC surfaces incubated at a WSS of  $7 \text{ dyn cm}^{-2}$  was significantly higher than those that were incubated with  $17 \text{ dyn cm}^{-2}$ . However, similar to whole blood incubation, no differences were observed for the anti-adhesive AP surface. Actually, bacterial coverage was reduced for both shear settings in comparison to initial colonization at  $t = 0 \text{ h}$ . However, this ratio changed significantly after an incubation of 24 hours. On PC, no differences in bacterial coverage were observed as most surfaces were almost completely covered, regardless of the occurring WSS. In contrast, the dependence of bacterial coverage and WSS now became apparent on anti-adhesive AP 10-30-16-2, as absolute values were much lower. Here, bacterial coverage was reduced from 7.2 % to 0.9 % (8-fold reduction) by applying the higher WSS.

These observations demonstrate that the introduced *in vitro* model is able to successfully reproduce the well-documented dependence of bacterial colonization and occurring shear stresses. The decrease in bacterial coverage in response to elevated WSS is mainly attributed to the fact that increased drag forces more often exceed adhesion forces between bacteria and surface [63]. As a consequence, loosely bound bacteria “slide and roll” over the surface and become detached more easily [65, 66]. However, it has been reported that bacteria that withstand detachment due to high shear stresses form very elastic and rigid biofilms, thus allowing to resist mechanical failure and detachment to a greater extent [64, 72]. Although such a relationship was not investigated within the scope of this work, the introduced model provides multiple opportunities to test such observations under the influence of an immune response and physiological flow conditions.

Incubation with varying flow conditions showed increased bacterial colonization in response to reduced WSS. Accordingly, it was demonstrated that the model is capable of representing the well-documented dependence of bacterial colonization and the flow conditions that occur.

## 4.7 Discussion

The objective of the second part of the thesis was the development of an *in vitro* model that allows the evaluation of antimicrobial coatings under *in vivo*-like conditions. To check whether this objective was fulfilled, the model was subjected to a verification and validation process after the development process was completed. Thereby, verification revealed that all previously defined requirements were actually met. Among other things, this confirmed that the model did indeed allow incubation under conditions similar to those *in vivo*. Moreover, validation confirmed that the model was able to differentiate the investigated antimicrobial surfaces and even reflect the dependence between bacterial colonization and occurring shear stresses. Thus, the intended purpose of the model was fulfilled and it could be confirmed that the blood flow model is applicable for the evaluation of antimicrobial coatings for blood-contacting medical devices.

In order to investigate whether the newly developed *in vitro* model actually provided additional information in comparison to state-of-the-art *in vitro* tests, the obtained results from the validation process were compared with the data acquired in the first part of the thesis. In particular, the detection of antimicrobial activity, the activation of whole blood, and the influence of the immune reaction were considered in more detail.

### Detection of antimicrobial efficacy

Table 4.1 presents the reduction of bacterial coverage that was achieved by the antimicrobial coatings AP 10-30-16-2 and AP 10-30-16-2-Hex in dependence of the performed *in vitro* test. Values were normalized to the control surface PC in order to allow for a better comparison of the results. The normalized values highlight the dependence of bacterial coverage on the occurring flow conditions, which is particularly strong for the anti-adhesive 10-30-16-2. While bacterial colonization (after 4 hours) was only reduced by 63.8 % (3-fold reduction) under static conditions, a reduction of 96.7 % (32-fold reduction, whole blood) and 94.2 % (17-fold reduction, LB medium) was achieved under dynamic conditions. In contrast, reduction in bacterial

colonization by AP 10-30-16-2-Hex was relatively independent of the performed *in vitro* method and ranged from 98.3 % (58-fold reduction) to 98.9 % (95-fold reduction) for static and dynamic incubation, respectively.

**Table 4.1:** Reduction of bacterial coverage by anti-adhesive and contact-killing AP coating in dependence of the performed *in vitro* test, normalized to control surface PC .

| Bacterial coverage normalized to PC |                       | 10-30-16-2 | 10-30-16-2-Hex |
|-------------------------------------|-----------------------|------------|----------------|
| 4 h                                 | static (M9* medium)   | 63.8 %     | 98.3 %         |
|                                     | dynamic (whole blood) | 96.7 %     | 98.9 %         |
|                                     | dynamic (LB medium)   | 94.2 %     | -              |
| 24 h                                | static (M9* medium)   | 81.0 %     | 99.0 %         |
|                                     | dynamic (whole blood) | -          | -              |
|                                     | dynamic (LB medium)   | 99.0 %     | -              |

As described above, reduced bacterial coverage in the presence of high WSS is mainly attributed to increased drag forces that exceed adhesion forces between bacteria and surface and consequently cause detachment. This effect is particularly strong for the AP 10-30-16-2 as the anti-adhesive properties of PEG further reduce the prevalent adhesion forces, thus facilitating the removal of bacteria by increasing fluid flow. In contrast, the biocidal effect of hexetidine in AP 10-30-16-2-Hex acts on all adhering bacteria, regardless of the flow conditions that occur. The obtained data illustrate that the full potential of the anti-adhesive coating only becomes apparent under dynamic test conditions. The introduced flow model is able to capture these influences and thus provides an essential value for the analysis of anti-adhesive and contact-killing coatings under physiological conditions.

### Activation of whole blood

While established *in vitro* models only investigate hemocompatibility and antimicrobial activity separately, the newly developed model offers a possibility to combine these evaluations. Here, it was found that assessment of blood activation with the *in vitro* flow model provides another indicator for bacterial colonization; however it does not replace established hemocompatibility tests to evaluate the activating effects of the materials themselves. Due to the simultaneous incubation of blood, bacteria and material surface, effects of bacteria and material surface on blood activation are overlapping. However, the activating effects of bacteria seem to be stronger than those of the material surface. This becomes particularly evident when considering the



cellular inflammatory response (CD11b) of the anti-adhesive AP 10-30-16-2. During quasi-static hemocompatibility testing, CD11b expression was lower than on AP 10-30-16-2-Hex, but increased compared to control surface PC. However, results obtained with the *in vitro* blood flow model revealed an opposite trend, showing the strongest activation on PC and the lowest activation on 10-30-16-2-Hex. As this tendency correlated with bacterial colonization, it is assumed that the strong blood activation due to *S. aureus* (see Figure 4.7) masks the effect of the material surfaces. Accordingly, the detection of blood activation with the *in vitro* model can serve as an excellent indirect indicator for the antimicrobial efficacy of the materials.

### **Influence of immune reactions**

Considering the influence of the immune defense, it becomes evident that incubation with whole blood only had a minor effect on *S. aureus* coverage. After 4 hours blood incubation, bacterial coverage on anti-adhesive AP 10-30-16-2 was reduced by 96.7 % (30-fold reduction), whereas a reduction by 94.2 % (17-fold reduction) was observed after incubation with LB medium. It is suspected that a small part of the present bacteria was eliminated by the immune cells of the whole blood; however, a larger proportion was able to evade the mechanisms of the host defense. The excellent evasion strategies of *S. aureus* strains are well documented and base on the secretion of proteins that target antibody opsonization and phagocytosis, protecting them from elimination by immune cells, as well as on the tendency to aggregate and encapsulate themselves in layers of EPS, thus impeding recognition and phagocytosis by immune cells [76] (see Chapter 2.1.4). Data obtained within this study suggest that this is also valid for the utilized *S. aureus* strain, thus making it very suitable for the evaluation of antimicrobial materials regarding their ability to prevent device-related bloodstream infections. In contrast, cells of the *E. coli* strain (MG1655) that was evaluated in preliminary experiments were eliminated by the immune system within less than 30 minutes. Accordingly, the introduced model also provides an excellent platform for the selection of clinically relevant laboratory strains.

## Conclusion

The comparison between the different methods confirmed the advantage of the newly developed blood flow model over state-of-the-art *in vitro* assays to realistically evaluate antimicrobial coatings. The direct comparison of bacterial coverage revealed that evaluation under physiological flow conditions is particularly relevant for anti-adhesive surfaces. Moreover, incubation with whole blood offers numerous advantages. On the one hand, it is presumably the best way to provide a physiological nutrient environment, as there is no growth medium that accurately represents the nutrients present in blood. In addition, incubation with whole blood induces an immune response that attacks the bacteria. Thus, only those bacteria species that have developed effective evading strategies against the human immune response succeed to colonize the surface. Consequently, the model does not only provide a realistic growth environment for bacteria, but also offers a possibility to identify bacteria that are relevant in device-related blood stream infections.

## 5 Summary and outlook

The objective of this thesis was the development and application of an *in vitro* model that allows the evaluation of antimicrobial coatings under *in vivo*-like conditions. Previously developed *in vitro* tests do not adequately represent physiological conditions as they neglect the mutual influence of blood, bacteria, and the material surface of interest. To compensate for this deficiency, researchers widely perform animal studies during pre-clinical evaluation. The new *in vitro* model aimed to reduce the need for these highly controversial animal tests by providing data about the antimicrobial coatings that cannot be obtained with established state-of-the-art *in vitro* tests.

As a first application case, the model was intended to be directly used to evaluate recently in-house developed antimicrobial coatings, so-called anchor polymers (APs) [18]. For this purpose, the project was divided into two parts. While the first part focused on a preliminary evaluation of AP coatings with established *in vitro* tests, the second part dealt with the development and application of the new realistic *in vitro* model.

The AP coatings studied in the first part of the work are PEGylated styrene-maleic acid copolymers that physically adsorb to various polymer substrates. Due to their hydrophilic PEG chains, they exhibit strong anti-adhesive properties, while further functionalization with hexetidine allows the creation of contact-killing surfaces. Depending on the molecular architecture of the SMA backbone and PEG side chains, APs present a wide range of properties, providing a large library of available coatings. Thus, the objective of this part was to identify the most promising molecular architecture, and to provide a general assessment of the APs in terms of their applicability as antimicrobial coatings in medical devices. Moreover, the detailed characterization was intended to enable subsequent comparison between the newly developed model and *in vitro* tests according to the state of the art.

In this respect, the AP coatings were subjected to various tests regarding their adsorption and stability properties on two medically relevant polymers (TPU and PC), their antimicrobial activity, as well as their biological safety. The measurements revealed that all investigated APs adsorbed on both tested polymer substrates and formed stable adsorbate layers. The long-term stability was maintained even under more challenging conditions, such as the presence of proteins, under shear stresses,

and during incubation at body temperature. However, the stability of the adsorbate layers was clearly superior on PC compared to TPU. For this reason, the use of AP coatings on TPU is mainly recommended for devices with only transient contact time. Alternatively, it is proposed to apply AP coatings as “sacrificial layers”, where controlled desorption can either release specific active substances or impede bacterial colonization on the surface. A more detailed investigation of these approaches is suggested for additional research studies.

Further evaluation revealed the strong antimicrobial efficacy of the AP coatings. Thereby, coatings with a high PEG density were most effective in reducing bacterial colonization, whereas the length of the PEG chains only had a minor impact. The additional antimicrobial effect due to the hexetidine functionalization resulted in further reduction of bacterial colonization on the surfaces. To exploit the full potential of the modular AP technology, functionalization with additional bioactive substances is recommended for further studies. In this respect, antimicrobial peptides and phenolic compounds have already shown promising results in preliminary tests. Beyond that, combinatorial approaches should also be considered. Functionalization with two different bioactives has the potential to either exploit synergies of the active ingredients or increase the action spectrum against different bacterial species.

Investigations regarding the biological safety of the AP coatings also showed promising results. Hemocompatibility assessment (ISO 10993-4) demonstrated a low hemostasis response that was comparable or even reduced to clinically approved control surfaces. Inflammation reaction caused by the AP coatings was considered acceptable despite slightly elevated values. Moreover, *in vitro* cytotoxicity (ISO 10993-5) assays performed in previous studies have demonstrated the excellent biocompatibility of the coatings. However, to gain approval for the application on medical devices, the AP coatings need to undergo further testing, including the evaluation of systemic cytotoxicity (ISO 10993-11), the identification and quantification of degradation products (ISO 10993-13), as well as the establishment of allowable limits for leachable substances (ISO 10993-17). The performance of these investigations is recommended for further studies.

Overall, the investigation of adsorption behavior, stability, antimicrobial efficacy and biological safety revealed a high potential of the AP coatings for future applications in blood-contacting devices. However, for a more profound consideration it is essential to evaluate the coatings under more realistic conditions. To reduce the necessity of animal studies for this purpose, the second part of the work aimed at developing a model setup that facilitates this investigation *in vitro*.

In order to define the requirements for such a model, the first step was to identify the limitations of current test systems. These included, in particular, the use of non-representative microorganisms and nutrients, uncharacteristic flow conditions, and the absence of an immune response. All these aspects were addressed by the presented model setup. A representative nutrient environment and the inclusion of an immune response were realized by utilizing freshly drawn human blood. The modular pumping system, provided by the Fraunhofer IWS, facilitated the adjustment of characteristic flow conditions. *S. aureus* was selected as a representative microorganism species as they are among the most common pathogens causing device-related bloodstream infections.

The validation of the blood flow model was performed with one anti-adhesive and one contact-killing AP coating in comparison to the control surface PC and confirmed the model's ability to differentiate between tested surfaces. Inflammatory and coagulant blood activation correlated slightly with bacterial coverage, which in turn was strongly dependent on the investigated material surface. Incubation with varying flow conditions showed increased bacterial colonization in response to reduced wall shear stresses, thus demonstrating the capability of the model to reflect the well-documented dependence of bacterial colonization and occurring flow conditions. This ability represents one of the greatest benefits of the model, as current *in vitro* models either neglect the relevance of occurring shear stresses completely or represent them only inaccurately. A further advantage of the model is the simultaneous incubation of blood, bacteria, and test surface that allows analysis of the mutual interactions between the three parameters. Overall, validation confirmed the suitability of the blood flow model to evaluate novel antimicrobial materials for their applicability in blood-contacting devices. The obtained results suggest that the model could indeed play a vital role in the quest to reduce the need of animal studies.

In this work, the *in vitro* model was only validated for the application of anti-adhesive and contact-killing materials. In order to verify whether the model can also be applied for release-based materials, it is recommended to perform a corresponding investigation in further studies. Moreover, the model could be adapted to study alternative routes of infection. By pre-colonizing the surfaces with bacteria prior to blood contact, the results obtained in this study represent contamination through the skin during the insertion of the medical device. Switching this order and adding bacteria after blood contact could potentially simulate other infection routes, such as hematogenous seeding. Moreover, the model could be applied to analyze bacterial colonization by several other bacterial strains. In this regard, the use of clinical isolates is particularly recommended as it would further increase the clinical relevance of the data obtained.

In addition to the realistic evaluation of antimicrobial materials, the *in vitro* blood flow model also has great potential for biofilm research. Previous studies have shown that biofilms differ greatly in size and shape depending on whether they were formed *in vitro* or *in vivo*. In particular, the frequently described mushroom structure in matured *in vitro* biofilms was almost never observed on catheters [9]. Therefore, performing detailed biofilm studies with the introduced *in vitro* model might provide new insights on biofilm formation under *in vivo*-like conditions. In this regard, it is also recommended to examine the formation of multi-species biofilms by incubating various bacterial strains simultaneously. Here, the inclusion of an immune response is particularly important, as each bacterial strain possesses different evading strategies, which could provide them with a growth advantage over other strains.

## 6 Experimental part

### 6.1 Surface preparation

#### 6.1.1 Polycarbonate

PC substrates (Makrofol<sup>®</sup> DE 1-1 000000) were purchased from Covestro (Leverkusen, Germany) and utilized as supplied, except for QCM measurements. For QCM analysis, PC substrates were dissolved ( $c = 0.5$  wt %) in dichloromethane (DCM) (Sigma-Aldrich, St. Louis, USA), and subsequently filtered (0.2  $\mu$ m PTFE syringe filter, Sigma-Aldrich) to remove remaining particles. In parallel, QCM crystals (QSX 303 SiO<sub>2</sub>, Biolin Scientific, Västra Frölunda, Sweden) were cleaned using a standard Radio Corporation of America (RCA) cleaning-protocol [238], and silanized with hexamethyldisilazane (HMDS) (Sigma-Aldrich). Subsequently, PC solution was spin-coated on QCM crystals (LabSpin 6 semi-automatic spin-coater, Süß MicroTec, München, Germany), applying the following parameters: time = 30 s, speed = 4000 rpm, and acceleration = 1500 rpm s<sup>-1</sup>. Afterwards, QCM crystals were dried at 60 °C for 2 hours. The identity of the spin-coated layers was confirmed by a shift in wettability and surface roughness.

#### 6.1.2 Thermoplastic polyurethane

Medical-grade TPU (Tecoflex<sup>™</sup>SG-80A, Lubrizol, Wickliffe, USA) was spin-coated on glass coverslips (Thermo Fisher Scientific, Waltham, USA), glass disks (Borofloat<sup>®</sup>, Berliner Glas KG, Berlin, Germany) and QCM crystals (QSX 303 SiO<sub>2</sub>, Biolin Scientific) to receive thin polymer films. For that purpose, TPU granulate was dissolved ( $c = 0.5$  wt %) in tetrahydrofuran (THF) (Sigma-Aldrich), and subsequently filtered (0.2  $\mu$ m PTFE syringe filter, Sigma-Aldrich). RCA cleaning, silanization, spin-coating, and drying procedure were performed analogously to the method described for PC. The identity of the spin-coated layers was confirmed by ellipsometry and a shift in wettability and surface roughness.

### 6.1.3 Teflon AF

For the fabrication of Teflon AF surfaces, a solution of Teflon<sup>®</sup> AF (DuPont, Neu-Isenburg, Germany) and solvent Fluorinert<sup>™</sup> FC-77 (Sigma-Aldrich) was prepared in a ratio of 1:5 and subsequently filtered (0.2  $\mu\text{m}$  PTFE syringe filter, Sigma-Aldrich). In parallel, glass coverslips (Thermo Fisher Scientific) or glass disks (Borofloat<sup>®</sup>, Berliner Glas KG) were cleaned according to standard RCA cleaning-protocol [238], air-plasma treated (plasma cleaner, Harrick Scientific Products, USA), and silanized with HMDS (Sigma-Aldrich). Subsequently, surfaces were spin-coated (LabSpin 6, Süß MicroTec) applying the following parameters: time = 30 s, speed = 3000 rpm, and acceleration = 3000 rpm s<sup>-1</sup> and dried at 160 °C for 1 hour. Spin-coating parameters were established in previous studies [87, 239].

### 6.1.4 Glass

Glass coverslips (Thermo Fisher Scientific) or glass disks (Borofloat<sup>®</sup>, Berliner Glas KG) were cleaned according to standard RCA cleaning-protocol [238] and placed into deionized water until usage.

## 6.2 Anchor polymer coatings

All AP coatings used in this study were synthesized and kindly provided by André Ruland. The detailed synthesis strategy is described in [18] and briefly summarized here for a better understanding of the project.

### 6.2.1 Synthesis of modified styrene-maleic acid copolymers

Styrene-maleic anhydride (SMAnh) copolymers XIRAN<sup>®</sup> SZ 10010, 26120, and 30010 were kindly provided by Polyscope Polymers (Geleen, the Netherlands); homofunctional polyethylene glycols ( $\alpha$ -Methoxy- $\omega$ -amino PEG, H<sub>2</sub>N-PEG-Me) were purchased from Rapp Polymere (Tübingen, Germany). After transferring SMAnh granulate into powder form, it was dissolved in THF; PEG was dissolved in a mixture of THF and deionized water (ratio 10:1). For PEGylation reaction, both solutions were combined under vigorous stirring for 48 hours at room temperature (RT). Subsequently, the reaction mixture was purified by dialysis against 1 M NaCl (3 $\times$ ) and deionized water (3 $\times$ ), lyophilized, and stored at RT until usage. The molar excess of PEG for this synthesis was calculated as a function of the polymerization degree



of maleic anhydride monomers and the anticipated degree of PEGylation (50 % and 100 %, respectively). The reaction scheme of this process is presented in Figure 6.1.

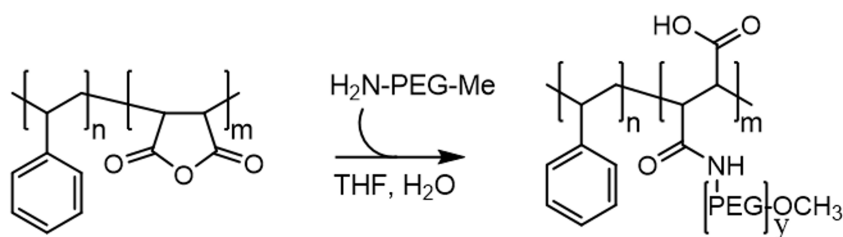


**Figure 6.1:** Synthesis of AP derivatives: APs were obtained by amide bond formation between SManh and  $\alpha$ -Methoxy- $\omega$ -amino PEG, from [18].

The resulting AP derivatives were named according to the following nomenclature:

$$\text{MW}_{\text{bb}} - \text{MA}\% - \text{PEG}/\text{S} - \text{MW}_{\text{PEG}}$$

Hereby,  $\text{MW}_{\text{bb}}$  refers to the average molecular weight of the backbone in kDa, MA % to the percentage of maleic acid groups, PEG/S to the number of PEG monomer units per number of styrene monomer units, and  $\text{MW}_{\text{PEG}}$  to the average molecular weight of the PEG chain in kDa.

Table 6.1 presents all AP derivatives applied in this study.

**Table 6.1:** Synthesized AP derivates applied in this study including SManh backbone, PEGylation degree, and molecular weight of PEG.

| AP derivative | SManh (brand name)          | PEGylation degree | $\text{MW}_{\text{PEG}}$ |
|---------------|-----------------------------|-------------------|--------------------------|
| 10-10-6-2     | XIRAN <sup>®</sup> SZ 10010 | 100 %             | 2 kDa                    |
| 120-30-13-2   | XIRAN <sup>®</sup> SZ 26120 | 100 %             | 2 kDa                    |
| 10-30-16-2    | XIRAN <sup>®</sup> SZ 30010 | 100 %             | 2 kDa                    |
| 10-30-8-2     | XIRAN <sup>®</sup> SZ 30010 | 50 %              | 2 kDa                    |
| 10-30-165-20  | XIRAN <sup>®</sup> SZ 30010 | 100 %             | 20 kDa                   |

### 6.2.2 Hexetidine functionalization

For hexetidine functionalization of APs, hexetidine-maleimide was first synthesized by mixing a solution of N-(3-maleimidopropionyloxy)-succinimide (Merck, Darmstadt, Germany) and hexetidine (Merck) in dimethylformamide (DMF).

In parallel, SMANh copolymer XIRAN<sup>®</sup> SZ 30010 and heterofunctional PEG ( $\alpha$ -amino- $\omega$ -tritylthio, H<sub>2</sub>N-PEG-S-Trt) (Rapp Polymere) were dissolved, combined, stirred for 5 days at RT, purified via dialysis, and lyophilized. Subsequently, trityl protection group of the resulting AP was deprotected by dissolving it in a mixture of trifluoroacetic acid (TFA), phenol, tri-isopropyl silane and deionized water. The reaction mixture was stirred for 3 hours at RT, diluted and dialyzed. To prevent oxidation of the thiol groups, the dialysis solution was vigorously saturated by bubbled nitrogen. Subsequently, the product was purified and lyophilized.

To functionalize the resulting AP-SH with hexetidine-maleimide, the products were dissolved in DMF and phosphate buffered saline (PBS) (Sigma-Aldrich), respectively. Both solutions were combined, stirred for 4 h at RT, purified by dialysis, lyophilized, and stored at -20 °C until usage. The chemical reaction of this process is presented in Figure 6.2.

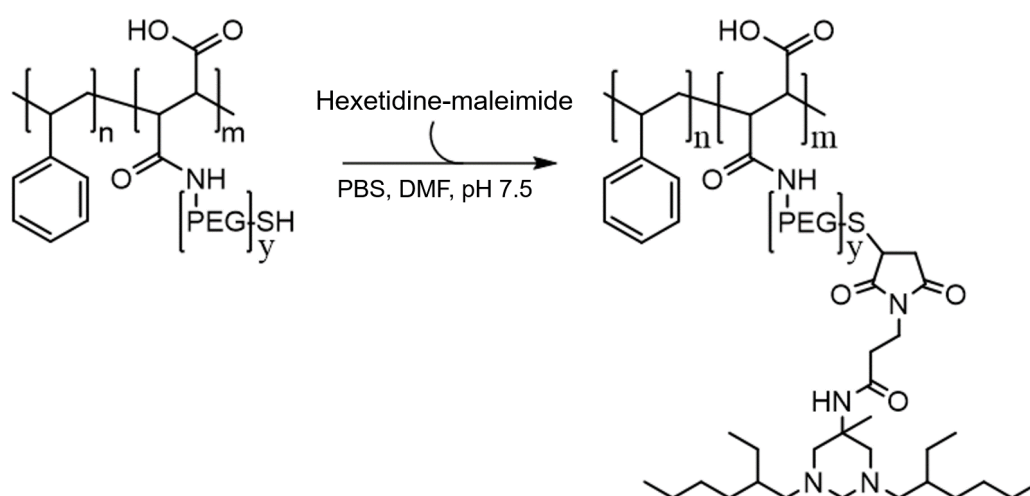


**Figure 6.2:** Synthesis of hexetidine functionalized AP derivatives: Conjugation of hexetidine-maleimide to free thiol moieties of  $\alpha$ -amino- $\omega$ -tritylthio PEG was achieved by Michael type (click)-reactions, from [18].

### 6.2.3 Fluorescence functionalization

To obtain fluorescence-labeled APs (AP-Atto 647N), fluorescent dye Atto 647N-NH<sub>2</sub> (Atto-TEC GmbH, Siegen, Germany), SMAnh copolymers (XIRAN<sup>®</sup> SZ 30010), and PEG ( $\alpha$ -Methoxy- $\omega$ -amino) were first dissolved in THF or THF-dionized water mixture. Then, Atto 647N-NH<sub>2</sub> solution was combined with SMAnh solution, N,N-Diisopropylethylamine (Merck) was supplemented, and after 10 minutes stirring at RT, the PEG solution was finally added. The reaction mixture was stirred for 5 days at RT, purified by dialysis, lyophilized, and stored at -20 °C until usage.

### 6.2.4 Application

APs were dissolved in PBS to a concentration of 1 g L<sup>-1</sup> and evenly distributed on polymer substrates PC and TPU. After 1 hour incubation time at RT, the AP solution was removed, and surfaces were rinsed twice in PBS. Coated surfaces were stored in PBS until usage (up to 24 hours).

## 6.3 Characterisation

### 6.3.1 Quartz crystal microbalance

QCM measurements with dissipation monitoring were performed on a QSense E4 (Biolin Scientific) using precoated QCM crystals. The QCM crystals are characterized by a fundamental resonance frequency of  $f_0 = 5$  MHz and a sensitivity constant of  $C = 0.177$  mg m<sup>2</sup> Hz<sup>-1</sup>. To establish a stable baseline, PBS was first pumped over the crystals within the flow cell. Subsequently, it was replaced by the AP solution ( $c = 1$  g L<sup>-1</sup> in PBS), which was then pumped through the cell at a flow rate of 0.1 mL min<sup>-1</sup>. After the baseline was stable again, the AP solution was replaced by PBS to remove loosely bound polymer chains. Polymer adsorption was measured for the 3rd to 11th overtone of the fundamental frequency at 20 °C. QSense Dfind software (Biolin) was used to collect and analyze data applying the Sauerbrey model [240]. Thickness of the polymer layers were determined after initial adsorption and after desorption process (rinsing with PBS). Retention  $R$  was calculated as presented in Equation 6.1, with  $l_{ads}$  as layer thickness after initial adsorption and  $l_{des}$  as layer thickness after subsequent desorption process.

$$R = \frac{l_{des}}{l_{ads}} \cdot 100 \% \quad (6.1)$$

### 6.3.2 Contact angle

Surface wettability was determined via dynamic contact angle measurements using an OCA30 goniometer (Data Physics Instruments GmbH, Filderstadt, Germany). Operational mode “sessile drop - needle in” was applied to measure advancing and receding contact angle. Here, an automated syringe dispensed a 2  $\mu\text{L}$  droplet of degassed deionized water to build a bridge between needle and sample surface. After defining a baseline between droplet and surface using image processing software SCA202, the automated syringe dispensed 20  $\mu\text{L}$  water at a speed of 0.5  $\mu\text{L min}^{-1}$ . After stabilization of the droplet shape, the volume of 20  $\mu\text{L}$  was re-dispensed. Values of contact angles were permanently obtained by the “tracking mode” of the software. Contact angle hysteresis was calculated as the difference between maximum and minimum contact angle.

### 6.3.3 Protein adsorption

Fluorescence-labeled bovine serum albumin (BSA) and fibrinogen (FGN) were used to analyze protein adsorption on AP coatings. Alexa Fluor 488-conjugated FGN (Invitrogen™ Fibrinogen from human plasma, Alexa Fluor™ 488 Conjugate) was purchased from Sigma-Aldrich, BSA was conjugated with Atto 565 NHS ester (Sigma-Aldrich) according to the manufacturer’s instructions. The average labelling degree for BSA Atto 565 was 0.7 mol of dye per mol of protein. BSA Atto 565 and FGN Alexa Fluor 488 were dissolved in PBS to a concentration of 100  $\mu\text{g mL}^{-1}$ . AP coated and control surfaces were immersed in BSA and FGN solutions, respectively. Fluorescence intensity (indicating protein adsorption) was analyzed after 1 h, 4 h, and 24 h using a Leica confocal laser scanning microscope SP5 (Leica Microsystems, Germany) equipped with a 40 $\times$ , NA1.25 oil immersion objective (Leica) with appropriate filter setting for Atto 488 and Alexa Fluor 565. Each surface was imaged on at least five randomly selected locations. Raw data images were processed by open-source software Fiji [217]. Measured fluorescence intensities were normalized to values of the control surfaces (PC or TPU) at each time point.

### 6.3.4 Long-term stability

To analyze the long-term stability of AP coatings, pre-coated coverslips ( $d = 13 \text{ mm}$ ) were exposed to various physiological media for up to 14 days. Therefore, PC and TPU surfaces were coated with 1  $\text{g L}^{-1}$  AP-Atto 647N. After 1 hour incubation time, the surfaces were rinsed in PBS and placed into 24-well plates (TPP tissue culture plates, Merck). To remove unbound AP, the coverslips were immersed into 1 mL

PBS supplemented with 0.1 % ProClin™ 950 (Sigma-Aldrich) and incubated for 24 h at 37 °C under constant agitation. Thereafter, initial fluorescence intensity values were determined using fluorescence scanner FLA 5100 (Fujifilm, Minato, Japan). Subsequently, PBS was replaced by one of the following solutions: a buffer solution of tris-(hydroxymethyl)-aminomethan (Tris)-HCl (50 mM) and BSA (40 mg mL<sup>-1</sup>), citrated plasma (sodium citrate dihydrate 0.14 M, Haema, Leipzig, Germany), Tween20 (4 mM) and freshly prepared PBS. Again, 0.1 % ProClin™ 950 was added to each solution to avoid bacterial contaminations. Fluorescence intensity of the surfaces was examined every 3 to 4 days. The media were removed for the measurement and subsequently replaced with fresh solutions. In between measurements, all well plates were incubated at 37 °C under constant agitation. Data collection and analysis was performed using multi gauge software (Minato). Measured intensities were normalized to initial fluorescence intensity as presented in Equation 6.2, with  $F_r$  as relative fluorescence intensity in %,  $F_{t=i}$  as fluorescence intensity at different time points, and  $F_{t=0}$  as initial fluorescence intensity.

$$F_r(t) = \frac{F_{t=i}}{F_{t=0}} \cdot 100 \% \quad (6.2)$$

### 6.3.5 Hemocompatibility

This section focuses on the procedure and analysis for quasi-static hemocompatibility assessment. However, selected analytical methods were applied analogously during the development of the introduced *in vitro* flow model (described in Chapter 4).

#### Quasi-static blood incubation

The quasi-static assessment of hemocompatibility was performed with in-house designed incubation chambers [169] (see Figure 6.3). For this purpose, venous blood was freshly drawn from two ABO-compatible healthy donors who stated that they had not taken any anti-inflammatory medication within the last 10 days. The obtained blood was anticoagulated with 1.5 IU mL<sup>-1</sup> heparin (Ratiopharm, Ulm, Germany) and pooled after excluding an elevated inflammation level (mö-quick CRP-Test, möLab, Langenfeld, Germany). Here, a blood sample was taken and analyzed as initial sample. The materials to be investigated (either spin-coated on Borofloat® glass disks or punched to a diameter of 25 mm), were installed as top and bottom surfaces in the incubation chambers. After rinsing the cavity of the chambers with PBS, they were filled with 1.95 mL of blood. All blood chambers were incubated for 2 hours under permanent overhead rotation to avoid sedimentation of blood cells. Subsequently,

both whole blood and incubated surfaces were removed from the chambers for further analysis.



**Figure 6.3:** Blood incubation chamber for quasi-static hemocompatibility assessment.

### Blood sample analysis

The collected blood samples were analyzed for inflammatory and hemostasis parameters as well as hemolysis, blood gas stability, and pH.

Leukocyte and platelet numbers were analyzed with whole blood cell counter Coulter Ac-T diff Hematology Analyzer (Beckman Coulter GmbH, Krefeld, Germany). Each sample was analyzed at least three times to compensate for measurement inaccuracies of the instrument. To calculate leukocyte and platelet loss after incubation, the obtained cell counts were normalized to the initial sample.

Fluorescence-activated cell scanning (FACS) (LSRFortessa™, BD Biosciences, Franklin Lakes, USA) was deployed to analyze granulocyte and platelet activation. For that purpose, blood cells were stained for 30 minutes with anti-CD11b-PacificBlue (BioLegend, San Diego, USA), anti-CD14-APC (BD Biosciences), anti-CD15-PE (BioLegend), and anti-CD41a-FITC (BD Biosciences). In addition, NaN<sub>3</sub> (0.1 % sodium azide, Sigma-Aldrich) was supplemented to inhibit cell activation during the staining process [241]. Subsequent to staining, FACSlyse (BD Biosciences) was added to the samples to lyse erythrocytes and fix remaining cells. As positive activation control, initial blood was incubated with 100 EU mL<sup>-1</sup> control standard endotoxin (CSE, Associates of Cape Cod, East Falmouth, USA) for 2 h at 37 °C. Raw FACS data were evaluated using FACS Diva software (BD Biosciences). Leukocytes were identified according to their characteristic pattern in the forward vs. side scatter plot and further differentiated in monocytes (CD14<sup>+</sup> cells) and granulocytes (CD15<sup>+</sup> cells).

Granulocytes that were also CD41<sup>+</sup> were regarded as granulocyte-platelet-conjugates. The median of CD11b signal intensity of the granulocyte population was quantified and normalized to the intensity of endotoxin-activated granulocytes.

Commercial enzyme-linked immunosorbent assays (ELISAs) were utilized to analyze the release of PF4 (Zymutest PF4, Hyphen BioMed, Neuville-sur-Oise, France), complement fragment 5a (C5a) (Enzygnost C5a micro, DRG Diagnostica, Marburg, Germany), and F1+2 (Enzygnost F1+2, Siemens Healthcare, Marburg, Germany). For this purpose, the collected blood was anticoagulated and centrifuged, and the obtained plasma was stored at -80°C until analysis. Measurements were performed according to the manufacturer's instructions.

Hemolysis was analyzed by a colorimetric assay using Drabkin's solution. For this purpose, whole blood was anticoagulated with 10 mM ethylenediaminetetraacetic acid (EDTA) (Merck, Darmstadt, Germany) and centrifuged for 30 minutes at 2600 g (Benchtop Centrifuge, Sigma-Aldrich). 20 µL of the collected plasma was then mixed with 180 µL of Drabkin's solution and examined for the formation of cyanmethemoglobin in a platereader (Spark<sup>®</sup> Multimode Microplate Reader, Tecan, Crailsheim, Germany) with a wavelength of 540 nm. A mixture of whole blood and distilled water (ratio 1:10) served as reference for 10 % hemolysis, and a serial dilution of it was applied as standard.

The stability of blood gases and pH was controlled with blood gas analyzer Combiline (Eschweiler, Kiel, Germany).

### Sample surface analysis

Subsequent to blood incubation, test surfaces were removed from the chambers and washed three times in PBS to remove all non-adherent cells.

Samples for fluorescence microscopy were fixed in 2 % formaldehyde (Sigma-Aldrich) for at least 1 hour, and washed in PBS (3×). Subsequently, adherent cells were permeabilized in 0.2 % saponin (Sigma-Aldrich) and stained with 4,6-diamidine-2-phenylindole-dihydrochlorid (DAPI) and 3,3'-dihexyl-oxacarbocyaniniodid (DiOC<sub>6</sub>). Both dyes were utilized in a concentration of 1 µg mL<sup>-1</sup>. The test surfaces were imaged using a wide-field fluorescence microscope (Zeiss Axio Observer, equipped with a Zeiss EC Plan-Neofluar 20×/0.5 Ph2 objective, Zeiss, Jena, Germany) at appropriate filter setting for DAPI and DiOC<sub>6</sub>. On each surface, five images of randomly selected locations were taken and analyzed for cell adhesion and morphological changes.

Samples for scanning electron microscopy (SEM) were fixed with 2 % glutaraldehyde (AppliChem, Darmstadt, Germany) for at least 1 hour, washed in PBS (3×), de-

hydrated in ascending ethanol series, and air-dried. Before SEM imaging (ESEM Quattro S, Thermo Fisher Scientific), all samples were sputtered with gold (SCD 050, BAL-TEC, Schalksmühle, Germany). SEM analysis was performed in high vacuum mode, using an analytical working distance of 10 mm and acceleration voltage of 10 kV. Three images were acquired from each test surface at magnifications of both  $1.000\times$  and  $5.000\times$  to analyze blood cell adhesion and morphology changes due to immune reactions.

### **Ethical approval**

The study was approved by the Ethics Committee of the Sächsische Landesärztekammer. All blood experiments were performed in compliance with the relevant laws and institutional guidelines. Informed consent of the donors was obtained for any experimentation with human whole blood.

### **6.3.6 Bacteria experiments**

#### **Bacterial strain**

GFP-expressing Gram-positive *S. aureus* RN4220 lab strain (GFP *S. aureus*) was applied to assess antimicrobial properties of the coatings. Fluorescence expression was achieved by replacement of the *spa* gene by pN25-gfpP7 [242, 243]. The strain was kindly provided by Mariana Pinho (ITQB, Lisbon, Portugal) and stored in glycerol stocks at  $-80^{\circ}\text{C}$ .

#### **Bacterial cultivation and surface incubation**

Bacteria from  $-80^{\circ}\text{C}$  storage were streaked on blood agar plates that were previously prepared with blood agar base (Sigma-Aldrich), supplemented with 5 % defibrinated sheep blood (Thermo Fisher Scientific). After overnight incubation at  $37^{\circ}\text{C}$ , plates were stored at  $4^{\circ}\text{C}$  until usage.

For bacterial assays, single bacterial colonies were harvested from the agar plates and incubated overnight in 2 mL lysogeny broth (LB) media (Sigma-Aldrich) at  $37^{\circ}\text{C}$  under constant shaking (220 rpm). Overnight cultures were then centrifuged, the supernatant discarded, and the bacterial pellet resuspended in PBS. The optical density of the suspension was determined by spectrophotometer (Eppendorf BioPhotometer<sup>®</sup>, Eppendorf, Hamburg, Germany) using a wavelength of 600 nm, and subsequently diluted to a value of  $\text{OD}_{600} = 0.1$ .



For surface incubation, the prepared bacterial suspensions were pipetted onto the samples until they were completely covered. This was followed by a one-hour incubation period at 37 °C under static conditions. The surfaces were then rinsed with PBS to remove non-adherent bacteria and used immediately.

### **Bacterial coverage under static conditions**

AP coated and pre-colonized test surfaces were placed into sterile 6-well plates containing fresh low-nutrient M9\* medium (M9 medium supplemented with 2 % casein hydrolysate broth and 0.4 % glucose, diluted 1:100 in sterile water). Bacterial colonization was assessed by phase-contrast-microscopy (Zeiss Axiovert 200, Zeiss), equipped with an Axiocam 503 mono CCD and a Zeiss EC Plan-Neofluar 40×/0.6NA objective) initially and after 4 and 24 hours incubation time at 37 °C. At least ten images were taken from each sample at randomly selected locations. Between measurements, samples were incubated at 37 °C in fresh M9\* medium. In addition, surfaces were gently washed before each measurement to remove non-adherent cells. Microscopy images were analyzed with the open-source software Fiji [217] using a bandpass filter and manual threshold to determine the total bacterial coverage (as percentage of the covered surface area).

## **6.4 *In vitro* flow model**

### **6.4.1 Rotation device**

The detailed design of the rotation device is described in Chapter 4.3.4. The components utilized for this project are displayed in Table 6.2. They were either purchased by Eckstein Komponente (Clausthal-Zellerfeld, Germany) or Conrad Electronic (Hirschau, Germany). The software describing the movement of the motor (20 half-turns per minute) was written in C++ using open-source Arduino Software (see Listings A.1).

The design for casing and plate holder was created using the software Autodesk® Inventor (San Rafael, USA). The resulting 3D models were imported to Ultimaker Cura software (Ultimaker, Utrecht, Netherlands), where they were sliced into layers and converted into the printer-specific g-code. The subsequent printing was performed on an Ultimaker 3 (Ultimaker) 3D printer using polylactid (PLA – M0751 white filament, Ultimaker) as print material.

**Table 6.2:** List of components for construction of the rotation device.

| Component                                      | Distributor         |
|--|---------------------|
| Pololu Stepper Motor NEMA 17                   | Eckstein Komponente |
| Pololu DRV8825 Stepper Motor Driver Carrier    | Eckstein Komponente |
| Arduino Board Nano ATmega328                   | Conrad Electronic   |
| Europalatin Hartpapier SU527453                | Conrad Electronic   |
| Faber Litze SiF 1 x 0.50 mm <sup>2</sup>       | Conrad Electronic   |
| Elektrolytkondensator, 1000 $\mu$ F $\pm$ 20 % | Conrad Electronic   |
| Buchsenleiste 40 BL40/1G8                      | Conrad Electronic   |
| Steckernetzteil SYS 1308-2412-W2E EURO         | Conrad Electronic   |
| Niedervolt-Steckverbinder Buchse DC12-F        | Conrad Electronic   |
| Anschlusskabel Digitus USB 2.0                 | Conrad Electronic   |

### 6.4.2 Model setup

The general setup of the *in vitro* flow model is elucidated in Chapter 4.4.1. Here, applied materials and components as well as manufacturing processes are described in more detail.

#### Pumping unit

All components of the pumping unit were kindly provided by Fraunhofer IWS (Fraunhofer Institute for Material and Beam Technology IWS, Dresden, Germany). To operate the triple-pump-chip, it had to be clamped into a holder that is connected to compressed air. The control unit “MPScontrol” (Fraunhofer IWS, Dresden, Germany) regulated the compressed air and vacuum that was responsible for membrane deflection in the triple-pump-chip. Here, maximum pressure was set to 300 mbar. The control unit allows to set the frequency of the pumping cycle between 1 and 150 beats per minute (bpm), corresponding to pumping speeds of 5.4 to 600  $\mu$ L min<sup>-1</sup>. In this study, a pumping frequency of 6 bpm (32.4  $\mu$ L min<sup>-1</sup>) was applied. The intermediary air chambers (15 mL, 50 mL, or 250 mL) within the damper “MPShemodyn” (Fraunhofer IWS) dampened the pressure of the air flow, thus influencing the hemodynamic pumping behavior (see Chapter 4.4.3.)

#### Blood stream unit

The microchannel chips were manufactured and kindly provided by Fraunhofer IWS. Top and intermediate layers of the chips are made of PC, while the material of the bottom layer is adaptable. Here, the materials PC, TPU, Teflon, and glass were

applied, after being prepared as described in Chapter 6.1. The intermediate layer was treated by a laser cutter (microSTRUCT<sup>TM</sup> vario, 3D-Micromac AG) to obtain the desired channel geometry. Depending on the material of the bottom, the single layers were either merged by thermal bonding (LaboPress P300S, Vogt Maschinenbau GmbH) (PC), or by adhesive tape (3M<sup>TM</sup>Adhesive Transfer Tape 94714 LE, 3M, Neuss, Germany) (TPU, Teflon AF, glass). The Luer Lock connectors (Fluidic 303, Microfluidic ChipShop) for in- and outlet were bonded to the top layer by 2-component liquid epoxy adhesive Loctite<sup>®</sup> EA M-31 CL (Henkel). In general, the design of the channels is customizable: here, dimensions of 3 mm × 40 mm (channel area), and 0.25 mm (channel height) were used.

Whole blood was stored in a blood bag for veterinary medicine (feline blood collection bag, Alvedia, Limonest, France) that holds up to 100 mL. From the reservoir, blood was directed through Luer Lock connection tubes (B. Braun, Melsungen, Germany) and separated into the three independent channels by three-way stopcocks (Fresenius Kabi, Bad Homburg, Germany). After passing through the microchannel chips, blood was collected in 5 mL reaction tubes (Eppendorf, Hamburg, Germany). The whole blood stream unit was placed into an incubator set to 37 °C and 5 % CO<sub>2</sub>.

### 6.4.3 Micro-particle image velocimetry

Micro-PIV measurements were performed by Stephan Behrens (Fraunhofer IWS), as described elsewhere [244]. In brief, the *in vitro* flow model was operated with a suspension containing 10 µm CML latex beads (4 w/v %, 10 µm, Life Technologies, Schwerte, Germany) and a mixture of water, glycerin and xanthan gum that mimics the viscoelastic shear thinning behavior of blood [245]. The motion of the latex beads was tracked in the middle of the microchannel chip using a Zeiss Primovert inverted microscope (Zeiss) coupled with a high-speed camera (Baumer HXC40, Baumer Optronic, Radeberg, Germany). The measured volume flow ( $Q$ ), viscosity of whole blood ( $\eta = 3.5$  cP), as well as channel height ( $h = 250$  µm) and width ( $w = 3$  mm) were applied to calculate the corresponding WSS ( $\tau$ ) (see Equation 6.3). Measurements were performed with a pumping speed of 6 bpm and damping adjustments of 0, 15, and 50 mL.

$$\tau = \frac{6 \cdot Q \cdot \eta}{w \cdot h^2} \quad (6.3)$$

#### 6.4.4 Workflow

Figure 6.4 presents the workflow of the developed *in vitro* flow model.

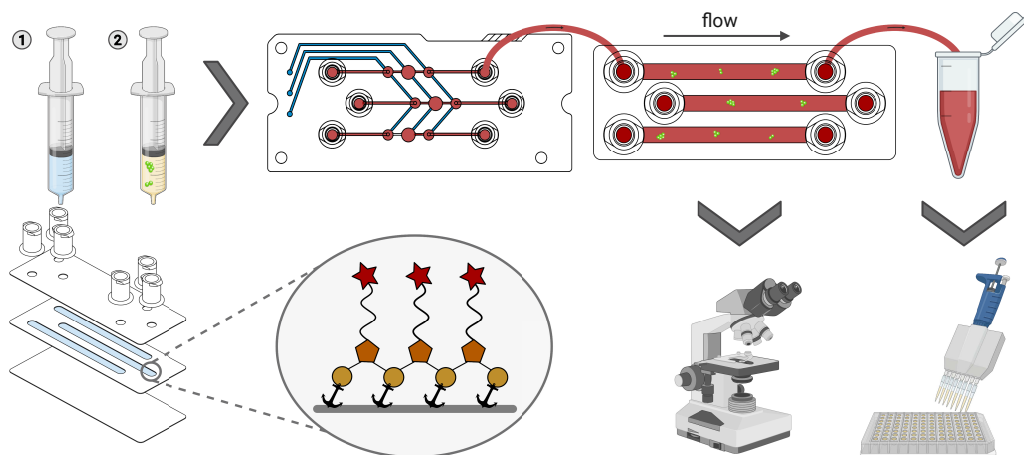


**Figure 6.4:** Workflow of *in vitro* blood flow model; Preparation: the three-layer microchannel chip was coated with the AP solution (1 hour at RT) and subsequently incubated with bacterial solution (1 hour at 37°C); Experiment: whole blood is pumped from a rotating reservoir over the pre-treated microchannel chip using a pneumatic-driven triple-pump-chip; Analysis: fluorescence microscopy of microchannel chip, and FACS and ELISA measurements of collected blood samples.

As a first step, microchannel chips had to undergo a pre-treatment. To apply antimicrobial coatings, prepared AP solutions ( $c = 1 \text{ g L}^{-1}$  in PBS) were filled into syringes and injected into the channels through Luer Locks connectors. After an incubation time of 1 hours at RT, the channels were rinsed with PBS in order to remove unbound polymer. For control surfaces, this step was skipped. The second part of pre-treatment comprised the pre-colonization of the test surfaces with bacteria. For this purpose, an overnight culture of GFP *S. aureus* was diluted to an optical density of  $\text{OD}_{600} = 0.1$  in PBS. The bacterial suspension was then injected into the microchannel chips and incubated for 1 hour at a temperature of 37°C. After incubation, the chip was carefully rinsed with PBS to remove non-adherent bacteria. After pre-treatment, the microchannel chip was inserted into the model setup between triple-pump-chip and collection tubes.

Directly after completing pre-treatment of the microchannel chip, the whole system including both chips and connection tubes was carefully flushed with PBS. In addition, the pump was activated and used to pump PBS over the system during blood collection. Whole blood was then drawn from two ABO-compatible healthy donors (40 mL each), anticoagulated with 5  $\mu\text{M}$  hirudin (Refludan, Celgene, Munich, Germany), and pooled.

After filling whole blood into the blood bag and placing it onto the rotation device, it was interconnected with the connection tubes of the flow model. In consequence, blood was drawn from the reservoir over the triple-pump chip to the microchannel chip. After passing the microchannel chip with the test surface, blood was collected in 5 mL tubes. To allow time-dependent analysis, tubes were exchanged after every hour. To exclude the possibility that inflammatory and hemostatic reactions had already occurred within the blood reservoir, another blood sample was taken from the blood bag after the incubation period of 4 hours.

Blood samples were analyzed for the following parameters: granulocyte-platelet-conjugates and PF4 (hemostasis), C5a and CD11b (inflammation), hemolysis, pH, and blood gas stability. Measurements were performed analogously to the methods used for static hemocompatibility assessment (see Chapter 6.3.5). Subsequent to blood incubation, bacterial colonization of the microchannel chip was quantified. Therefore, test surfaces were imaged with a wide-field fluorescence microscope (Zeiss Axio Observer, equipped with a Zeiss EC Plan-Neofluar 20 $\times$ /0.5 Ph2 objective, Zeiss) using appropriate filter settings for GFP. At least ten images from different locations were taken of each test surface. Open-source software Fiji [217] was applied for raw image processing, determining bacterial coverage in percent.

To examine the impact of WSS on bacterial coverage over a longer time period, the flow model was also operated without blood. The general setup was identical as described above, but whole blood was replaced by LB medium. Bacterial colonization was quantified after 4 and 24 hours via phase-contrast microscopy (Zeiss Axiovert 200 equipped with an Axiocam 503 mono CCD and a Zeiss EC Plan-Neofluar 40 $\times$ /0.6NA objective, Zeiss) and image-processing software Fiji. The LB medium was discarded after passing the microchannel chip. The available blood volume allowed parallel testing of two different surface materials (= two microchannel chips).

## 6.5 Statistical analysis

Data are either presented in box plots with whiskers indicating the 5-95 percentile (mean is shown as +), bar charts presenting mean  $\pm$  standard deviation, or line charts presenting the mean  $\pm$  standard deviation of each time point. Statistical analysis was performed by unpaired two-tailed t-tests or one-way analysis of variance (ANOVA) with subsequent Holm-Sidak multiple comparisons. Statistical significance was defined as  $p < 0.05$  (\* $p < 0.05$ , \*\* $p < 0.01$ ).

# List of Figures

|      |   |    |
|------|---|----|
| 1.1  | Approach of the thesis project, divided into two parts: Coating evaluation and model development . . . . .  | 4  |
| 2.1  | Infection pathways of medical devices illustrated by the example of a catheter . . . . .  | 7  |
| 2.2  | Biofilm life cycle showing the five phases of biofilm development: attachment, multiplication, exodus, maturation, and dispersal . . . . .  | 8  |
| 2.3  | Single bacteria and biofilms under the influence of flow conditions . . .   | 11 |
| 2.4  | Simplified illustration of the intrinsic and extrinsic pathways of coagulation cascade, triggered by the presence of bacteria . . . . .   | 15 |
| 2.5  | Categories of antimicrobial coatings commonly applied in medical devices  | 17 |
| 2.6  | Procedure of medical device development in accordance to Medical Device Regulation including design, evidence collection, conformity assessment, and post-market surveillance . . . . . | 22 |
| 3.1  | Scheme of compositional and functional features of AP coatings . . . .  | 26 |
| 3.2  | Chemical structure of PC including aromatic hydroxy compounds . . .   | 27 |
| 3.3  | Chemical structure of aliphatic polyether-based TPU . . . . .   | 28 |
| 3.4  | QCM-based measurements displaying adsorption and retention properties of selected anti-adhesive APs . . . . .   | 29 |
| 3.5  | Dynamic water contact angle of AP coated and uncoated polymer substrates PC and TPU . . . . .   | 31 |
| 3.6  | Adsorption of fluorescence-labeled BSA and FGN on AP coatings, normalized to the bare bare polymer substrate . . . . .  | 33 |
| 3.7  | Long-term stability of AP 10-30-16-2 under physiological conditions . .   | 34 |
| 3.8  | Static hemocompatibility assessment of anti-adhesive AP coatings in comparison to untreated polymer substrate PC . . . . .  | 36 |
| 3.9  | Antimicrobial activity of the investigated AP coatings compared to reference surface PC . . . . .   | 38 |
| 3.10 | Static hemocompatibility assessment of AP 10-30-16-2 and 10-30-16-2-Hex in comparison to control surfaces glass, Teflon AF, TPU, and PC . . . .   | 41 |
| 3.11 | Analysis of antimicrobial activity on the examined surfaces PC, 10-30-16-2, and 10-30-16-2-Hex after static incubation in M9* media at 37 °C . . . .                                    | 43 |
| 4.1  | Hemolysis caused by the anti-sedimentation prototype of the commercial pumping system from Biophysical Tools . . . . .  | 54 |

|      |  |       |
|------|--|-------|
| 4.2  | Schematic topview of the triple-pump-chip by Fraunhofer IWS with fluidic parts in red and pneumatic parts in blue . . . . .                  | 55    |
| 4.3  | Exploded view of microchannel chip design, composed of three layers . .  | 56    |
| 4.4  | Circuit diagram for a rotation device with micro-controller, motor driver carrier, and stepper motor . . . . .                               | 58    |
| 4.5  | Models for 3D printing of casing and holder for rotation device . . . . .  | 59    |
| 4.6  | Photograph of final rotation device . . . . .  | 60    |
| 4.7  | Exemplary image of GFP-expressing <i>S. aureus</i> on PC after blood incubation  | 63    |
| 4.8  | General setup of the <i>in vitro</i> flow model . . . . .  | 65    |
| 4.9  | Effects of blood incubation with heparin-anticoagulated blood in microchannel chip . . . . .   | 66    |
| 4.10 | Sedimentation of blood cells within the connection tubes . . . . .   | 68    |
| 4.11 | Female Luer Lock connectors, before enlarging the diameter . . . . .   | 69    |
| 4.12 | Blood activation in dependence of channel height . . . . .   | 71    |
| 4.13 | Volume flow and corresponding WSS in the microchannel chip . . . . .   | 72    |
| 4.14 | Validation of the <i>in vitro</i> flow model: Antimicrobial activity . . . . .   | 76    |
| 4.15 | Validation of the <i>in vitro</i> flow model: Blood activation . . . . .   | 77    |
| 4.16 | Validation of the <i>in vitro</i> flow model: Influence of WSS . . . . .   | 79    |
| 6.1  | Synthesis of AP derivatives . . . . .  | 91    |
| 6.2  | Synthesis of hexetidine functionalized AP derivatives . . . . .  | 92    |
| 6.3  | Blood incubation chamber for quasi-static hemocompatibility assessment   | 96    |
| 6.4  | Workflow of <i>in vitro</i> blood flow model . . . . .   | 102   |
| A.1  | Static hemocompatibility assessment of anti-adhesive AP coatings, additional data . . . . .  | xxi   |
| A.2  | Static hemocompatibility assessment of AP 10-30-16-2 and 10-30-16-2-Hex in comparison to various control surfaces, additional data . . . . . | xxii  |
| A.3  | Exemplary phase-contrast microscopy images taken after 0, 4, and 24 hours incubation in M9* medium on antimicrobial surfaces . . . . .       | xxiii |
| A.4  | Blood activation in reservoir after 4 hours incubation time . . . . .  | xxiii |
| A.5  | Blood activation of materials incorporated in microchannel chip . . . . .  | xxiv  |
| A.6  | Blood activation induced by GFP <i>S. aureus</i> pre-seeded on TPU . . . . .   | xxv   |
| A.7  | Validation of the <i>in vitro</i> flow model: Formation of granulocyte-platelet-conjugates . . . . .   | xxv   |
| A.8  | Validation of the <i>in vitro</i> flow model: Correlation between bacterial coverage and blood activation . . . . .                          | xxvi  |
| A.9  | Technical drawing of casing body for rotation device . . . . .   | xxix  |
| A.10 | Technical drawing of casing cover for rotation device . . . . .  | xxx   |
| A.11 | Technical drawing of blood bag holder for rotation device . . . . .  | xxxi  |

# List of Tables

|     |   |     |
|-----|---|-----|
| 3.1 | Range of molecular characteristics of selected AP coatings . . . . .  | 27  |
| 4.1 | Reduction of bacterial coverage by anti-adhesive and contact-killing AP coating in dependence of the performed <i>in vitro</i> test . . . . . | 82  |
| 6.1 | Synthesized AP derivates applied in this study including SMAnh backbone, PEGylation degree, and molecular weight of PEG . . . . .             | 91  |
| 6.2 | List of components for construction of the rotation device . . . . .  | 100 |



# Bibliography

- [1] M. B. Bracken, “Why animal studies are often poor predictors of human reactions to exposure”, *Journal of the Royal Society of Medicine* **2009**, *102*, 120–122.
- [2] N. Shanks, R. Greek, J. Greek, “Are animal models predictive for humans?”, *Philosophy ethics and humanities in medicine: PEHM* **2009**, *4*, 2.
- [3] D. G. Hackam, D. A. Redelmeier, “Translation of research evidence from animals to humans”, *JAMA* **2006**, *296*, 1731–1732.
- [4] M. I. Martić-Kehl, R. Schibli, P. A. Schubiger, “Can animal data predict human outcome? Problems and pitfalls of translational animal research”, *European journal of nuclear medicine and molecular imaging* **2012**, *39*, 1492–1496.
- [5] A. Akhtar, “The flaws and human harms of animal experimentation”, *Cambridge quarterly of healthcare ethics: CQ: the international journal of healthcare ethics committees* **2015**, *24*, 407–419.
- [6] W. M. S. Russell, R. L. Burch, “The Principles of Humane Experimental Technique”, *Medical Journal of Australia* **1960**, *1*, 500.
- [7] European Parliament and the Council, Directive 2010/63/EU on the protection of animals used for scientific purposes, **2010**.
- [8] M. Malone, D. M. Goeres, I. Gosbell, et al., “Approaches to biofilm-associated infections: the need for standardized and relevant biofilm methods for clinical applications”, *Expert Review of Anti-infective Therapy* **2017**, *15*, 147–156.
- [9] A. E. L. Roberts, K. N. Kragh, T. Bjarnsholt, et al., “The Limitations of In Vitro Experimentation in Understanding Biofilms and Chronic Infection”, *Journal of molecular biology* **2015**, *427*, 3646–3661.
- [10] T. F. Moriarty, D. W. Grainger, R. G. Richards, “Challenges in linking preclinical anti-microbial research strategies with clinical outcomes for device-associated infections”, *European cells & materials* **2014**, *28*, 112–28, discussion 128.
- [11] B. Gottenbos, H. C. van der Mei, F. Klatter, et al., “In vitro and in vivo antimicrobial activity of covalently coupled quaternary ammonium silane coatings on silicone rubber”, *Biomaterials* **2002**, *23*, 1417–1423.
- [12] G. Subbiahdoss, I. C. S. Fernández, J. F. d. S. Domingues, et al., “In vitro interactions between bacteria, osteoblast-like cells and macrophages in the pathogenesis of biomaterial-associated infections”, *PloS one* **2011**, *6*, e24827.
- [13] A. K. Nussbaumer-Pröll, S. Knotzer, S. Eberl, et al., “Impact of erythrocytes on bacterial growth and antimicrobial activity of selected antibiotics”, *European journal of clinical microbiology & infectious diseases : official publication of the European Society of Clinical Microbiology* **2019**, *38*, 485–495.
- [14] S. Schulz, M. Maitz, S. Hänsel, et al., “Analyzing the antiseptic capacity of silver-functionalized poly(ethylene glycol)-heparin hydrogels after human whole blood exposure”, *Biomaterials science* **2018**, *6*, 1129–1139.

- [15] R. Murga, J. M. Miller, R. M. Donlan, “Biofilm formation by gram-negative bacteria on central venous catheter connectors: effect of conditioning films in a laboratory model”, *Journal of clinical microbiology* **2001**, *39*, 2294–2297.
- [16] S. Sapatnekar, K. M. Kieswetter, K. Merritt, et al., “Blood-biomaterial interactions in a flow system in the presence of bacteria: effect of protein adsorption”, *Journal of biomedical materials research* **1995**, *29*, 247–256.
- [17] M. R. Brunstedt, S. Sapatnekar, K. R. Rubin, et al., “Bacteria/blood/material interactions. I. Injected and preseeded slime-forming *Staphylococcus epidermidis* in flowing blood with biomaterials”, *Journal of biomedical materials research* **1995**, *29*, 455–466.
- [18] A. Ruland, S. Schenker, L. Schirmer, et al., “Amphiphilic Copolymers for Versatile, Facile, and In Situ Tunable Surface Biofunctionalization”, *Advanced materials* **2021**, *33*, e2102489.
- [19] S. S. Magill, J. R. Edwards, W. Bamberg, et al., “Multistate point-prevalence survey of health care-associated infections”, *The New England journal of medicine* **2014**, *370*, 1198–1208.
- [20] V. D. Rosenthal, H. M. Al-Abdely, A. A. El-Kholy, et al., “International Nosocomial Infection Control Consortium report, data summary of 50 countries for 2010-2015: Device-associated module”, *American journal of infection control* **2016**, *44*, 1495–1504.
- [21] T. C. Horan, M. Andrus, M. A. Dudeck, “CDC/NHSN surveillance definition of health care-associated infection and criteria for specific types of infections in the acute care setting”, *American journal of infection control* **2008**, *36*, 309–332.
- [22] S. D. Elek, P. E. Conen, “The Virulence of *Staphylococcus pyogenes* for Man. A Study of the Problems of Wound Infection”, *British journal of experimental pathology* **1957**, *38*, 573–586.
- [23] W. Zimmerli, P. D. Lew, F. A. Waldvogel, “Pathogenesis of foreign body infection. Evidence for a local granulocyte defect”, *The Journal of clinical investigation* **1984**, *73*, 1191–1200.
- [24] P. E. Vaudaux, G. Zulian, E. Huggler, et al., “Attachment of *Staphylococcus aureus* to polymethylmethacrylate increases its resistance to phagocytosis in foreign body infection”, *Infection and immunity* **1985**, *50*, 472–477.
- [25] R. Gahlot, C. Nigam, V. Kumar, et al., “Catheter-related bloodstream infections”, *International Journal of Critical Illness and Injury Science* **2014**, *4*, 162–167.
- [26] B. Böll, E. Schalk, D. Buchheidt, et al., “Central venous catheter-related infections in hematology and oncology: 2020 updated guidelines on diagnosis, management, and prevention by the Infectious Diseases Working Party (AG-IHO) of the German Society of Hematology and Medical Oncology (DGHO)”, *Annals of hematology* **2021**, *100*, 239–259.
- [27] R. Abd El-Hamid El-Kady, D. Waggas, A. AkL, “Microbial Repercussion on Hemodialysis Catheter-Related Bloodstream Infection Outcome: A 2-Year Retrospective Study”, *Infection and drug resistance* **2021**, *14*, 4067–4075.

- 
- [28] M. Marcos, A. Soriano, A. Iñurrieta, et al., “Changing epidemiology of central venous catheter-related bloodstream infections: increasing prevalence of Gram-negative pathogens”, *The Journal of antimicrobial chemotherapy* **2011**, *66*, 2119–2125.
- [29] K. Blot, N. Hammami, S. Blot, et al., “Gram-negative central line-associated bloodstream infection incidence peak during the summer: a national seasonality cohort study”, *Scientific reports* **2022**, *12*, 5202.
- [30] E. Bouza, A. Eworo, C. A. Fernández, et al., “Catheter-related bloodstream infections caused by Gram-negative bacteria”, *The Journal of hospital infection* **2013**, *85*, 1–11.
- [31] R. Mukherji, A. Patil, Prabhune A., “Role of Extracellular Proteases in Biofilm Disruption of Gram Positive Bacteria with Special Emphasis on *Staphylococcus aureus* Biofilms”, *Enzyme Engineering* **2014**, *04*, 1–7.
- [32] J. W. Costerton, K. J. Cheng, G. G. Geesey, et al., “Bacterial biofilms in nature and disease”, *Annual review of microbiology* **1987**, *41*, 435–464.
- [33] A. L. S. D. Santos, A. C. M. Galdino, T. P. de Mello, et al., “What are the advantages of living in a community? A microbial biofilm perspective!”, *Memorias do Instituto Oswaldo Cruz* **2018**, *113*, e180212.
- [34] H. J. Busscher, H. C. van der Mei, “How Do Bacteria Know They Are on a Surface and Regulate Their Response to an Adhering State?”, *PLoS pathogens* **2012**, *8*, e1002440.
- [35] J. M. Rodríguez-Martínez, A. Pascual, “Antimicrobial resistance in bacterial biofilms”, *Reviews in Medical Microbiology* **2006**, *17*, 65–75.
- [36] E. Giaouris, E. Heir, M. Desvaux, et al., “Intra- and inter-species interactions within biofilms of important foodborne bacterial pathogens”, *Frontiers in microbiology* **2015**, *6*, 1–26.
- [37] D. E. Moormeier, K. W. Bayles, “*Staphylococcus aureus* Biofilm: A Complex Developmental Organism”, *Molecular microbiology* **2017**, *104*, 365–376.
- [38] V. A. Carneiro, R. S. Melo, A. M. G. Pereira, et al. in *Bacterial Biofilms*, (Eds.: S. Dincer, M. Sümengen Özdenefe, A. Arkut), IntechOpen, Erscheinungsort nicht ermittelbar, **2020**.
- [39] P. Kuusela, “Fibronectin binds to *Staphylococcus aureus*”, *Nature* **1978**, *276*, 718–720.
- [40] J. Hawiger, S. Timmons, D. D. Strong, et al., “Identification of a region of human fibrinogen interacting with staphylococcal clumping factor”, *Biochemistry* **1982**, *21*, 1407–1413.
- [41] P. Speziale, G. Raucci, L. Visai, et al., “Binding of collagen to *Staphylococcus aureus* Cowan 1”, *Journal of bacteriology* **1986**, *167*, 77–81.
- [42] R. Vasudevan, “Biofilms: Microbial Cities of Scientific Significance”, *Journal of Microbiology & Experimentation* **2014**, *1*, 84–98.
- [43] M. Gross, S. E. Cramton, F. Götz, et al., “Key role of teichoic acid net charge in *Staphylococcus aureus* colonization of artificial surfaces”, *Infection and immunity* **2001**, *69*, 3423–3426.

- 
- [44] C. A. Kennedy, J. P. O’Gara, “Contribution of culture media and chemical properties of polystyrene tissue culture plates to biofilm development by *Staphylococcus aureus*”, *Journal of medical microbiology* **2004**, *53*, 1171–1173.
- [45] J. A. Geoghegan, R. M. Corrigan, D. T. Gruszka, et al., “Role of surface protein SasG in biofilm formation by *Staphylococcus aureus*”, *Journal of bacteriology* **2010**, *192*, 5663–5673.
- [46] P. Speziale, G. Pietrocola, T. J. Foster, et al., “Protein-based biofilm matrices in *Staphylococci*”, *Frontiers in cellular and infection microbiology* **2014**, *4*, 1–10.
- [47] L. Foulston, A. K. W. Elsholz, A. S. DeFrancesco, et al., “The Extracellular Matrix of *Staphylococcus aureus* Biofilms Comprises Cytoplasmic Proteins That Associate with the Cell Surface in Response to Decreasing pH”, *mBio* **2014**, *5*, 1–9.
- [48] D. E. Moormeier, J. L. Bose, A. R. Horswill, et al., “Temporal and Stochastic Control of *Staphylococcus aureus* Biofilm Development”, *mBio* **2014**, *5*, 1–12.
- [49] N. M. Mackey-Lawrence, D. E. Potter, N. Cerca, et al., “*Staphylococcus aureus* immunodominant surface antigen B is a cell-surface associated nucleic acid binding protein”, *BMC microbiology* **2009**, *9*, 61.
- [50] M. J. Huseby, A. C. Kruse, J. Digre, et al., “Beta toxin catalyzes formation of nucleoprotein matrix in staphylococcal biofilms”, *Proceedings of the National Academy of Sciences* **2010**, *107*, 14407–14412.
- [51] K. Schwartz, M. Ganesan, D. E. Payne, et al., “Extracellular DNA facilitates the formation of functional amyloids in *Staphylococcus aureus* biofilms”, *Molecular microbiology* **2015**, *99*, 123–134.
- [52] L. Hall-Stoodley, J. W. Costerton, P. Stoodley, “Bacterial biofilms: from the natural environment to infectious diseases”, *Nature reviews. Microbiology* **2004**, *2*, 95–108.
- [53] P. S. Stewart, M. J. Franklin, “Physiological heterogeneity in biofilms”, *Nature reviews. Microbiology* **2008**, *6*, 199–210.
- [54] M. Oliveira, S. F. Nunes, C. Carneiro, et al., “Time course of biofilm formation by *Staphylococcus aureus* and *Staphylococcus epidermidis* mastitis isolates”, *Veterinary microbiology* **2007**, *124*, 187–191.
- [55] M. B. Miller, B. L. Bassler, “Quorum sensing in bacteria”, *Annual review of microbiology* **2001**, *55*, 165–199.
- [56] J. W. Costerton, Z. Lewandowski, D. E. Caldwell, et al., “Microbial biofilms”, *Annual review of microbiology* **1995**, *49*, 711–745.
- [57] B. R. Boles, A. R. Horswill, “agr-Mediated Dispersal of *Staphylococcus aureus* Biofilms”, *PLoS pathogens* **2008**, *4*, 1–13.
- [58] S. Periasamy, H.-S. Joo, A. C. Duong, et al., “How *Staphylococcus aureus* biofilms develop their characteristic structure”, *Proceedings of the National Academy of Sciences of the United States of America* **2012**, *109*, 1281–1286.
- [59] B. R. Boles, A. R. Horswill, “*Staphylococcal* biofilm disassembly”, *Trends in microbiology* **2011**, *19*, 449–455.

- 
- [60] J. M. Yarwood, D. J. Bartels, E. M. Volper, et al., “Quorum sensing in *Staphylococcus aureus* biofilms”, *Journal of bacteriology* **2004**, *186*, 1838–1850.
- [61] C. Vuong, H. L. Saenz, F. Götz, et al., “Impact of the *agr* quorum-sensing system on adherence to polystyrene in *Staphylococcus aureus*”, *The Journal of infectious diseases* **2000**, *182*, 1688–1693.
- [62] P. Stoodley, Z. Lewandowski, J. D. Boyle, et al., “Structural deformation of bacterial biofilms caused by short-term fluctuations in fluid shear: An in situ investigation of biofilm rheology”, *Biotechnology and Bioengineering* **1999**, *65*, 83–92.
- [63] A. Persat, C. D. Nadell, M. K. Kim, et al., “The Mechanical World of Bacteria”, *Cell* **2015**, *161*, 988–997.
- [64] E. S. Gloag, S. Fabbri, D. J. Wozniak, et al., “Biofilm mechanics: Implications in infection and survival”, *Biofilm* **2020**, *2*, 100017.
- [65] C. J. Rupp, C. A. Fux, P. Stoodley, “Viscoelasticity of *Staphylococcus aureus* biofilms in response to fluid shear allows resistance to detachment and facilitates rolling migration”, *Applied and environmental microbiology* **2005**, *71*, 2175–2178.
- [66] M. R. Nejadnik, H. C. van der Mei, W. Norde, et al., “Bacterial adhesion and growth on a polymer brush-coating”, *Biomaterials* **2008**, *29*, 4117–4121.
- [67] B. Purevdorj, J. W. Costerton, P. Stoodley, “Influence of hydrodynamics and cell signaling on the structure and behavior of *Pseudomonas aeruginosa* biofilms”, *Applied and environmental microbiology* **2002**, *68*, 4457–4464.
- [68] Y. Liu, J.-H. Tay, “The essential role of hydrodynamic shear force in the formation of biofilm and granular sludge”, *Water research* **2002**, *36*, 1653–1665.
- [69] A.-A. D. Jones, C. R. Buie, “Continuous shear stress alters metabolism, mass-transport, and growth in electroactive biofilms independent of surface substrate transport”, *Scientific reports* **2019**, *9*, 2602.
- [70] A. Rochex, J.-J. Godon, N. Bernet, et al., “Role of shear stress on composition, diversity and dynamics of biofilm bacterial communities”, *Water research* **2008**, *42*, 4915–4922.
- [71] V. Kostenko, M. M. Salek, P. Sattari, et al., “*Staphylococcus aureus* biofilm formation and tolerance to antibiotics in response to oscillatory shear stresses of physiological levels”, *FEMS immunology and medical microbiology* **2010**, *59*, 421–431.
- [72] P. Stoodley, R. Cargo, C. J. Rupp, et al., “Biofilm material properties as related to shear-induced deformation and detachment phenomena”, *Journal of industrial microbiology & biotechnology* **2002**, *29*, 361–367.
- [73] O. Galy, P. Latour-Lambert, K. Zrelli, et al., “Mapping of Bacterial Biofilm Local Mechanics by Magnetic Microparticle Actuation”, *Biophysical Journal* **2012**, *103*, 1400–1408.

- 
- [74] *Janeway Immunologie*, 9. Aufl. 2018, (Eds.: K. Murphy, C. Weaver), Springer Berlin Heidelberg, Berlin, Heidelberg, **2018**.
- [75] S. Antoniak, “The coagulation system in host defense”, *Research and Practice in Thrombosis and Haemostasis* **2018**, 2, 549–557.
- [76] L. de Vor, S. H. M. Rooijackers, J. A. G. van Strijp, “Staphylococci evade the innate immune response by disarming neutrophils and forming biofilms”, *FEBS letters* **2020**, 594, 2556–2569.
- [77] N. K. Archer, M. J. Mazaitis, J. W. Costerton, et al., “Staphylococcus aureus biofilms: properties, regulation, and roles in human disease”, *Virulence* **2011**, 2, 445–459.
- [78] E. J. Giamarellos-Bourboulis, M. Raftogiannis, “The immune response to severe bacterial infections: consequences for therapy”, *Expert Review of Anti-infective Therapy* **2012**, 10, 369–380.
- [79] J. S. Marshall, R. Warrington, W. Watson, et al., “An introduction to immunology and immunopathology”, *Allergy Asthma and Clinical Immunology : Official Journal of the Canadian Society of Allergy and Clinical Immunology* **2018**, 14, 5–14.
- [80] H. Karauzum, S. K. Datta, “Adaptive Immunity Against Staphylococcus aureus”, *Current topics in microbiology and immunology* **2017**, 409, 419–439.
- [81] S. Chamrathy in *Pathobiology of human disease*, (Eds.: L. M. McManus, R. N. Mitchell), Academic Press, Amsterdam, **2014**, pp. 1544–1552.
- [82] E. S. Kalter, W. C. van Dijk, A. Timmerman, et al., “Activation of purified human plasma prekallikrein triggered by cell wall fractions of Escherichia coli and Staphylococcus aureus”, *The Journal of infectious diseases* **1983**, 148, 682–691.
- [83] E. T. M. Berends, A. Kuipers, M. M. Ravesloot, et al., “Bacteria under stress by complement and coagulation”, *FEMS microbiology reviews* **2014**, 38, 1146–1171.
- [84] R. Pawlinski, J.-G. Wang, A. P. Owens, et al., “Hematopoietic and non-hematopoietic cell tissue factor activates the coagulation cascade in endotoxemic mice”, *Blood* **2010**, 116, 806–814.
- [85] A. Shibamiya, K. Hersemeyer, T. Schmidt Wöll, et al., “A key role for Toll-like receptor-3 in disrupting the hemostasis balance on endothelial cells”, *Blood* **2009**, 113, 714–722.
- [86] C. T. Esmon, J. Xu, F. Lupu, “Innate immunity and coagulation”, *Journal of thrombosis and haemostasis : JTH* **2011**, 9 Suppl 1, 182–188.
- [87] C. Sperling, M. F. Maitz, S. Grasso, et al., “A Positively Charged Surface Triggers Coagulation Activation Through Factor VII Activating Protease (FSAP)”, *ACS applied materials & interfaces* **2017**, 9, 40107–40116.
- [88] S. Massberg, L. Grahl, M.-L. von Bruehl, et al., “Reciprocal coupling of coagulation and innate immunity via neutrophil serine proteases”, *Nature Medicine* **2010**, 16, 887–896.

- 
- [89] A. Forsgren, J. Sjöquist, "Protein A" from *S. aureus*. I. Pseudo-immune reaction with human gamma-globulin", *Journal of immunology (Baltimore Md. : 1950)* **1966**, *97*, 822–827.
- [90] L. Zhang, K. Jacobsson, J. Vasi, et al., "A second IgG-binding protein in *Staphylococcus aureus*", *Microbiology (Reading England)* **1998**, *144* ( Pt 4), 985–991.
- [91] J. L. Woehl, D. A. C. Stapels, B. L. Garcia, et al., "The extracellular adherence protein from *Staphylococcus aureus* inhibits the classical and lectin pathways of complement by blocking formation of the C3 proconvertase", *Journal of immunology (Baltimore Md. : 1950)* **2014**, *193*, 6161–6171.
- [92] I. Jongerius, B. L. Garcia, B. V. Geisbrecht, et al., "Convertase Inhibitory Properties of Staphylococcal Extracellular Complement-binding Protein \*\*", *Journal of Biological Chemistry* **2010**, *285*, 14973–14979.
- [93] S. H. M. Rooijackers, M. Ruyken, A. Roos, et al., "Immune evasion by a staphylococcal complement inhibitor that acts on C3 convertases", *Nature Immunology* **2005**, *6*, 920–927.
- [94] S. Anwar, L. R. Prince, S. J. Foster, et al., "The rise and rise of *Staphylococcus aureus*: laughing in the face of granulocytes", *Clinical and Experimental Immunology* **2009**, *157*, 216–224.
- [95] De Jong, Nienke W. M., K. P. M. van Kessel, J. A. G. van Strijp, "Immune Evasion by *Staphylococcus aureus*", *Microbiology Spectrum* **2019**, *7*, 1–27.
- [96] D. F. Bainton, R. Takemura, P. E. Stenberg, et al., "Rapid fragmentation and reorganization of Golgi membranes during frustrated phagocytosis of immobile immune complexes by macrophages", *The American Journal of Pathology* **1989**, *134*, 15–26.
- [97] C. Vuong, J. M. Voyich, E. R. Fischer, et al., "Polysaccharide intercellular adhesin (PIA) protects *Staphylococcus epidermidis* against major components of the human innate immune system", *Cellular Microbiology* **2004**, *6*, 269–275.
- [98] H. A. Crosby, J. Kwiecinski, A. R. Horswill, "Staphylococcus aureus Aggregation and Coagulation Mechanisms, and Their Function in Host-Pathogen Interactions", *Advances in applied microbiology* **2016**, *96*, 1–41.
- [99] M. McAdow, D. M. Missiakas, O. Schneewind, "Staphylococcus aureus Secretes Coagulase and von Willebrand Factor Binding Protein to Modify the Coagulation Cascade and Establish Host Infections", *Journal of Innate Immunity* **2012**, *4*, 141–148.
- [100] J. Sjollem, S. A. J. Zaat, V. Fontaine, et al., "In vitro methods for the evaluation of antimicrobial surface designs", *Acta Biomaterialia* **2018**, *70*, 12–24.
- [101] G. R. Collin, "Decreasing catheter colonization through the use of an antiseptic-impregnated catheter: a continuous quality improvement project", *Chest* **1999**, *115*, 1632–1640.
- [102] H. Tsuchiya, T. Shirai, H. Nishida, et al., "Innovative antimicrobial coating of titanium implants with iodine", *Journal of orthopaedic science : official journal of the Japanese Orthopaedic Association* **2012**, *17*, 595–604.

- 
- [103] J. M. Schierholz, K. Nagelschmidt, M. Nagelschmidt, et al., “Antimicrobial central venous catheters in oncology: efficacy of a rifampicin-miconazole-releasing catheter”, *Anticancer research* **2010**, *30*, 1353–1358.
- [104] H. Wang, H. Tong, H. Liu, et al., “Effectiveness of antimicrobial-coated central venous catheters for preventing catheter-related blood-stream infections with the implementation of bundles: a systematic review and network meta-analysis”, *Annals of intensive care* **2018**, *8*, 71.
- [105] C. M. C. Faustino, S. M. C. Lemos, N. Monge, et al., “A scope at antifouling strategies to prevent catheter-associated infections”, *Advances in colloid and interface science* **2020**, *284*, 102230.
- [106] A. Shahid, B. Aslam, S. Muzammil, et al., “The prospects of antimicrobial coated medical implants”, *Journal of applied biomaterials & functional materials* **2021**, *19*, 22808000211040304.
- [107] Z. K. Zander, M. L. Becker, “Antimicrobial and Antifouling Strategies for Polymeric Medical Devices”, *ACS Macro Letters* **2018**, *7*, 16–25.
- [108] I. Francolini, C. Vuotto, A. Piozzi, et al., “Antifouling and antimicrobial biomaterials: an overview”, *APMIS* **2017**, *125*, 392–417.
- [109] X. H. Wu, Y. K. Liew, C.-W. Mai, et al., “Potential of Superhydrophobic Surface for Blood-Contacting Medical Devices”, *International Journal of Molecular Sciences* **2021**, *22*, 1–16.
- [110] C. L. Ventola, “The Antibiotic Resistance Crisis: Part 1: Causes and Threats”, *Pharmacy and Therapeutics* **2015**, *40*, 277–283.
- [111] A. Panáček, L. Kvítek, M. Smékalová, et al., “Bacterial resistance to silver nanoparticles and how to overcome it”, *Nature nanotechnology* **2018**, *13*, 65–71.
- [112] D. I. Andersson, D. Hughes, “Microbiological effects of sublethal levels of antibiotics”, *Nature reviews. Microbiology* **2014**, *12*, 465–478.
- [113] N. Kashef, M. Akbarizare, S. K. Kamrava, “Effect of sub-lethal photodynamic inactivation on the antibiotic susceptibility and biofilm formation of clinical *Staphylococcus aureus* isolates”, *Photodiagnosis and photodynamic therapy* **2013**, *10*, 368–373.
- [114] S. Pavlukhina, Y. Lu, A. Patimetha, et al., “Polymer multilayers with pH-triggered release of antibacterial agents”, *Biomacromolecules* **2010**, *11*, 3448–3456.
- [115] Z. Lu, J. Zhang, Z. Yu, et al., “Hydrogel degradation triggered by pH for the smart release of antibiotics to combat bacterial infection”, *New Journal of Chemistry* **2017**, *41*, 432–436.
- [116] Y. Bourgat, C. Mikolai, M. Stiesch, et al., “Enzyme-Responsive Nanoparticles and Coatings Made from Alginate/Peptide Ciprofloxacin Conjugates as Drug Release System”, *Antibiotics (Basel Switzerland)* **2021**, *10*, 1–16.
- [117] V. V. Komnatnyy, W.-C. Chiang, T. Tolker-Nielsen, et al., “Bacteria-triggered release of antimicrobial agents”, *Angewandte Chemie (International ed. in English)* **2014**, *53*, 439–441.



- 
- [118] *Antimicrobial coatings and modifications on medical devices*, (Eds.: Z. Zhang, V. E. Wagner), Springer, Cham, **2017**.
- [119] H. Qiu, Z. Si, Y. Luo, et al., “The Mechanisms and the Applications of Antibacterial Polymers in Surface Modification on Medical Devices”, *Frontiers in bioengineering and biotechnology* **2020**, *8*, 910.
- [120] S. P. Denyer, “Mechanisms of action of antibacterial biocides”, *International Biodeterioration & Biodegradation* **1995**, *36*, 227–245.
- [121] C. Sperling, M. Fischer, M. F. Maitz, et al., “Neutrophil extracellular trap formation upon exposure of hydrophobic materials to human whole blood causes thrombogenic reactions”, *Biomaterials science* **2017**, *5*, 1998–2008.
- [122] J. L. Brash, T. A. Horbett, R. A. Latour, et al., “The blood compatibility challenge. Part 2: Protein adsorption phenomena governing blood reactivity”, *Acta Biomaterialia* **2019**, *94*, 11–24.
- [123] A. Asadinezhad, I. Novák, M. Lehocý, et al., “An in vitro bacterial adhesion assessment of surface-modified medical-grade PVC”, *Colloids and surfaces. B Biointerfaces* **2010**, *77*, 246–256.
- [124] K. Ozaltin, A. Di Martino, Z. Capakova, et al., “Plasma Mediated Chlorhexidine Immobilization onto Polylactic Acid Surface via Carbodiimide Chemistry: Antibacterial and Cytocompatibility Assessment”, *Polymers* **2021**, *13*, 1–11.
- [125] J. Pant, J. Gao, M. J. Goudie, et al., “A multi-defense strategy: Enhancing bactericidal activity of a medical grade polymer with a nitric oxide donor and surface-immobilized quaternary ammonium compound”, *Acta Biomaterialia* **2017**, *58*, 421–431.
- [126] P. N. Coneski, P. A. Fulmer, J. H. Wynne, “Enhancing the fouling resistance of biocidal urethane coatings via surface chemistry modulation”, *Langmuir : the ACS journal of surfaces and colloids* **2012**, *28*, 7039–7048.
- [127] M. Schmidt, S. Harmuth, E. R. Barth, et al., “Conjugation of Ciprofloxacin with Poly(2-oxazoline)s and Polyethylene Glycol via End Groups”, *Bioconjugate chemistry* **2015**, *26*, 1950–1962.
- [128] S. Degoutin, M. Jimenez, F. Chai, et al., “Simultaneous immobilization of heparin and gentamicin on polypropylene textiles: a dual therapeutic activity”, *Journal of biomedical materials research. Part A* **2014**, *102*, 3846–3854.
- [129] I. H. Jaffer, J. I. Weitz, “The blood compatibility challenge. Part 1: Blood-contacting medical devices: The scope of the problem”, *Acta Biomaterialia* **2019**, *94*, 2–10.
- [130] C. Mora-Solano, J. H. Collier, “Engaging adaptive immunity with biomaterials”, *Journal of materials chemistry. B* **2014**, *2*, 2409–2421.
- [131] L. Vroman, A. L. Adams, “Findings with the recording ellipsometer suggesting rapid exchange of specific plasma proteins at liquid/solid interfaces”, *Surface Science* **1969**, *16*, 438–446.
- [132] L. Vroman, A. L. Adams, G. C. Fischer, et al., “Interaction of high molecular weight kininogen, factor XII, and fibrinogen in plasma at interfaces”, *Blood* **1980**, *55*, 156–159.

- 
- [133] S. Irmscher, N. Döring, L. D. Halder, et al., “Kallikrein Cleaves C3 and Activates Complement”, *Journal of Innate Immunity* **2018**, *10*, 94–105.
- [134] R. Wiegner, S. Chakraborty, M. Huber-Lang, “Complement-coagulation crosstalk on cellular and artificial surfaces”, *Immunobiology* **2016**, *221*, 1073–1079.
- [135] M. Gorbet, C. Sperling, M. F. Maitz, et al., “The blood compatibility challenge. Part 3: Material associated activation of blood cascades and cells”, *Acta Biomaterialia* **2019**, *94*, 25–32.
- [136] C. Sperling, M. Fischer, M. F. Maitz, et al., “Blood coagulation on biomaterials requires the combination of distinct activation processes”, *Biomaterials* **2009**, *30*, 4447–4456.
- [137] P. L. den Exter, S. L. M. A. Beeres, J. Eikenboom, et al., “Anticoagulant treatment and bleeding complications in patients with left ventricular assist devices”, *Expert review of cardiovascular therapy* **2020**, *18*, 363–372.
- [138] S. Piran, S. Schulman, “Treatment of bleeding complications in patients on anticoagulant therapy”, *Blood* **2019**, *133*, 425–435.
- [139] D. S. Budnitz, M. C. Lovegrove, N. Shehab, et al., “Emergency hospitalizations for adverse drug events in older Americans”, *The New England journal of medicine* **2011**, *365*, 2002–2012.
- [140] M. F. Maitz, M. C. L. Martins, N. Grabow, et al., “The blood compatibility challenge. Part 4: Surface modification for hemocompatible materials: Passive and active approaches to guide blood-material interactions”, *Acta Biomaterialia* **2019**, *94*, 33–43.
- [141] W. R. Gombotz, G. H. Wang, T. A. Horbett, et al., “Protein adsorption to poly(ethylene oxide) surfaces”, *Journal of biomedical materials research* **1991**, *25*, 1547–1562.
- [142] M. Li, S. Jiang, J. Simon, et al., “Brush Conformation of Polyethylene Glycol Determines the Stealth Effect of Nanocarriers in the Low Protein Adsorption Regime”, *Nano letters* **2021**, *21*, 1591–1598.
- [143] S. Nagaoka, A. Nakao, “Clinical application of antithrombogenic hydrogel with long poly(ethylene oxide) chains”, *Biomaterials* **1990**, *11*, 119–121.
- [144] H. Guo, Y. Uehara, T. Matsuda, et al., “Surface charge dominated protein absorption on hydrogels”, *Soft matter* **2020**, *16*, 1897–1907.
- [145] J. Zhang, G. Li, J. Man, et al., “Mechanism of anti-proteins adsorption behavior on superhydrophobic titanium surface”, *Surface and Coatings Technology* **2021**, *421*, 127421.
- [146] C. P. Stallard, K. A. McDonnell, O. D. Onayemi, et al., “Evaluation of protein adsorption on atmospheric plasma deposited coatings exhibiting superhydrophilic to superhydrophobic properties”, *Biointerphases* **2012**, *7*, 31.
- [147] P. S. Fleser, V. K. Nuthakki, L. E. Malinzak, et al., “Nitric oxide-releasing biopolymers inhibit thrombus formation in a sheep model of arteriovenous bridge grafts”, *Journal of Vascular Surgery* **2004**, *40*, 803–811.

- 
- [148] V. B. Damodaran, V. Leszczak, K. A. Wold, et al., “Anti-thrombogenic properties of a nitric oxide-releasing dextran derivative: evaluation of platelet activation and whole blood clotting kinetics”, *RSC advances* **2013**, *3*, 24406–24414.
- [149] K. E. Kador, T. G. Mamedov, M. Schneider, et al., “Sequential co-immobilization of thrombomodulin and endothelial protein C receptor on polyurethane: activation of protein C”, *Acta Biomaterialia* **2011**, *7*, 2508–2517.
- [150] C. Sperling, K. Salchert, U. Streller, et al., “Covalently immobilized thrombomodulin inhibits coagulation and complement activation of artificial surfaces in vitro”, *Biomaterials* **2004**, *25*, 5101–5113.
- [151] F. Senatore, F. Bernath, K. Meisner, “Clinical study of urokinase-bound fibrocollagenous tubes”, *Journal of biomedical materials research* **1986**, *20*, 177–188.
- [152] Z. Wu, H. Chen, D. Li, et al., “Tissue plasminogen activator-containing polyurethane surfaces for fibrinolytic activity”, *Acta Biomaterialia* **2011**, *7*, 1993–1998.
- [153] R. Biran, D. Pond, “Heparin coatings for improving blood compatibility of medical devices”, *Advanced Drug Delivery Reviews* **2017**, *112*, 12–23.
- [154] European Parliament and the Council, Regulation (EU) 2017/745, **2017**.
- [155] European Parliament and the Council, Council Directive 93/42/EEC, **1993**.
- [156] International Organization for Standardization, Biological evaluation of medical devices — Part 4: Selection of tests for interactions with blood: DIN EN ISO 10993-4, **2017**.
- [157] B. D. Ratner, “The Catastrophe Revisited: Blood Compatibility in the 21st Century1”, *Biomaterials* **2007**, *28*, 5144–5147.
- [158] M. F. Wolf, G. Girdhar, A. A. Anderson, et al., “In vitro methodology for medical device material thrombogenicity assessments: A use condition and bio-analytical proof-of-concept approach”, *Journal of biomedical materials research. Part B Applied biomaterials* **2021**, *109*, 358–376.
- [159] International Organization for Standardization, Textiles — Determination of antibacterial activity of textile products: ISO 20743, **2021**.
- [160] International Organization for Standardization, Measurement of antibacterial activity on plastics and other non-porous surfaces: ISO 22196, **2011**.
- [161] D. G. Powell, “Medical Applications of Polycarbonate”, *Medical Plastics and Biomaterials Magazine* **1998**, 38–45.
- [162] X.-L. Li, X.-F. Guo, J.-L. Song, et al., “Research progress on hydrolytic stability of polyester polyurethane dispersions”, *Journal of Physics: Conference Series* **2020**, *1635*, 012109.
- [163] N. Mahajan, P. Gupta, “New insights into the microbial degradation of polyurethanes”, *RSC Advances* **2015**, *5*, 41839–41854.
- [164] M. A. Cohen Stuart in *Biopolymers at Interfaces; 2nd ed*, (Ed.: M. Malmsten), Dekker, **2003**, pp. 1–25.

- 
- [165] T. Tadros in *Encyclopedia of Colloid and Interface Science*, Springer, Berlin, Heidelberg, **2013**, pp. 945–962.
- [166] A. Sartori, A. Johner, J.-L. Viovy, et al., “Theoretical Study of Comb Polymers Adsorption on Solid Surfaces”, *Macromolecules* **2005**, *38*, 3432–3441.
- [167] D. Li, A. W. Neumann, “Surface heterogeneity and contact angle hysteresis”, *Colloid & Polymer Science* **1992**, *270*, 498–504.
- [168] L. W. Schwartz, S. Garoff, “Contact angle hysteresis on heterogeneous surfaces”, *Langmuir* **1985**, *1*, 219–230.
- [169] U. Streller, C. Sperling, J. Hübner, et al., “Design and evaluation of novel blood incubation systems for in vitro hemocompatibility assessment of planar solid surfaces”, *Journal of biomedical materials research. Part B Applied biomaterials* **2003**, *66*, 379–390.
- [170] B. Dong, S. Manolache, A. C. L. Wong, et al., “Antifouling ability of polyethylene glycol of different molecular weights grafted onto polyester surfaces by cold plasma”, *Polymer Bulletin* **2011**, *66*, 517–528.
- [171] L. Peng, L. Chang, X. Liu, et al., “Antibacterial Property of a Polyethylene Glycol-Grafted Dental Material”, *ACS applied materials & interfaces* **2017**, *9*, 17688–17692.
- [172] F. Afennich, D. E. Slot, N. Hossainian, et al., “The effect of hexetidine mouthwash on the prevention of plaque and gingival inflammation: a systematic review”, *International journal of dental hygiene* **2011**, *9*, 182–190.
- [173] H. Weidinger, H. J. Passloer, L. Kovacs, et al., “Nutzen der prophylaktischen Vaginalantiseptik mit Hexetidin in Geburtshilfe und Gynäkologie”, *Geburtshilfe und Frauenheilkunde* **1991**, *51*, 929–935.
- [174] M. Weber, H. Steinle, S. Golombek, et al., “Blood-Contacting Biomaterials: In Vitro Evaluation of the Hemocompatibility”, *Frontiers in bioengineering and biotechnology* **2018**, *6*, 1–11.
- [175] K. M. Kovach, J. R. Capadona, A. S. Gupta, et al., “The effects of PEG-based surface modification of PDMS microchannels on long-term hemocompatibility”, *Journal of biomedical materials research. Part A* **2014**, *102*, 4195–4205.
- [176] S.-F. Chou, B. A. Caltrider, A. Azghani, et al., “Inhibition of Platelet Adhesion from Surface Modified Polyurethane Membranes”, *Biomedical journal of scientific & technical research* **2020**, *32*, 24988–24993.
- [177] J. B. Kaplan, “Biofilm Dispersal: Mechanisms, Clinical Implications, and Potential Therapeutic Uses”, *Journal of Dental Research* **2010**, *89*, 205–218.
- [178] A. K. Muszanska, E. T. J. Rochford, A. Gruszka, et al., “Antiadhesive polymer brush coating functionalized with antimicrobial and RGD peptides to reduce biofilm formation and enhance tissue integration”, *Biomacromolecules* **2014**, *15*, 2019–2026.
- [179] H.-Y. Cheung, M. M.-K. Wong, S.-H. Cheung, et al., “Differential actions of chlorhexidine on the cell wall of *Bacillus subtilis* and *Escherichia coli*”, *PloS one* **2012**, *7*, e36659.

- 
- [180] T. B. Horwich, K. Kalantar-Zadeh, R. W. MacLellan, et al., “Albumin levels predict survival in patients with systolic heart failure”, *American heart journal* **2008**, *155*, 883–889.
- [181] M. K. L. N. Sikosana, Dissertation, TU Dresden, **2021**.
- [182] S. Ibbotson, T. Dettmer, S. Kara, et al., “Eco-efficiency of disposable and reusable surgical instruments—a scissors case”, *The International Journal of Life Cycle Assessment* **2013**, *18*, 1137–1148.
- [183] R. Konradi, V. B. Schwartz, M. Seufert, et al., US 2020/0148991 A1, **2020**.
- [184] A. B. Chandler, “In vitro thrombotic coagulation of the blood; a method for producing a thrombus”, *Laboratory investigation; a journal of technical methods and pathology* **1958**, *7* 2, 110–114.
- [185] K. Christensen, R. Larsson, H. Emanuelsson, et al., “Heparin coating of the stent graft — effects on platelets, coagulation and complement activation”, *Biomaterials* **2001**, *22*, 349–355.
- [186] G. Tepe, J. Schmehl, H. P. Wendel, et al., “Reduced thrombogenicity of nitinol stents—in vitro evaluation of different surface modifications and coatings”, *Biomaterials* **2006**, *27*, 643–650.
- [187] J. Andersson, J. Sanchez, K. N. Ekdahl, et al., “Optimal heparin surface concentration and antithrombin binding capacity as evaluated with human non-anticoagulated blood in vitro”, *Journal of biomedical materials research. Part A* **2003**, *67*, 458–466.
- [188] J. B. Slee, I. S. Alferiev, R. J. Levy, et al., “The use of the ex vivo Chandler Loop Apparatus to assess the biocompatibility of modified polymeric blood conduits”, *Journal of visualized experiments : JoVE* **2014**, 1–8.
- [189] S. Krajewski, R. Prucek, A. Panacek, et al., “Hemocompatibility evaluation of different silver nanoparticle concentrations employing a modified Chandler-loop in vitro assay on human blood”, *Acta Biomaterialia* **2013**, *9*, 7460–7468.
- [190] P. G. Kalman, D. A. McCullough, C. A. Ward, “Evacuation of microscopic air bubbles from Dacron reduces complement activation and platelet aggregation”, *Journal of Vascular Surgery* **1990**, *11*, 591–598.
- [191] T. Thorsen, H. Klausen, R. T. Lie, et al., “Bubble-induced aggregation of platelets: effects of gas species, proteins, and decompression”, *Undersea & hyperbaric medicine : journal of the Undersea and Hyperbaric Medical Society Inc* **1993**, *20*, 101–119.
- [192] N. M. Lamba, J. D. Gaylor, J. M. Courtney, et al., “Complement activation by cellulose: investigation of the effects of time, area, flow rate, shear rate and temperature on C3a generation in vitro, using a parallel plate flow cell”, *Journal of materials science. Materials in medicine* **1998**, *9*, 409–414.
- [193] S. Behrens, F. Schmieder, C. Polk, et al. in Microfluidics, BioMEMS, and Medical Microsystems XIX, (Ed.: B. Gray), SPIE / International Society for Optical Engineering, **2021**, p. 20.

- 
- [194] C. Dittfeld, M. Winkelkotte, S. Behrens, et al., “Establishment of a resazurin-based aortic valve tissue viability assay for dynamic culture in a microphysiological system”, *Clinical hemorheology and microcirculation* **2021**, 79, 167–178.
- [195] T. J. Kolanowski, M. Busek, M. Schubert, et al., “Enhanced structural maturation of human induced pluripotent stem cell-derived cardiomyocytes under a controlled microenvironment in a microfluidic system”, *Acta Biomaterialia* **2020**, 102, 273–286.
- [196] F. Schmieder, S. Behrens, N. Reustle, et al., “A microphysiological system to investigate the pressure dependent filtration at an artificial glomerular kidney barrier”, *Current Directions in Biomedical Engineering* **2019**, 5, 389–391.
- [197] D. P. Bakker, A. van der Plaats, G. J. Verkerke, et al., “Comparison of velocity profiles for different flow chamber designs used in studies of microbial adhesion to surfaces”, *Applied and environmental microbiology* **2003**, 69, 6280–6287.
- [198] M. Pilecky, A. Schildberger, L. Knabl, et al., “Influence of antibiotic treatment on the detection of *S. aureus* in whole blood following pathogen enrichment”, *BMC microbiology* **2019**, 19, 180.
- [199] S. L. J. Blok, G. E. Engels, W. van Oeveren, “In vitro hemocompatibility testing: The importance of fresh blood”, *Biointerphases* **2016**, 11, 029802.
- [200] S. Braune, M. Walter, F. Schulze, et al., “Changes in platelet morphology and function during 24 hours of storage”, *Clinical hemorheology and microcirculation* **2014**, 58, 159–170.
- [201] M. Antonelli, G. de Pascale, V. M. Ranieri, et al., “Comparison of triple-lumen central venous catheters impregnated with silver nanoparticles (AgTive®) vs conventional catheters in intensive care unit patients”, *The Journal of hospital infection* **2012**, 82, 101–107.
- [202] T. Ostendorf, A. Meinhold, C. Harter, et al., “Chlorhexidine and silver-sulfadiazine coated central venous catheters in haematological patients—a double-blind, randomised, prospective, controlled trial”, *Supportive care in cancer : official journal of the Multinational Association of Supportive Care in Cancer* **2005**, 13, 993–1000.
- [203] M. D. Khare, S. S. Bukhari, A. Swann, et al., “Reduction of catheter-related colonisation by the use of a silver zeolite-impregnated central vascular catheter in adult critical care”, *The Journal of infection* **2007**, 54, 146–150.
- [204] D. G. Maki, F. Jarrett, H. W. Sarafin, “A semiquantitative culture method for identification of catheter-related infection in the burn patient”, *Journal of Surgical Research* **1977**, 22, 513–520.
- [205] R. J. Sherertz, I. I. Raad, A. Belani, et al., “Three-year experience with sonicated vascular catheter cultures in a clinical microbiology laboratory”, *Journal of clinical microbiology* **1990**, 28, 76–82.
- [206] D. J. Cleri, M. L. Corrado, S. J. Seligman, “Quantitative culture of intravenous catheters and other intravascular inserts”, *The Journal of infectious diseases* **1980**, 141, 781–786.

- 
- [207] N. Tripathi, A. Sapra, *Gram Staining*, StatPearls Publishing, Treasure Island (FL), **2022**.
- [208] P. R. Langer-Safer, M. Levine, D. C. Ward, “Immunological method for mapping genes on *Drosophila* polytene chromosomes”, *Proceedings of the National Academy of Sciences* **1982**, *79*, 4381–4385.
- [209] V. Krimmer, H. Merkert, C. von Eiff, et al., “Detection of *Staphylococcus aureus* and *Staphylococcus epidermidis* in Clinical Samples by 16S rRNA-Directed In Situ Hybridization”, *Journal of clinical microbiology* **1999**, *37*, 2667–2673.
- [210] A. Tavares, J. Inácio, J. Melo-Cristino, et al., “Use of fluorescence in situ hybridization for rapid identification of staphylococci in blood culture samples collected in a Portuguese hospital”, *Journal of clinical microbiology* **2008**, *46*, 3097–3100.
- [211] E. Prudent, D. Raoult, “Fluorescence in situ hybridization, a complementary molecular tool for the clinical diagnosis of infectious diseases by intracellular and fastidious bacteria”, *FEMS microbiology reviews* **2019**, *43*, 88–107.
- [212] R. O. Schlechter, H. Jun, M. Bernach, et al., “Chromatic Bacteria - A Broad Host-Range Plasmid and Chromosomal Insertion Toolbox for Fluorescent Protein Expression in Bacteria”, *Frontiers in microbiology* **2018**, *9*, 3052.
- [213] T. Kondo, S. Yumura, “An improved molecular tool for screening bacterial colonies using GFP expression enhanced by a *Dictyostelium* sequence”, *BioTechniques* **2020**, *68*, 91–95.
- [214] F. Kato, M. Nakamura, M. Sugai, “The development of fluorescent protein tracing vectors for multicolor imaging of clinically isolated *Staphylococcus aureus*”, *Scientific reports* **2017**, *7*, 2865.
- [215] K. P. Scott, D. K. Mercer, A. J. Richardson, et al., “Chromosomal integration of the green fluorescent protein gene in lactic acid bacteria and the survival of marked strains in human gut simulations”, *FEMS microbiology letters* **2000**, *182*, 23–27.
- [216] P. Gu, F. Yang, T. Su, et al., “A rapid and reliable strategy for chromosomal integration of gene(s) with multiple copies”, *Scientific reports* **2015**, *5*, 9684.
- [217] J. Schindelin, I. Arganda-Carreras, E. Frise, et al., “Fiji: an open-source platform for biological-image analysis”, *Nature methods* **2012**, *9*, 676–682.
- [218] J. Valtin, S. Behrens, M. F. Maitz, et al., “A modular in vitro flow model to analyse blood-surface interactions under physiological conditions”, *Current Directions in Biomedical Engineering* **2021**, *7*, 171–174.
- [219] R. Kopp, R. Bernsberg, A. Kashefi, et al., “Effect of hirudin versus heparin on hemocompatibility of blood contacting biomaterials: an in vitro study”, *The International journal of artificial organs* **2005**, *28*, 1272–1277.
- [220] T. E. Mollnes, O.-L. Brekke, M. Fung, et al., “Essential role of the C5a receptor in *E. coli*-induced oxidative burst and phagocytosis revealed by a novel lepirudin-based human whole blood model of inflammation”, *Blood* **2002**, *100*, 1869–1877.

- 
- [221] Y. J. Chuang, R. Swanson, S. M. Raja, et al., “Heparin enhances the specificity of antithrombin for thrombin and factor Xa independent of the reactive center loop sequence. Evidence for an exosite determinant of factor Xa specificity in heparin-activated antithrombin”, *The Journal of biological chemistry* **2001**, *276*, 14961–14971.
- [222] F. Bexborn, A. E. Engberg, K. Sandholm, et al., “Hirudin versus heparin for use in whole blood in vitro biocompatibility models”, *Journal of biomedical materials research. Part A* **2009**, *89*, 951–959.
- [223] K. Fu, R. Izquierdo, J. M. Walenga, et al., “Comparative study on the use of anticoagulants heparin and recombinant hirudin in a rabbit traumatic anastomosis model”, *Thrombosis Research* **1995**, *78*, 421–428.
- [224] T. N. Estep, R. A. Pedersen, T. J. Miller, et al., “Characterization of erythrocyte quality during the refrigerated storage of whole blood containing di-(2-ethylhexyl) phthalate”, *Blood* **1984**, *64*, 1270–1276.
- [225] R. S. Labow, R. T. Card, G. Rock, “The effect of the plasticizer di(2-ethylhexyl)phthalate on red cell deformability”, *Blood* **1987**, *70*, 319–323.
- [226] B. Horowitz, M. H. Stryker, A. A. Waldman, et al., “Stabilization of red blood cells by the plasticizer, diethylhexylphthalate”, *Vox sanguinis* **1985**, *48*, 150–155.
- [227] C. V. Prowse, D. de Korte, J. R. Hess, et al., “Commercially available blood storage containers”, *Vox sanguinis* **2014**, *106*, 1–13.
- [228] J. Simmchen, R. Ventura, J. Segura, “Progress in the removal of di-2-ethylhexyl-phthalate as plasticizer in blood bags”, *Transfusion medicine reviews* **2012**, *26*, 27–37.
- [229] L. Peng, Y. Qiu, Z. Huang, et al., “Numerical Simulation of Hemodynamic Changes in Central Veins after Tunneled Cuffed Central Venous Catheter Placement in Patients under Hemodialysis”, *Scientific reports* **2017**, *7*, 15955.
- [230] R. Mongrain, J. Rodés-Cabau, “Role of Shear Stress in Atherosclerosis and Restenosis After Coronary Stent Implantation”, *Revista Española de Cardiología (English Edition)* **2006**, *59*, 1–4.
- [231] International Organization for Standardization, Quality management systems - Fundamentals and vocabulary: ISO 9000, **2015**.
- [232] C. R. Arciola, D. Campoccia, L. Montanaro, “Implant infections: adhesion, biofilm formation and immune evasion”, *Nature reviews. Microbiology* **2018**, *16*, 397–409.
- [233] S. Misra, D. A. Woodrum, J. Homburger, et al., “Assessment of wall shear stress changes in arteries and veins of arteriovenous polytetrafluoroethylene grafts using magnetic resonance imaging”, *Cardiovascular and interventional radiology* **2006**, *29*, 624–629.
- [234] M. Wolff, S. Handtke, R. Palankar, et al., “Activated platelets kill *Staphylococcus aureus*, but not *Streptococcus pneumoniae*-The role of Fc $\gamma$ RIIa and platelet factor 4/heparinantibodies”, *Journal of thrombosis and haemostasis : JTH* **2020**, *18*, 1459–1468.



- 
- [235] K. Krauel, C. Pötschke, C. Weber, et al., “Platelet factor 4 binds to bacteria, inducing antibodies cross-reacting with the major antigen in heparin-induced thrombocytopenia”, *Blood* **2011**, *117*, 1370–1378.
- [236] K. P. M. van Kessel, J. Bestebroer, J. A. G. van Strijp, “Neutrophil-Mediated Phagocytosis of *Staphylococcus aureus*”, *Frontiers in immunology* **2014**, *5*, 467.
- [237] T. Tanaka in *Encyclopedia of immunobiology*, (Ed.: M. J. Ratcliffe), Academic Press is an imprint of Elsevier, Amsterdam, **2016**, pp. 505–511.
- [238] W. Kern, “The Evolution of Silicon Wafer Cleaning Technology”, *Journal of The Electrochemical Society* **1990**, *137*, 1887–1892.
- [239] A. L. Cordeiro, M. Rückel, F. Bartels, et al., “Protein adsorption dynamics to polymer surfaces revisited-A multisystems approach”, *Biointerphases* **2019**, *14*, 051005.
- [240] G. Sauerbrey, “Verwendung von Schwingquarzen zur Wägung dünner Schichten und zur Mikrowägung”, *Z. Physik (Zeitschrift für Physik)* **1959**, *155*, 206–222.
- [241] E. L. Yeo, J. A. Sheppard, I. A. Feuerstein, “Role of P-selectin and leukocyte activation in polymorphonuclear cell adhesion to surface adherent activated platelets under physiologic shear conditions (an injury vessel wall model)”, *Blood* **1994**, *83*, 2498–2507.
- [242] A. C. Fisher, M. P. DeLisa, “Laboratory evolution of fast-folding green fluorescent protein using secretory pathway quality control”, *PloS one* **2008**, *3*, e2351.
- [243] P. M. Pereira, H. Veiga, A. M. Jorge, et al., “Fluorescent reporters for studies of cellular localization of proteins in *Staphylococcus aureus*”, *Applied and environmental microbiology* **2010**, *76*, 4346–4353.
- [244] M. Busek, S. Gruenzner, T. Steege, et al., “Design, characterization, and modeling of microcirculation systems with integrated oxygenators”, *Journal of Sensors and Sensor Systems* **2016**, *5*, 221–228.
- [245] C. Roloff, R. Bordás, R. Nickl, et al., “Investigation of the velocity field in a full-scale model of a cerebral aneurysm”, *International Journal of Heat and Fluid Flow* **2013**, *43*, 212–219.

# A Appendix

## A.1 Supplementary results

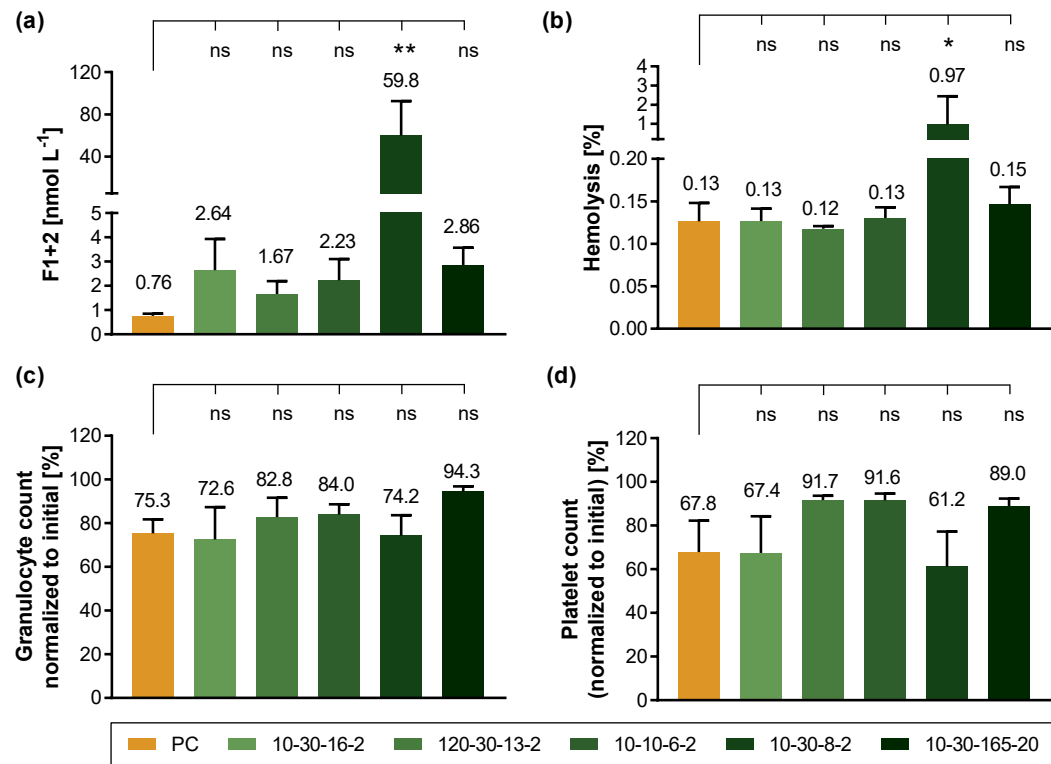


**Figure A.1:** Static hemocompatibility assessment of anti-adhesive AP coatings in comparison to untreated polymer substrate PC; statistical significance was determined in comparison to the control surface PC using ANOVA and Holm-Sidak's multiple comparisons test (\* p < 0.05, \*\* p < 0.01, ns: not significant), n = 9; **(a)** Expression of prothrombin fragment F1+2, **(b)** Material-induced hemolysis, **(c)** Granulocyte count normalized to initial, **(d)** Platelet count normalized to initial.

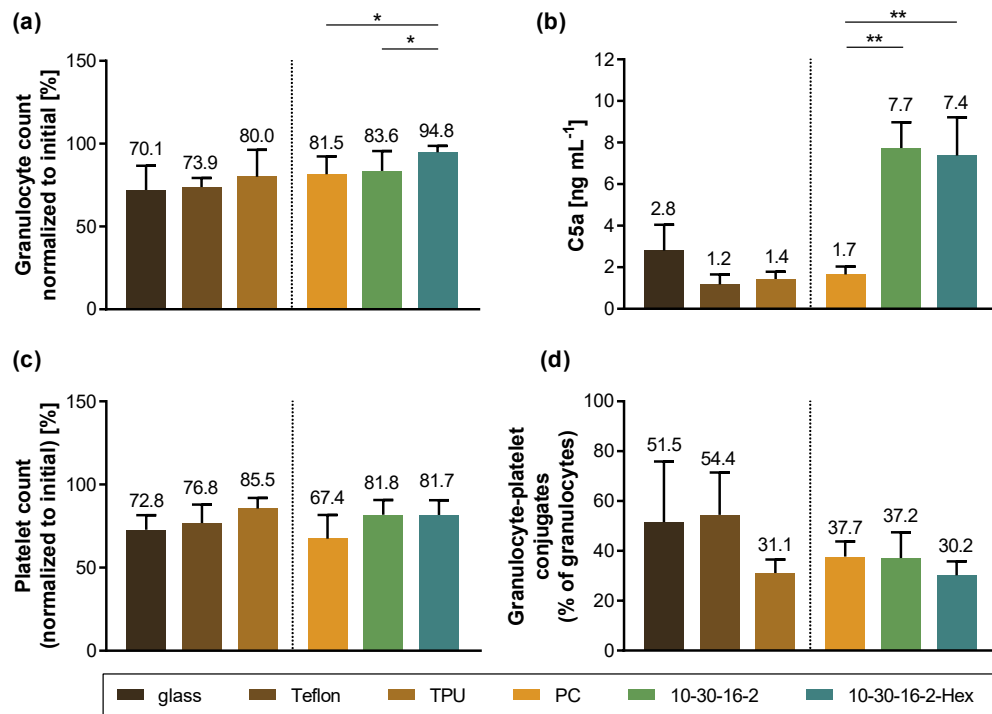


**Figure A.2:** Static hemocompatibility assessment of AP 10-30-16-2 and 10-30-16-2-Hex in comparison to control surfaces: glass, Teflon AF, TPU, and PC; statistical significance between PC, 10-30-16-2, and 10-30-16-2-Hex was determined using ANOVA and Holm-Sidak's multiple comparisons test (\*  $p < 0.05$ , \*\*  $p < 0.01$ ),  $n=9$ ; (a) Granulocyte count normalized to initial, (b) Expression of complement factor C5a, (c) Platelet count normalized to initial, (d) Granulocyte-platelet-conjugates normalized to total granulocyte count.

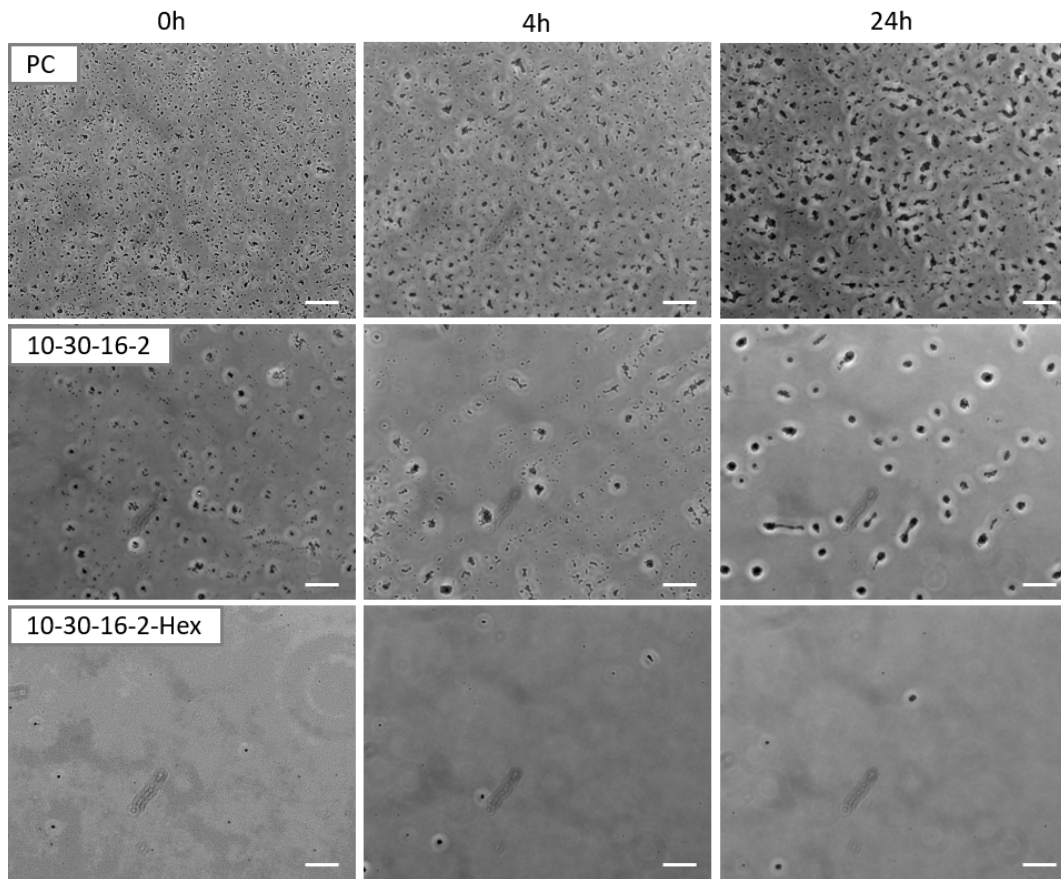


**Figure A.3:** Exemplary phase-contrast microscopy images taken after 0, 4, and 24 hours incubation in M9\* medium on PC, 10-30-16-2, and 10-30-16-2-Hex surfaces, scale bar: 20  $\mu\text{m}$ .

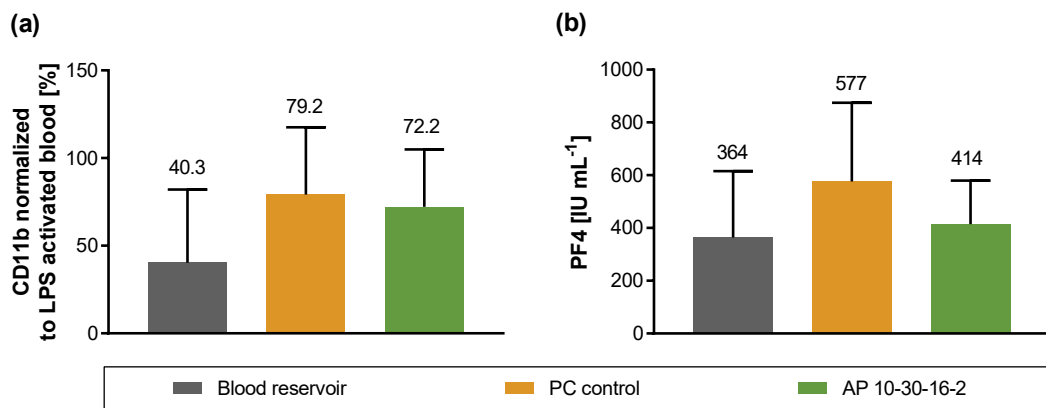


**Figure A.4:** Activation of blood samples collected from blood reservoir after 4 hours incubation time in comparison to blood samples that have passed the pre-seeded microchannel chip,  $n=2$ ; (a) Expression of inflammation parameter CD11b on granulocytes, normalized to LPS activated blood, (b) PF4 release as a parameter for platelet activation.

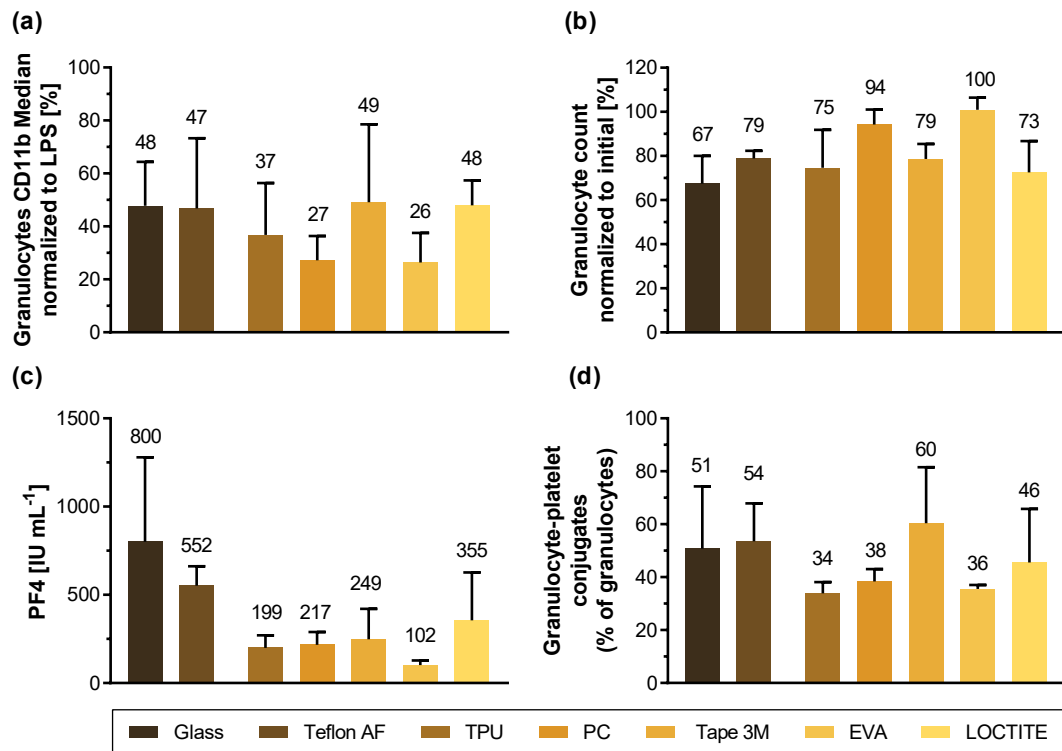


**Figure A.5:** Blood activation of materials incorporated in microchannel chip in comparison to control surfaces glass and Teflon AF,  $n = 3$ ; **(a)** Expression of inflammation parameter CD11b on granulocytes, normalized to LPS activated blood, **(b)** Granulocyte count normalized to initial, **(c)** PF4 release as parameter for platelet activation, **(d)** Granulocyte-platelet-conjugates normalized to total granulocytes.

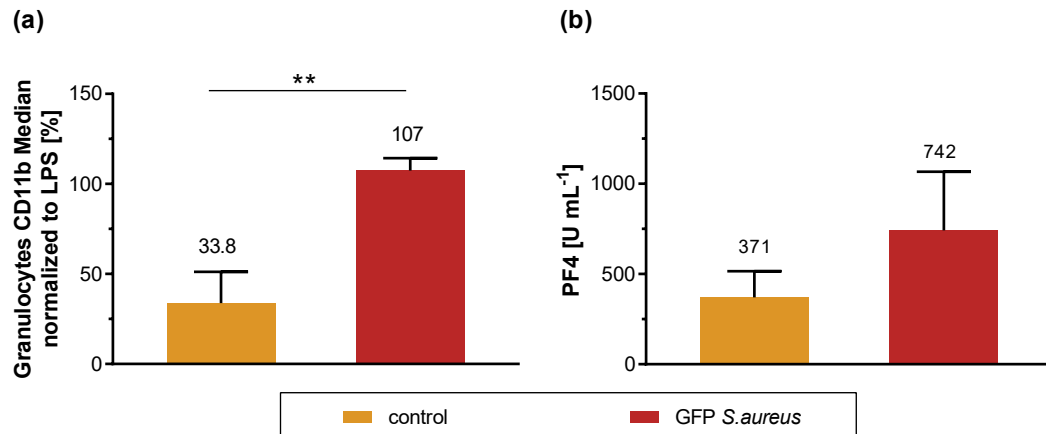


**Figure A.6:** Blood activation induced by GFP *S. aureus* pre-seeded on TPU compared to TPU control surface; statistical significance was determined using unpaired, two-tailed t-tests (\*  $p < 0.05$ , \*\*  $p < 0.01$ ),  $n = 3$ ; (a) Expression of inflammation parameter CD11b on granulocytes, normalized to LPS activated blood, (b) PF4 release as parameter for platelet activation.

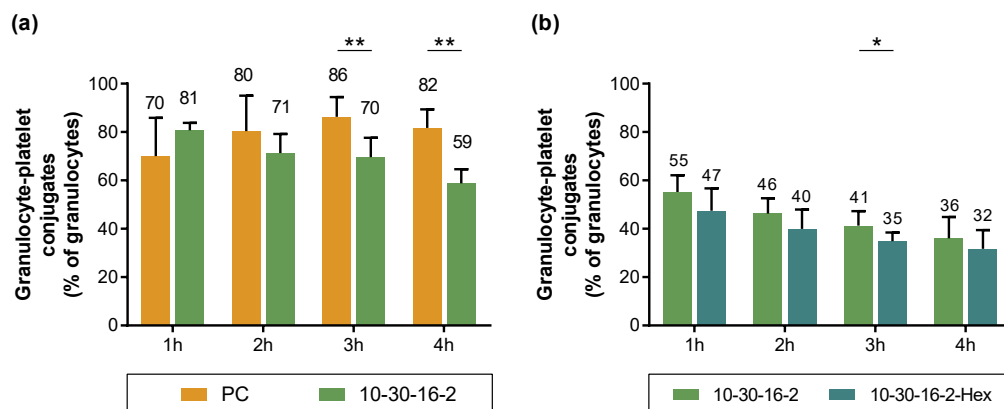


**Figure A.7:** Validation of the *in vitro* flow model: Formation of granulocyte-platelet-conjugates normalized to total granulocytes in blood samples collected after every hour during 4 hours incubation time; statistical significance was determined using unpaired, two-tailed t-tests for each time point (\*  $p < 0.05$ , \*\*  $p < 0.01$ ),  $n = 6$ ; (a) Comparison between control surface PC and anti-adhesive AP 10-30-16-2, (b) Comparison between anti-adhesive AP 10-30-16-2 and contact-killing AP 10-30-16-2-Hex.

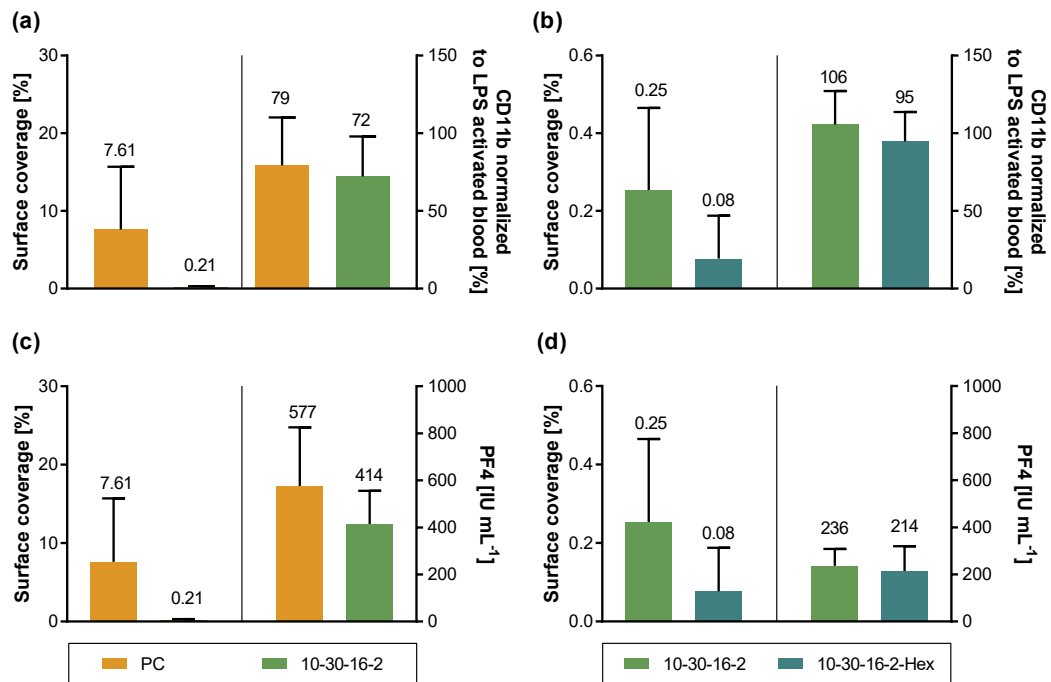


**Figure A.8:** Validation of the *in vitro* flow model: Correlation between bacterial surface coverage of microchannel chip and activation of collected blood samples after 4 hours incubation time,  $n = 6$ ; **(a)** Surface coverage vs. inflammation parameter CD11b for PC and AP 10-30-16-2, **(b)** Surface coverage vs. inflammation parameter CD11b for AP 10-30-16-2 and AP 10-30-16-2-Hex, **(c)** Surface coverage vs. platelet activation (release of PF4) for PC and AP 10-30-16-2, **(d)** Surface coverage vs. platelet activation (release of PF4) for AP 10-30-16-2 and AP 10-30-16-2-Hex.

## A.2 Source code

**Listing A.1:** Code for micro-controller of rotation device, written in C++.

```
1  // Arduino code for rotation device
2  // Juliane Valtin, 13.05.2020
3
4  // defines pin numbers
5  const int dirPin = 4;
6  const int stepPin = 5;
7  const int MS1 = 8;
8  const int MS2 = 9;
9  const int MS3 = 10;
10
11 void setup() {
12     // sets step and direction pins as output
13     pinMode(dirPin, OUTPUT);
14     pinMode(stepPin, OUTPUT);
15     // sets MS1-MS3 as output
16     pinMode(MS1, OUTPUT);
17     pinMode(MS2, OUTPUT);
18     pinMode(MS3, OUTPUT);
19 }
20
21 void loop() {
22     // enables the motor to move in a particular direction
23     digitalWrite(dirPin, HIGH);
24     digitalWrite(MS1, HIGH);
25     digitalWrite(MS2, HIGH);
26     digitalWrite(MS3, HIGH);
27
28     // makes 3200 pulses (microsteps) for making one half
        turn
29     for(int x = 0; x < 3200; x++) {
30         digitalWrite(stepPin, HIGH);
31         delay(2);
32         digitalWrite(stepPin, LOW);
33         delay(2);
34     }
35
```



```
36    // wait one second before change of direction
37    delay(1000);
38
39    //changes the rotation direction
40    digitalWrite(dirPin, LOW);
41
42    // makes 3200 pulses (microsteps) for making one half
    turn
43    for(int x = 0; x < 3200; x++) {
44        digitalWrite(stepPin, HIGH);
45        delay(2);
46        digitalWrite(stepPin, LOW);
47        delay(2);
48    }
49
50    // wait one second before restart of loop
51    delay(1000);
52 }
```

### A.3 Technical drawings

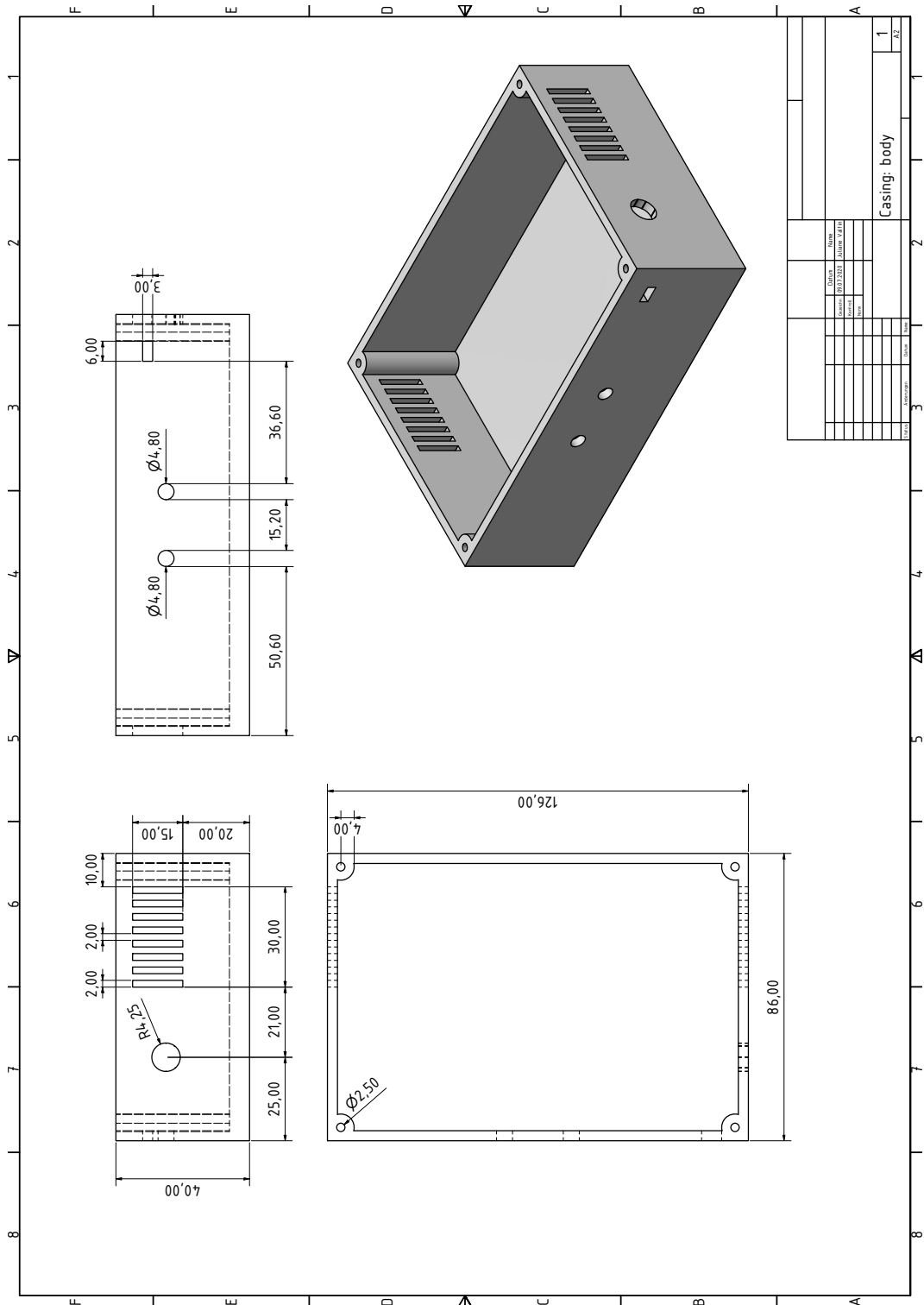


Figure A.9: Technical drawing of casing body for rotation device.

XXX

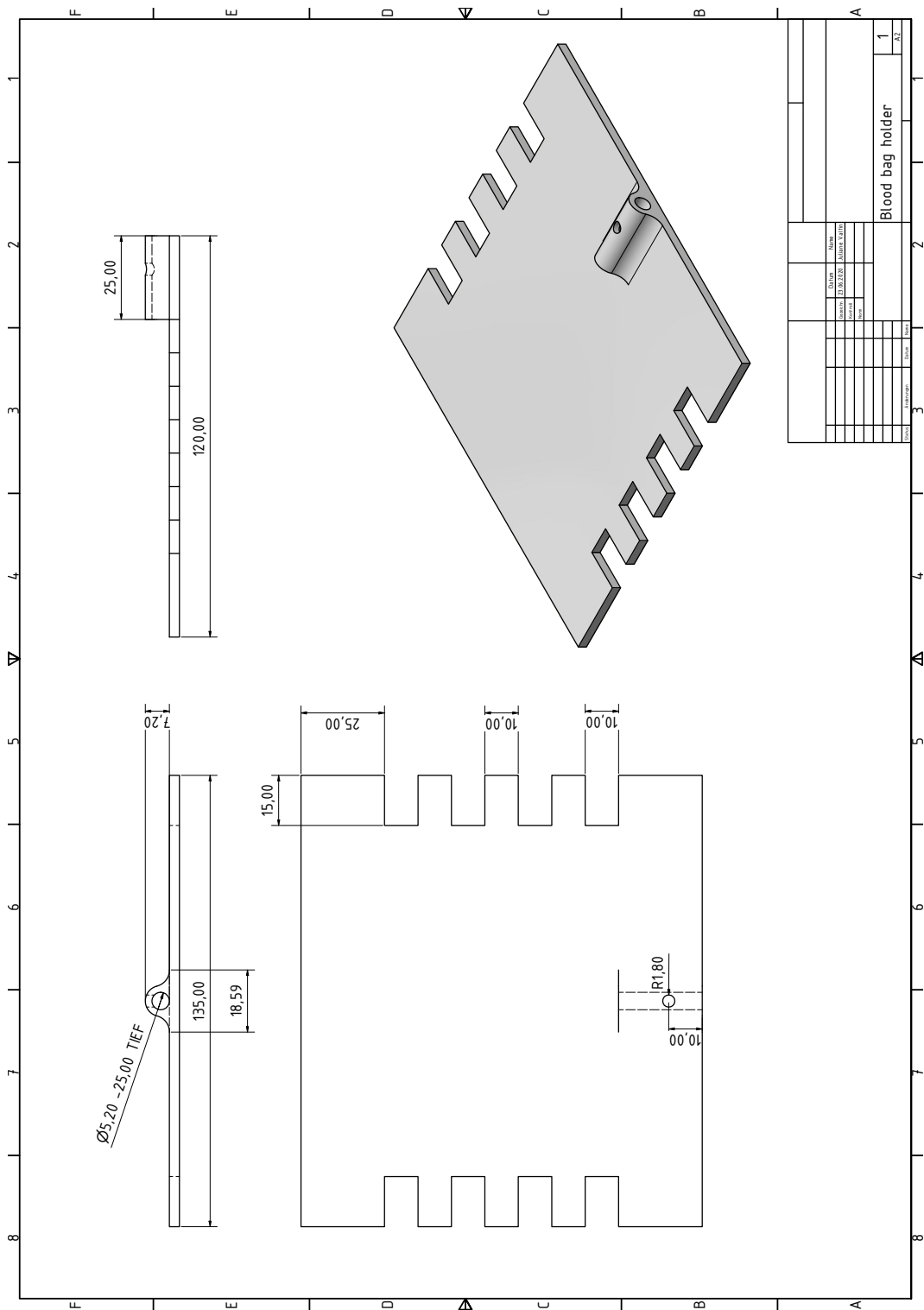


Figure A.11: Technical drawing of blood bag holder for rotation device.

## A.4 Publications and conference contributions

### Publications

André Ruland, Saskia Schenker, Lucas Schirmer, Jens Friedrichs, Andrea Meinhardt, Véronique B. Schwartz, Nadine Kaiser, Rupert Konradi, William MacDonald, Tina Helmecke, Melissa K. L. N. Sikosana, Juliane Valtin, Dominik Hahn, Lars D. Renner, Carsten Werner\*, Uwe Freudenberg\*. **Amphiphilic Copolymers for Versatile, Facile, and In Situ Tunable Surface Biofunctionalization**, in: *Advanced Materials* (2021), 33, e2102489

Juliane Valtin, Stephan Behrens, Manfred F. Maitz, Florian Schmieder, Frank Sonntag, Carsten Werner\*. **A modular *in vitro* flow model to analyse blood-surface interactions under physiological conditions**, in: *Current Directions in Biomedical Engineering* (2021), 7(2): 171-174

Juliane Valtin, Stephan Behrens, André Ruland, Florian Schmieder, Frank Sonntag, Lars D. Renner, Manfred F. Maitz, Carsten Werner\*. ***In vitro* blood flow model to evaluate antimicrobial materials under physiological conditions** - manuscript in preparation

### Conference contributions

**55<sup>th</sup> Annual Conference of the German Society for Biomedical Engineering**, 05.-07.10.2021, “A modular *in vitro* flow model to analyse blood-surface interactions under physiological conditions”, oral presentation

**31<sup>th</sup> Annual Conference of the European Society for Biomaterials**, 05.-09.09.2021, “Development of an *in vitro* flow model to test antimicrobial coatings for blood-contacting materials”, oral presentation

**11<sup>th</sup> World Biomaterials Congress**, 11.-15.12.2020, “On-demand antimicrobial coatings to combat biofilm formation on blood-contacting materials”, oral presentation performed by co-author André Ruland

---

\*corresponding author

## A.5 Selbstständigkeitserklärung

1. Hiermit versichere ich, dass ich die vorliegende Arbeit ohne unzulässige Hilfe Dritter und ohne Benutzung anderer als der angegebenen Hilfsmittel angefertigt habe; die aus fremden Quellen direkt oder indirekt übernommenen Gedanken sind als solche kenntlich gemacht.
2. Bei der Auswahl und Auswertung des Materials sowie bei der Herstellung des Manuskripts habe ich Unterstützungsleistungen von folgenden Personen erhalten:
  - Prof. Dr. Carsten Werner
  - Dr. Manfred F. Maitz
  - Dr. Lars D. Renner
3. Weitere Personen waren an der geistigen Herstellung der vorliegenden Arbeit nicht beteiligt. Insbesondere habe ich nicht die Hilfe eines kommerziellen Promotionsberaters bzw. einer kommerziellen Promotionsberaterin in Anspruch genommen. Dritte haben von mir weder unmittelbar noch mittelbar geldwerte Leistungen für Arbeiten erhalten, die im Zusammenhang mit dem Inhalt der vorgelegten Dissertation stehen.
4. Die Arbeit wurde bisher weder im Inland noch im Ausland in gleicher oder ähnlicher Form einer anderen Prüfungsbehörde vorgelegt und ist auch noch nicht veröffentlicht worden.
5. Ich bestätige, dass ich die Promotionsordnung der Fakultät Maschinenwesen der Technischen Universität Dresden anerkenne.

Dresden, 04.08.2022

Juliane Valtin